

Fall 12-6-2023

Comparative Evaluation of Propulsive Power Transmission Technologies for High-Speed Vertical Takeoff and Landing (HSVTOL) Cargo Aircraft

Xinyu Yang

Embry-Riddle Aeronautical University, yangx5@my.erau.edu

Follow this and additional works at: <https://commons.erau.edu/edt>



Part of the [Propulsion and Power Commons](#)

Scholarly Commons Citation

Yang, Xinyu, "Comparative Evaluation of Propulsive Power Transmission Technologies for High-Speed Vertical Takeoff and Landing (HSVTOL) Cargo Aircraft" (2023). *Doctoral Dissertations and Master's Theses*. 783.

<https://commons.erau.edu/edt/783>

This Thesis - Open Access is brought to you for free and open access by Scholarly Commons. It has been accepted for inclusion in Doctoral Dissertations and Master's Theses by an authorized administrator of Scholarly Commons. For more information, please contact commons@erau.edu.

COMPARATIVE EVALUATION OF PROPULSIVE POWER TRANSMISSION TECHNOLOGIES
FOR HIGH-SPEED VERTICAL TAKEOFF AND LANDING (HSVTOL) CARGO AIRCRAFT

By
Xinyu Yang

A Thesis Submitted to the Faculty of Embry-Riddle Aeronautical University
In Partial Fulfillment of the Requirements for the Degree of
Master of Science in Aerospace Engineering

December 2023

Embry-Riddle Aeronautical University
Daytona Beach, Florida

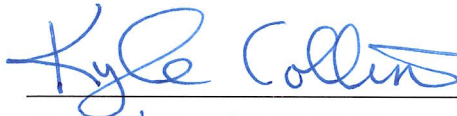
COMPARATIVE EVALUATION OF PROPULSIVE POWER TRANSMISSION TECHNOLOGIES
FOR HIGH-SPEED VERTICAL TAKEOFF AND LANDING (HSVTOL) CARGO AIRCRAFT

By

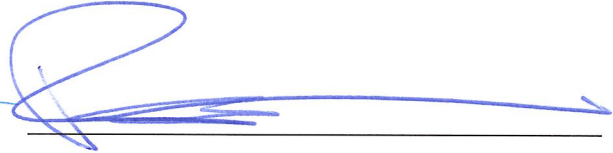
Xinyu Yang

This Thesis was prepared under the direction of the candidate's Thesis Committee Co-chair, Dr. Kyle B. Collins, Dr. Richard P. Anderson, Dr. Alberto W Mello, Department of Aerospace Engineering, and has been approved by the members of the Thesis Committee. It was submitted to the Office of the Senior Vice President for Academic Affairs and Provost, and was accepted in the partial fulfillment of the requirements for the Degree of Master of Science in Aerospace Engineering.

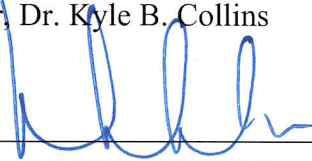
THESIS COMMITTEE



Co-chair, Dr. Kyle B. Collins



Co-chair, Dr. Richard P. Anderson



Co-chair, Dr. Alberto W Mello

Graduate Program Coordinator,
Dr. Hever Moncayo

Date

Dean of the College of Engineering,
Dr. James W. Gregory

Date

Associate Provost of Academic Support,
Dr. Kelly Austin

Date

ACKNOWLEDGEMENTS

I want to convey my sincere appreciation to my committee for their steadfast support, invaluable guidance, and insightful feedback, which have been instrumental in shaping the direction of this study.

I am also deeply grateful to my family for their unwavering encouragement, love, and understanding during the challenging phases of this academic journey. Their unwavering support has been a constant source of motivation.

I'd like to extend my acknowledgment to the Eagle Flight Research Center for providing the essential resources and research opportunities. The collaborative environment and resources they offer have played a pivotal role in the successful completion of this study.

ABSTRACT

Designing High-Speed Vertical Takeoff and Landing (HSVTOL) cargo aircraft capable of both low downwash velocity hovering and high subsonic speed cruising presents a significant engineering challenge. This challenge, stemming from conflicting design requirements, has been substantially influenced by recent technological advancements, which have offered greater flexibility in rotor placement. Consequently, this has led to the emergence of innovative mission-specific designs that hold the potential to outperform traditional concepts. The central objective of this study is to evaluate the benefits of modern technologies for VTOL cargo aircraft and assess their performance relative to baseline VTOL aircraft. The results of this comparative analysis provide valuable insights into the strengths and limitations of propulsive power traditional and advanced transmission for HSVTOL aircraft. Additionally, the study provides a comprehensive methodology for transmission sizing and weight estimation, ultimately revealing the most suitable transmission type for HSVTOL applications across varying weight ranges, thereby offering valuable guidance for future design endeavors. Within this technical scope, the weight of hydraulic propulsive power transmission with a turbine-speed pump, and electric transmission featuring state-of-the-art industrial and high-temperature superconductive (HTS) components is evaluated. In comparison to traditional mechanical transmission, it is evident that implementing HTS cables is effective in reducing HSVTOL propulsive power transmission weight across all takeoff weight ranges. Additionally, non-cryogenically cooled electrical power transmission demonstrates advantages, particularly for takeoff weights below 50,000 pounds.

TABLE OF CONTENTS

ACKNOWLEDGEMENTS.....	i
ABSTRACT.....	ii
TABLE OF CONTENTS.....	iii
LIST OF FIGURES	vi
LIST OF TABLES	xi
NOMENCLATURE	xiv
LIST OF SYMBOLS	xvi
1 Introduction	1
1.1 History.....	1
1.2 Importance of Research	3
1.3 Relevance and Significance	4
1.4 Mission of HSVTOL.....	6
1.5 Technological Challenge	7
1.6 Level of Technology	7
2 Problem Definition.....	9
2.1 Review of HSVTOL Literature	9
2.2 Concept Selection	16
2.3 Folding Rotor	20
2.4 Convertible Engines.....	20
2.5 Transmission System	22
2.6 Hypothesis.....	29

3	Methodology	31
3.1	Research Approach	31
3.2	Design Constraints	32
3.3	Hydrostatic Transmission Sizing Methodology.....	34
3.3.1	Hydrostatic Pump Sizing	36
3.3.2	Hydraulic Motor Sizing	38
3.3.3	Hydraulic Hose Sizing	41
3.3.4	Accessory and Miscellaneous.....	45
3.3.5	Integration.....	50
3.4	Electric Transmission Sizing Methodology	53
3.4.1	Motor/Generator Sizing.....	55
3.4.2	Rectifier/Inverter	58
3.4.3	Wire Sizing	58
3.4.4	Thermal Management System (TMS) Sizing	62
3.4.5	Battery Sizing	64
3.4.6	Integration.....	66
3.5	Scaling.....	68
4	Results	72
4.1	30-TF Transmission Weight Results	72
4.2	15-TF Transmission Weight	75

4.3	Trend of Transmission Weight	77
4.4	Comparison	84
5	Discussions, Conclusions, and Recommendations	85
5.1	Discussion	85
5.2	Conclusions	87
	REFERENCES	89
	APPENDIX A – Design of HSVTOL Airframe	96
	APPENDIX B – Data Used for Sizing	104
	APPENDIX C– Additional Information	123

LIST OF FIGURES

Figure	Page
Figure 1.1 The Baynes “Heliplane” (left) and Model 1-G (right) [1].	1
Figure 1.2 The Bell XV-3 (left) [8] and XFV-1(center) [3], and Fairey Jet (right) [4].	2
Figure 1.3 Ryan X-13(left) [5], Short SC.1 (center) [6], and Ryan XV-5 (right) [7].	2
Figure 1.4 Canadair CL-84 (left) [9] and Dornier Do 31 (right) [10].	3
Figure 1.5 Proof of concept designs that entered the HSVTOL challenge.	5
Figure 1.6 AFWERX’s envision of HSVTOL [17].	6
Figure 1.7 TRL [19] requirements for HSVTOL from the VFS RFP.	8
Figure 2.1 Primary Mission Profile for HSVTOL [18].	9
Figure 2.2 V-22 Long Range Special Operation mission [20].	9
Figure 2.3 Hover vertical lift efficiency as a function of disc loading [23].	11
Figure 2.4 Fan-in-Wing [24], Thrust Augmented Wing [25], and Tilt Nacelle [26].	11
Figure 2.5 Demonstration of rotor disk with high forward speed [30, p. 221].	12
Figure 2.6 S-97 Raider (left) [27], X3 (center) [28], and S-72 (right) [29].	13
Figure 2.7 Typical propeller efficiency with specified pitch [31].	14
Figure 2.8 Propeller thrust trend over a range of speed with constant power [31].	14
Figure 2.9 Power requirements and cruise-speed of various aircraft types [32].	15
Figure 2.10 Pneumatic channel wing predicted Super-STOL takeoff performance [34].	16
Figure 2.11 Radar plot of representing designs’ performance WRT requirements.	17
Figure 2.12 Radar plot of tiltrotor VTOL performance WRT HSVTOL requirements.	18
Figure 2.13 Visual representation of considered concepts.	19
Figure 2.14 Rendering of Bell HSVTOL concepts (Retrieved from [35]).	19
Figure 2.15 Model 627 folding proprotor pod with fold stow slots [36].	20
Figure 2.16 Bell's HSVTOL test article is at Holloman Air Force Base [37].	20

Figure	Page
Figure 2.17 Cutaway and performance of TF34 engine with VIGV [39].	21
Figure 2.18 Schematics of the V-22 transmission system [43].	22
Figure 2.19 Tactical tiltrotor transmission in left nacelle [44].	23
Figure 2.20 Expected route of HSVTOL transmission (Concept from [45]).	24
Figure 2.21 Cross section of LF-336 1.3 pressure ratio lift fan [46].	25
Figure 2.22 Schematic layout of smart UAV propulsion system [47].	25
Figure 2.23 Typical CRW in UAV Configuration [48].	26
Figure 2.24 Schematic of Bell UH-1/T-53 Hydraulic Transmission System [49].	27
Figure 2.25 Quadcopter uses fluid for power transmission [50].	27
Figure 2.26 End view of turbine speed pump [51].	28
Figure 2.27 ABL concept [53](left), BLI (center) and engine layout (right) [54].	28
Figure 2.28 Concepts explored in this study.....	30
Figure 3.1 Hydrostatic transmission system components layout.....	35
Figure 3.2 Actuator weight vs. input pressure [57].	35
Figure 3.3 Pump weight scaling curve.....	37
Figure 3.4 Bosch axial piston motor (left) [59], and radial piston motor (right) [60].	38
Figure 3.5 The scaling curve for hydraulic motor weight.	39
Figure 3.6 Overlaid correlation between weight and rated torque [61].....	39
Figure 3.7 Motor outflow rate to power scaling curve.	40
Figure 3.8 Comparison between OTS hoses and AM 350 pipes.	44
Figure 3.9 General trend of AM 350 pipe weight wrt diameter.	44
Figure 3.10 The two tilting methods considered.	45
Figure 3.11 Moog Model 810 drawings [66].	47
Figure 3.12 MOOG Model 810 length scaling plot.....	48

Figure	Page
Figure 3.13 MOOG Model 810 weight scaling plot.....	48
Figure 3.14 Pipe friction pressure drop versus velocity [49].....	50
Figure 3.15 Transition of power density in electric and hydraulic motors [61].	53
Figure 3.16 Turboelectric transmission system components layout.....	54
Figure 3.17 Room temp. turboelectric (top) vs. Cryo superconductor (bottom) [70].	54
Figure 3.18 Specific power of the motor considered.....	57
Figure 3.19 Cable conductor area with respect to the current carried.	60
Figure 3.20 Battery specific energy and density trends [81].	66
Figure 3.21 The radius to half-span ratio of various tiltrotor aircraft.....	70
Figure 3.22 Aspect ratio of various tiltrotor aircraft (Figure A 6 - Figure A 9).	70
Figure 3.23 V-22 dimensions are defined by shipboard compatibility requirements [20].	71
Figure 4.1 The transmission weight versus maximum vertical takeoff weight.....	78
Figure 4.2 The transmission weight fraction versus maximum vertical takeoff weight.....	78
Figure 4.3 Trend of hydrostatic transmission component percentage weight.....	79
Figure 4.4 Trend of HTC GRC transmission component percentage weight.....	80
Figure 4.5 Trend of transmission component percentage weight with N3-X assumption.....	81
Figure 4.6 Trend of transmission component percentage weight using Helix motor.....	82
Figure 4.7 Trend of transmission component percentage weight using Helix & HTS.....	83
Figure 4.8 Transmission weight trend WRT total power.	84
Figure 5.1 Power transmission weight trend of all the reviewed concepts.....	87
Figure A 1 VTOL with existing prototype (VTOL wheel is from [33]).....	96
Figure A 2 Aircraft indicated speed records (constant) in KTAS at different altitude.....	97
Figure A 3 Design process of HSVTOL based on common aircraft design process.....	99
Figure A 4 Schematics of tiltrotor pylon with fixed engine arrangement [89].....	100

Figure	Page
Figure A 5 A representative tiltrotor aircraft configuration [88].	101
Figure A 6 XV-15 aspect ratio (Drawing from [83]).	102
Figure A 7 V-22 aspect ratio (Drawing from [84]).	102
Figure A 8 AW609 aspect ratio (Drawing from [85]).	103
Figure A 9 V-280 aspect ratio (Drawing from [86] & [87]).	103
Figure B 1 Pump flow rate WRT displacement.	105
Figure B 2 Pump power to flow rate relation.	105
Figure B 3 Pump dry weight to flow rate relation.	106
Figure B 4 Pump dry weight to power relation.	106
Figure B 5 Trend of the existing pump weight WRT rated power collected.	108
Figure B 6 Unit weight trend of Parker™ P35/P56 hydraulic hoses.	109
Figure B 7 Model 810 drawing with dimensions varying with variable dimensions.	112
Figure B 8 Electrical motor scaling trends from [72] [81].	113
Figure B 9 Motor weight scaling trend for all motors considered.	114
Figure B 10 Wire cross-sectional area WRT current comply with AC 43.13-1B.	116
Figure B 11 HWC 263 cross-sectional area WRT current.	117
Figure B 12 Cross-section of the cryogenic pipe and conductor [78].	118
Figure B 13 STARC-ABL architecture: baseline (left) & advanced concepts (right) [79].	119
Figure B 14 RVLTEAP architecture: baseline (left) & advanced concepts (right) [79].	119
Figure C 1 The hydraulic component weight trend over takeoff weight.	123
Figure C 2 GRC components weight trend over takeoff weight.	124
Figure C 3 N3-X assumption components weight trend over takeoff weight.	125
Figure C 4 Helix motor transmission weight over takeoff weight.	126
Figure C 5 Helix motor and HTS cable transmission weight over takeoff weight.	127

Figure	Page
Figure C 6 Typical transmission system in single-rotor helicopter from [82]......	128
Figure C 7 Weight trends for current helicopter drive trains from [82].	128

LIST OF TABLES

Table	Page
Table 2.1 Main difference between mission profile of HSVTOL(VFS) and V-22	10
Table 2.2 HSVTOL decision matrix.....	18
Table 3.1 Counterparts of the traditional mechanical transmission systems.....	31
Table 3.2 List of scaling factor for hydrostatic transmission misc. objects.....	49
Table 3.3 Sample transmission weight estimated for 30-TF with hydrostatic transmission. .	52
Table 3.4 Percentage power rejected and specific weight of RVLT TMS.	62
Table 3.5 30-TF concept room temperature TMS component size.	63
Table 3.6 30-TF concept Cryogenic TMS component size.	64
Table 3.7 TMS weight summary and comparison.	64
Table 3.8. Technology used for weight estimation.....	67
Table 3.9 Sample transmission weight estimated for 30-TF with hydrostatic transmission. .	68
Table 4.1 Weight of various transmission comparing to 30-TF HSVTOL baseline.	72
Table 4.2 Weight fraction of various transmission system comparing to 30-TF baseline.	73
Table 4.3 Percentage component weight of transmission for 30-TF HSVTOL.	74
Table 4.4 Different types of batteries sized for the 30-TF concept.	74
Table 4.5 Weight of various transmission comparing to 15-TF HSVTOL baseline.	75
Table 4.6 Weight fraction of various transmission system comparing to 15-TF baseline.	75
Table 4.7 Percentage component weight of transmission for 15-TF HSVTOL.	76
Table 4.8 Different types of batteries sized for the 15-TF concept.	76
Table 4.9 The design parameter used for a range of MTOW in pounds.	77
Table 4.10 The hydraulic component weight out of the total system weight.	79
Table 4.11 The percentage transmission component weight using HTS GRC components. .	80
Table 4.12 The percentage transmission component weight using N3-X assumption.	81

Table	Page
Table 4.13 The percentage transmission component weight using Helix motor.	82
Table 4.14 The percentage component weight using Helix motor + HTS wire.	83
Table 4.15 Power transmission weight scaling equation WRT power.	84
Table 5.1 Scaling equation of HSVTOL power transmission weight.	87
Table A 1 Public domain peed records of aircraft using various propulsion types.	96
Table A 2 Public domain data of existing VTOL vs. VFS design requirements.	98
Table B 1 Parker™ Aircraft Engine-Driven Pumps data.	104
Table B 2 Bosch™ axial piston fixed/plug-in motor A10 series data.	107
Table B 3 Bosch™ axial piston fixed/plug-in motor A4 series data.	107
Table B 4 P35/P56 hose specific weight with various pressure and diameter in [lb/ft].	108
Table B 5 Minimum required thickness for given inner diameter and pressure.	109
Table B 6 Minimum weight for AM 350 (DA) piping.	110
<i>Table B 7 Reference hydraulic component weight for 1,500 hp system [49].</i>	<i>111</i>
Table B 8 MOOG Model 810 Parameters [66].	112
Table B 9 Design assumption for Single-Aisle BLI electric weight estimates [53].	113
Table B 10 Current carrying capacity and resistance of copper wire [76].	115
Table B 11 HW263 cable data [77].	117
Table B 12 Weight per unit length of the cable system [78].	118
Table B 13 Rated current and weight-to-current per unit length [78].	118
Table B 14 Electrified aircraft cooling loop comparison [79].	120
Table B 15 Sizing relations for loops cooling converters in series with motors [79].	121
Table B 16 Tiltwing concept vehicle design [56].	122
Table C 1 The hydraulic component weight, of various takeoff weight.	123
Table C 2 The electric transmission component weight with GRC components.	124

Table	Page
Table C 3 The electric transmission component weight with N3-X assumption.	125
Table C 4 The electric transmission component weight using Helix motor.	126
Table C 5 Electric transmission component weight using Helix motor + HTS cable.	127

NOMENCLATURE

AR	Aspect Ratio
DL	Disk Loading
DOP	Design Operating Pressure
FM	Figure of Merit
FoS	Factor of Safety
GPM	Gallons Per Minute
GRC	Glenn Research Center
HSVTOL	High-Speed Vertical Takeoff and Landing
HTS	High Temp. Superconductor
ID	Inner Diameter
KTAS	Knots True Airspeed
MEP	Mission Equipment Package
MTOW	Maximum Takeoff Weight
NASA	National Aeronautics and Space Administration
NDARC	NASA Design and Analysis of Rotorcraft
OEI	One Engine Inoperative
OTS	Off-the-shelf
pax	Passengers
RFP	Request For Proposal
ROA	Radius of Action
ROM	Revolutions Per Minute
SOA	State-of-Art

SPRINT	SPEed and Runway INdependent Technologies
T/O	Takeoff
TF	Tilt and Fold
TMS	Thermal Management System
TR	Tiltrotor
TRL	Technology Readiness Level
TW	Tilt-wing
VDTR	Variable Diameter Tiltrotor
VFS	Vertical Flight Society
VIGV	Variable Inlet Guide Vanes
VTOL	Vertical Takeoff and Landing
WL	Wing Loading
WRT	With Respect To

LIST OF SYMBOLS

κ	Induced Losses Factor	σ_{tu}	Tensile Ultimate Strength
A_R	Rotor Disk Area	σ_y	Yield Strength
C_P	Power Coefficient	r	Rotor Radius
C_T	Thrust Coefficient	I	Current
$P_{()}$	Power of ()	Q	Torque
$S_{()}$	Area of ()	S	Wing Area
$SP_{()}$	Specific Power ()	b	Wingspan
$V_{()}$	Volume of ()	l	Length
\dot{V}	Volume Flow Rate	u	Velocity
V_{motor}	Motor Voltage	ρ	Density
$W_{()}$	Weight of ()	σ	Solidity
$n_{()}$	Number of ()		

1 Introduction

The concept of High-Speed Vertical Takeoff and Landing (HSVTOL) transport aircraft, while not new, has yet to be fully realized. The design challenge for HSVTOL cargo aircraft is to create a concept that can hover with low downwash velocity and cruise at high subsonic speed. This challenge is difficult due to conflicting requirements, but with the advancement of propulsion technology, more flexible rotor placement options have emerged, allowing for the creation of novel designs that are customized for specific missions.

1.1 History

The concept of tiltrotor VTOL aircraft traces back to year 1937 [1], when Leslie E. Baynes patented a “Heliplane” that employed large diameter propeller on tiltable pylons, see Figure 1.1. This was one year after the appearance of the first side-by-side rotorcraft that successfully demonstrated stable hover and translation maneuvers. Multiple concepts were presented and patented, but the first prototype to demonstrate in-flight transition was not seen for another 10 years. Known as the Transcendental Model 1-G, the demonstrator crashed prior to completion of a full conversion to the airplane mode, due to a mechanical control failure [1].

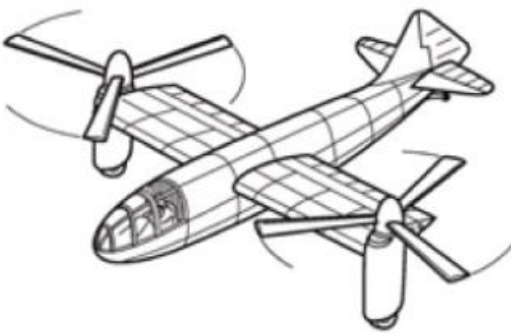


Figure 1.1 The Baynes “Heliplane” (left) and Model 1-G (right) [1].

Following up was the Bell XV-3, experienced severe vibration issue during conversion [2]. During the 50s, other configurations that convert between flight modes are being tested, such like XFV-1 tailsitter [3], Fairey Jet Gyrodyne compound gyroplane [4], X-13 vertijet [5], and SC.1 with lifting engines [6]. Although some of the concepts have demonstrated successful hover and transition, they carry little payload. In the 1960s Ryan XV-5A [7] with fan-in-wing design showed great potential but with the same problem in low reliability and usable load. Figures of the concepts mentioned above are depicted in Figure 1.2 and Figure 1.3.

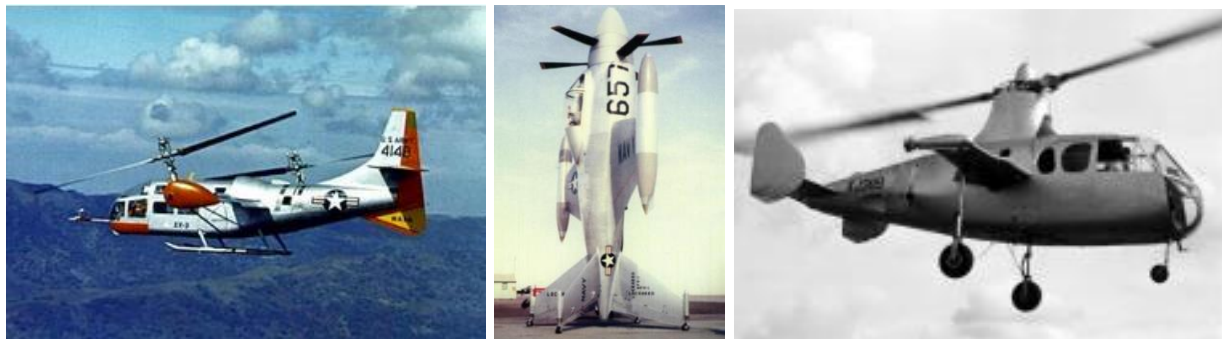


Figure 1.2 The Bell XV-3 (left) [8] and XFV-1(center) [3], and Fairey Jet (right) [4].

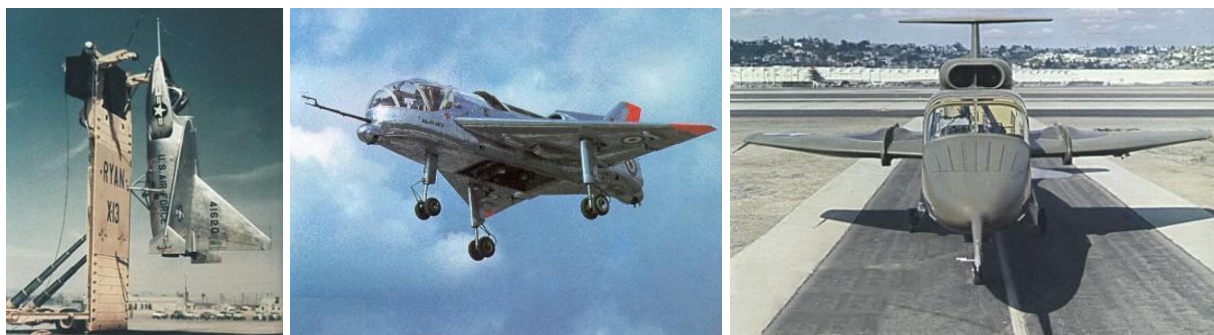


Figure 1.3 Ryan X-13(left) [5], Short SC.1 (center) [6], and Ryan XV-5 (right) [7].

The VTOL cargo plane design is particularly challenging, having no successful flights until the end of 1960s and early 70s. Canadair CL-84 tiltwing first flew in 1963 [9] but soon canceled

in early 70s. Dornier Do 31 with its unique tip-mounted lifting engines [10] has great cruise speed, but the usable load fraction is still marginal. See Figure 1.4 for photos of pictures of the airframe.

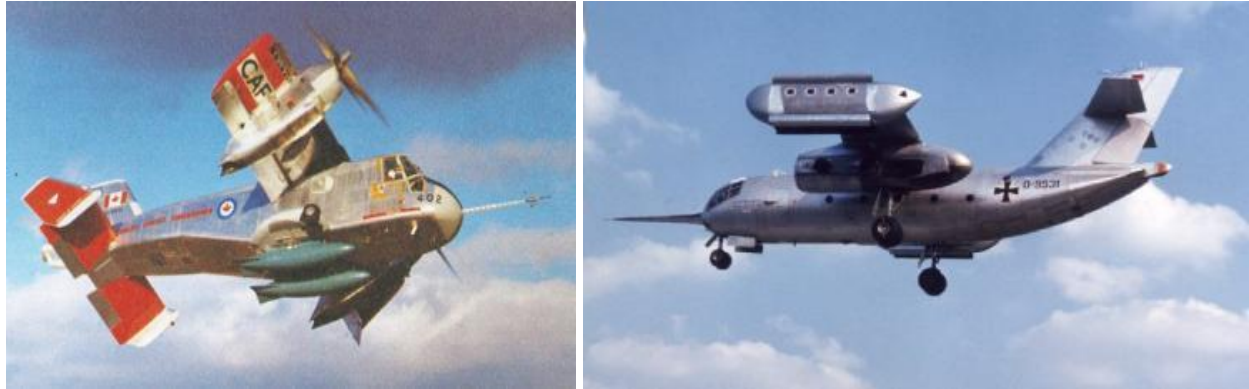


Figure 1.4 Canadair CL-84 (left) [9] and Dornier Do 31 (right) [10].

The Bell XV-15 tiltrotor is the closest to modern VTOL transport, with development started in 1972 and first flew in 1977. Bell's experience in designing XV-15 eventually initiated the design of V-22 tiltrotor, in 1986. To date, the V-22 Osprey has become a vital asset in armed forces, extending its reach across multiple military branches and countries. This study is conducted to seek for answers to design problem related to the next generation of VTOL transport, with missions similar to the V-22, but cruise at much higher airspeed.

1.2 Importance of Research

The importance of HSVTOL technology is underscored by its potential applications in various sectors. For the military, HSVTOL aircraft can be used for a wide range of applications, including reconnaissance, transportation, and logistics. The importance of runway independence is highlighted by the potential to operate aircraft on a vast scale, as noted by SOCOM Acquisitions Executive James Smith: *"The entire Indo-Pacific could be considered a runway."* [11] In addition, the high-speed and long-range capabilities of some HSVTOL designs make them suitable

for rapid deployment of troops and equipment in remote or difficult-to-access locations [12]. In the civilian sector, HSVTOL aircraft can be used for urban air mobility, cargo transportation, and emergency medical services, like concept explored in *Technology Needs for High Speed Rotorcraft* (3) [13].

Despite the potential benefits, the development of HSVTOL technology has been slow due to several technical and operational challenges. These include the need for high-performance convertible engines, the need for aerodynamic improvements for increasing range, the need for advanced control systems to manage the complex flight dynamics during transition, and the need for weight reduction to increase the payload weight reduction. A lack of historical resources further complicates the problem as it is more difficult to conduct preliminary design, and then compare with baseline or competitors for optimization purpose.

This study aims to provide a method of weight estimation in the early design stage, specifically the weight of transmission system. By estimating component weight, and comparing the integrated system utilizing traditional mechanical, hydrostatic, or electric transmission, the study will provide guidance for transmission system selection and sizing, for a range operating condition.

1.3 Relevance and Significance

The HSVTOL topic has long been of significant interest, and recent technological advancements and increasing demands have sparked a renewed focus. In January 2022, the US Air Force made a significant move by selecting eleven companies to embark on the conceptual development of a high-speed vertical takeoff and landing (HSVTOL) aircraft. This endeavor, initially known as the High-Speed VTOL Challenge, was initiated in the spring of 2021 as a collaborative effort between AFWERX, the Air Force's innovation hub, and the US Special Operations Command (SOCOM) [14]. The scope of this project is substantial, as evidenced by the

initial call for ideas, which drew a remarkable 218 proposals and was later narrowed down to 35 preliminary solutions by AFWERX in August 2021 [15], with a few of them shown in Figure 1.5.

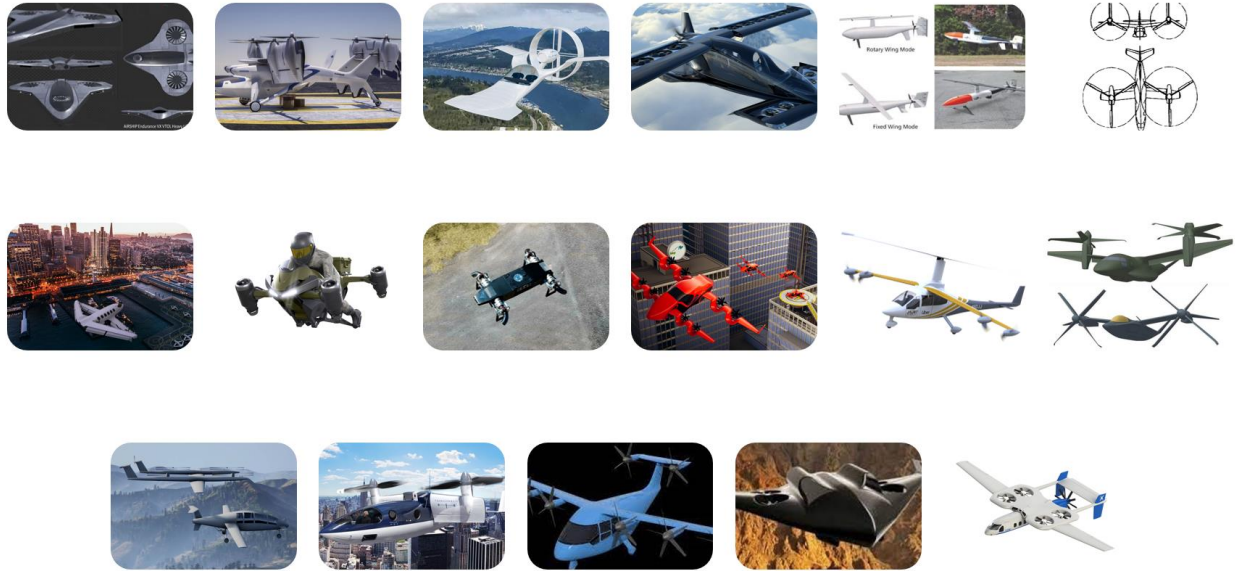


Figure 1.5 Proof of concept designs that entered the HSVTOL challenge.

Furthermore, in 2023, the Defense Advanced Research Projects Agency (DARPA) Tactical Technology Office (TTO) introduced the S^Peed and Runway INdependent Technologies (SPRINT) X-Plane Demonstrator program. This initiative resonates with the increasing interest in advancing air mobility platforms. The core objective of the SPRINT program is to design, build, certify, and successfully fly an X-plane that serves as a proof-of-concept technology demonstrator. It is tasked with showcasing the enabling technologies and integrated concepts essential for a revolutionary fusion of aircraft speed and runway independence, all in preparation for the next generation of air mobility platforms [16]. Notably, the ambitious timelines set by the SPRINT program underscore the drive to rapidly achieve its objectives. This study of HSVTOL

transmission weight may provide valuable insights into systems, power, and weight modeling, particularly benefiting the airframe developers participating in the program.

1.4 Mission of HSVTOL

The mission requirements for the HSVTOL program are centered on the development of an aircraft that could ultimately serve as a replacement for the Air Force's V-22 Osprey, offering a payload capacity on par with the V-22 but significantly higher cruise speeds. While the anticipated airframe will be multifunctional, including roles such as personnel infiltration, tactical mobility, and aeromedical evacuation, the initial focus of this study is on a predominant mission profile. The prioritization of this mission profile allows for further analysis and trade study between different missions to be conducted in future studies.

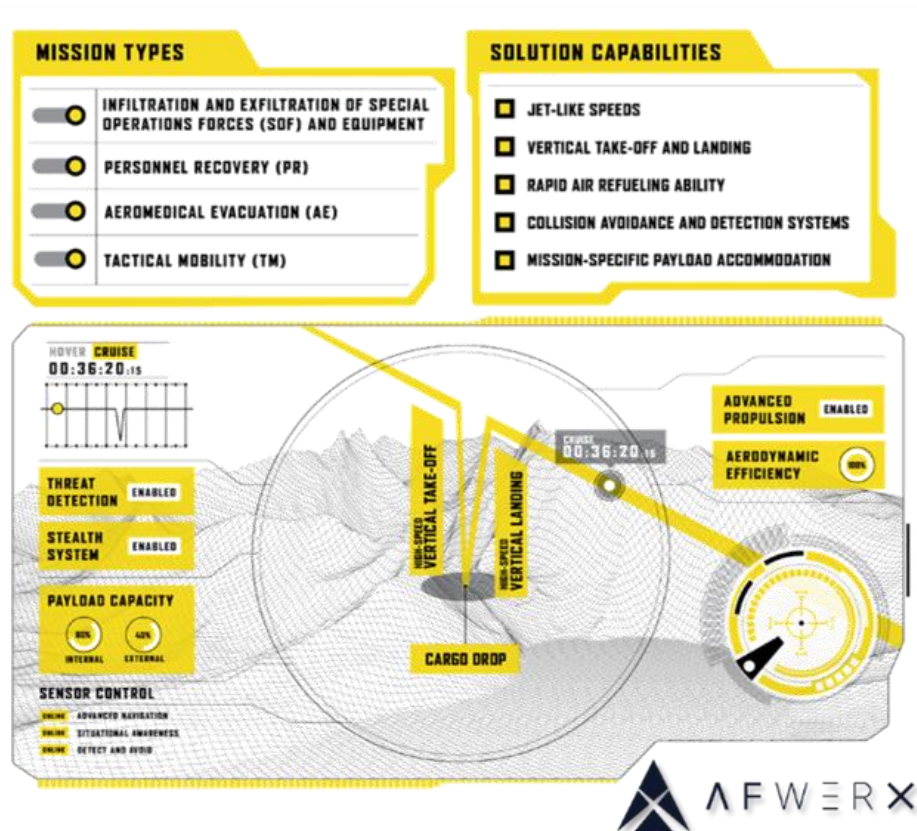


Figure 1.6 AFWERX's envision of HSVTOL [17].

Described on the AFWERX website, the primary mission profile necessitates jet-like speed, VTOL (Vertical Takeoff and Landing) capability, rapid aerial refueling ability, and specific requirements in terms of system functionalities and dimensional aspects, see Figure 1.6. This mission profile effectively narrows down the aircraft's configuration to a jet-propelled rotorcraft utilizing liquid fuel as the primary energy source. More specific mission requirements with specific speed and range values will be discussed in Section 2.

1.5 Technological Challenge

Following a thorough review of the mission profiles, the primary technological challenges can be briefly outlined. The HSVTOL program requires an aerodynamically efficient airframe to minimize profile drag in cruise, an advanced convertible engine capable of providing sufficient thrust during cruise and shaft power for hover, and a sophisticated control system designed to aid the pilot during flight mode transitions. While this paper aims to contribute to the solution by focusing on reducing transmission weight, thus lowering induced drag and power requirements for hover, it is imperative to select a concept with the appropriate configuration for accurate power estimation. A more comprehensive examination of these ongoing challenges will be presented in Section 2, along with an exploration of the assumptions underpinning the technologies employed.

1.6 Level of Technology

The responses to the recent HSVTOL challenge mark the onset of another significant technological advancement, centering around a particular issue. It's noteworthy that some of these emerging technologies are either still in the development phase or remain confined within non-public domains. While estimating technological progress based on historical trends is a customary approach, it's vital to consider the constraint posed by the Technology Readiness Level (TRL). This constraint sets a limit on the acceptable time frame for technological development. As

referenced in [18], the technology applied should have reached TRL 3 in 2021, attain TRL 6 by 2027, and eventually reach TRL 9 by 2035, see Figure 1.7. This constraint implies that relevant concepts must work in a controlled environment, and that prototype demonstrators can be effectively tested by 2027.

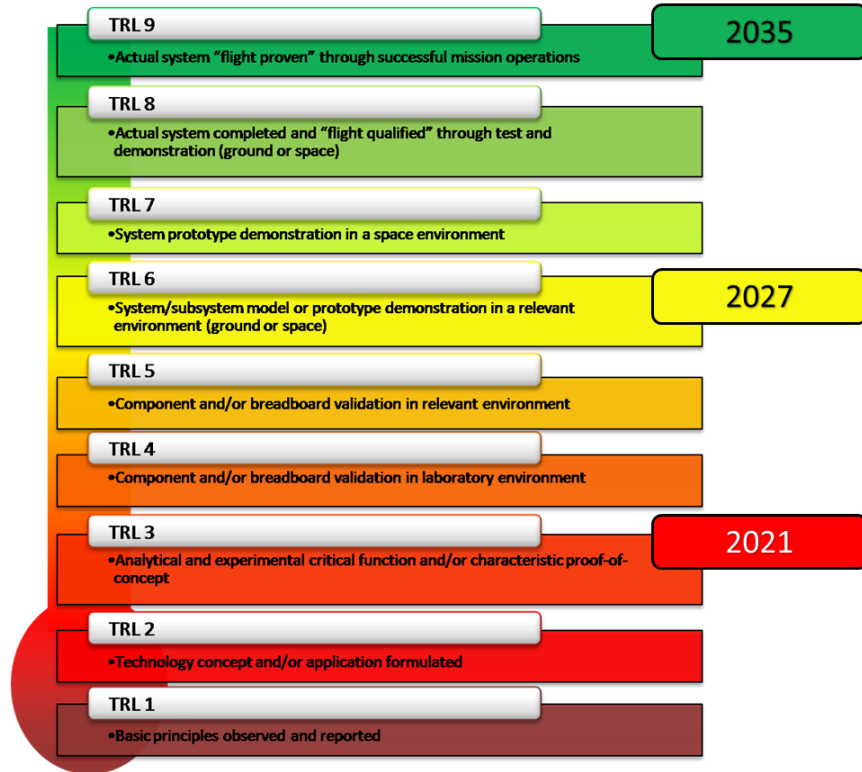


Figure 1.7 TRL [19] requirements for HSVTOL from the VFS RFP.

In conclusion, the concept of HSVTOL aircraft, while not new, has presented a complex and challenging technological endeavor. Recent advancements in technology, coupled with innovative design concepts, have brought the realization of HSVTOL aircraft closer to becoming a reality. This paper aims to contribute to this development by delving into the realm of hydraulic and electric transmissions for HSVTOL and offering insights into the associated changes in weight and performance.

2 Problem Definition

The problem definition section encompasses the review of mission requirements, a study on existing designs, selection of aircraft configuration, and specific technological challenges related to the topic. Beginning with a literature review, this section will elucidate the decisions made in the design process.

2.1 Review of HSVTOL Literature

The review of the literature section forms the foundation for understanding the conceptual landscape of HSVTOL aircraft technology. The selection of the concept under review was not arbitrary; it emerged from a meticulous evaluation of numerous conceptual designs. This evaluation involved a thorough analysis of previously explored technologies, setting the stage for the exploration of the chosen concept. Recognizing the pivotal role of mission profiles in shaping design, this section begins with a comprehensive review of mission parameters, as depicted in Figure 2.1, sourced from the Request for Proposals (RFP) for the 40th VFS student design competition, providing a guiding framework for the examination of the primary HSVTOL mission.

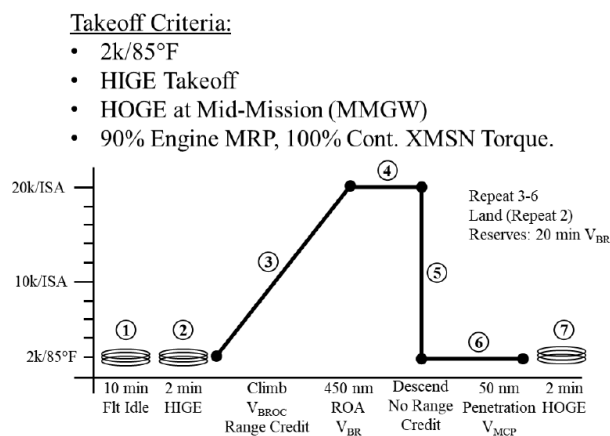


Figure 2.1 Primary Mission Profile for HSVTOL [18].

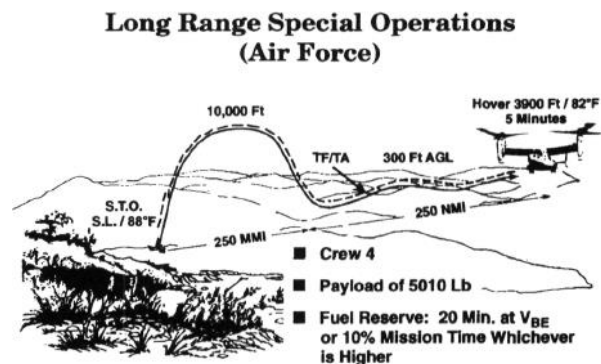


Figure 2.2 V-22 Long Range Special Operation mission [20].

Table 2.1 Main difference between mission profile of HSVTOL(VFS) and V-22.

Parameter	HSVTOL for VFS	V-22 Long Range Special Ops.
T/O Criteria	2,000 ft/85°F (0.002105 slug/ft ³)	0 ft/88°F (0.002251 slug/ft ³)
Hover Criteria	2,000 ft/85°F (0.002105 slug/ft ³)	3,000 ft/82°F (0.002040 slug/ft ³)
Cruise Alt	>20,000 ft (0.001364 slug/ft ³)	10,000 ft (0.001880 slug/ft ³)
Cruise Speed	>450 KTAS	~230 KTAS
Cruise ROA	450 nm	250 nm
Penetration ROA	50 nm	250 nm

The VFS mission profile of the HSVTOL shows significant similarities with the Long-Range Special Operation design mission for the V-22. However, notable distinctions are highlighted in Table 2.1. The HSVTOL's primary mission primarily encompasses covering the range by cruising at a thread avoidance altitude of no less than 20,000-feet MSL, achieving significantly higher speeds, and subsequently descend to low-level penetration at 2,000-feet with maximum continuous power for high-speed terminal penetration. The payload weights specified are in a similar range, approximately 5,000 lb, with the addition of 1,000 lb for the Mission Equipment Package (MEP) specified in the VFS primary mission.

Achieving the right balance between power requirements for vertical and horizontal flight is essential to minimize deadweight during each phase of flight. While it is possible to achieve vertical takeoff by vectoring jet thrust, the hover efficiency, also known as power loading, diminishes significantly as the disk loading increases. As illustrated in Figure 2.3, vectored jets exhibit the lowest power loading. However, for cargo airplanes, using the vectored jet for both configurations can result in an excessive amount of unused power during cruise. In contrast, helicopters with low disk loading experience the highest power loading, which is comparable to the power required in forward flight. This issue is exemplified by the Do 31 in [21], where eight lift engines are required in addition to the two engines for level flight with vectored thrust. On top

of the excessive amount of power required, airframe structures for vectored concepts must be further reviewed for higher working temperature, as a result of deflected exhaust air heating up the skin [21]. Additional non-cargo aircraft concepts with similar issue are shown in Figure 2.4 below. Additional performance information of thrust augmentation designs is available in [22].

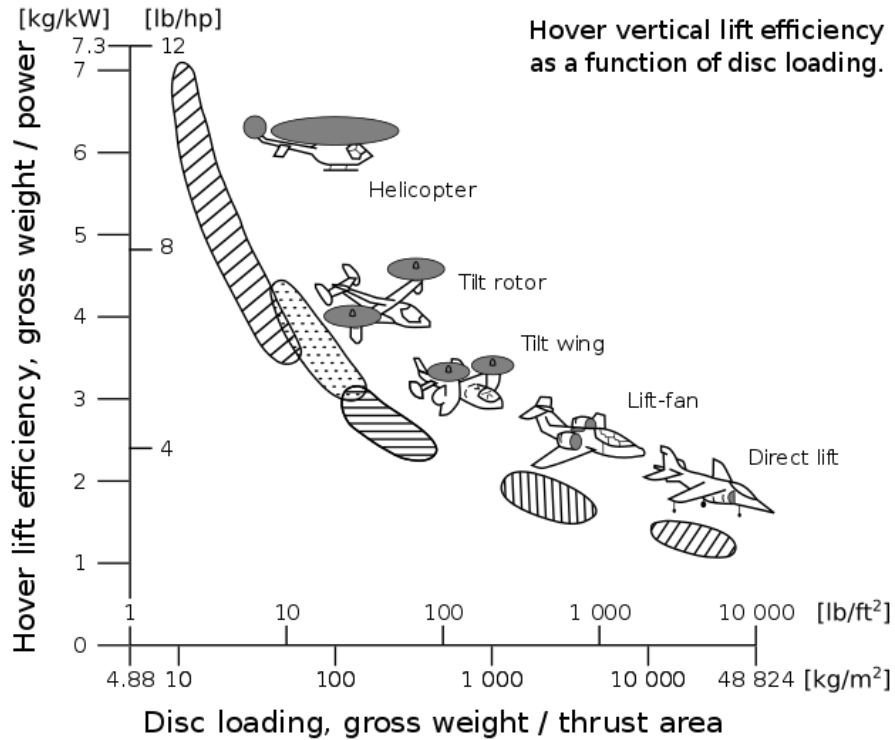


Figure 2.3 Hover vertical lift efficiency as a function of disc loading [23].

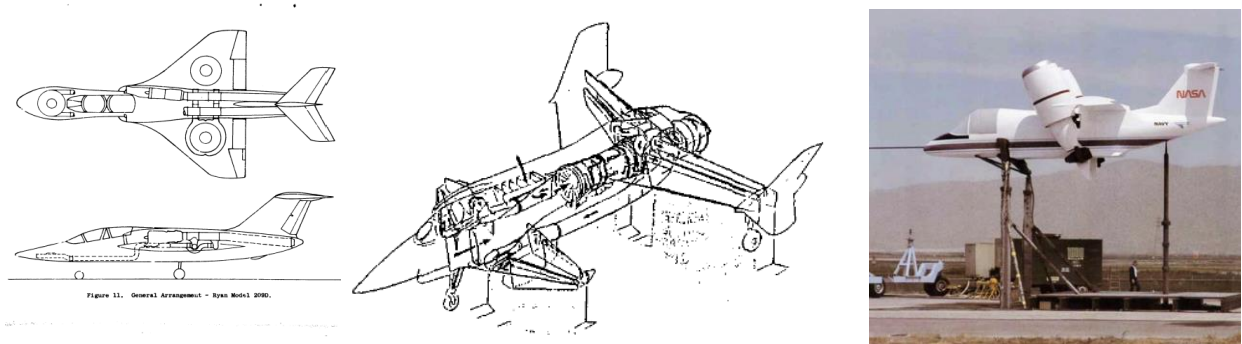


Figure 2.4 Fan-in-Wing [24], Thrust Augmented Wing [25], and Tilt Nacelle [26].

In contrast, rotors and traditional propellers are ill-suited for high-speed flight. Rotorcraft, for instance, has a top speed of around 200 knots due to the challenges posed by the varying loads on their advancing and retreating rotor blades, driven by their high forward speed. At these velocities, the tip speed on the advancing side exceeds the divergence Mach number, while on the retreating side, reversed flow begins from the root of the blades, shown in Figure 2.5. This results in an unsteady, uneven load distribution, causes difficulties in controlling the rotorcraft, increased structural stress, and increased drag. The issue isn't limited to traditional helicopters alone. Coaxial helicopters with pusher propellers, such as the Sikorsky S-97 Raider [27], and compound helicopters like the Eurocopter X3 [28] and Sikorsky S-72 [29], can achieve higher speeds than traditional helicopters but still fall short of the speeds attained by fixed-wing airplanes. This comparison is illustrated in Figure A 2, and the aircraft mentioned are shown in Figure 2.6.

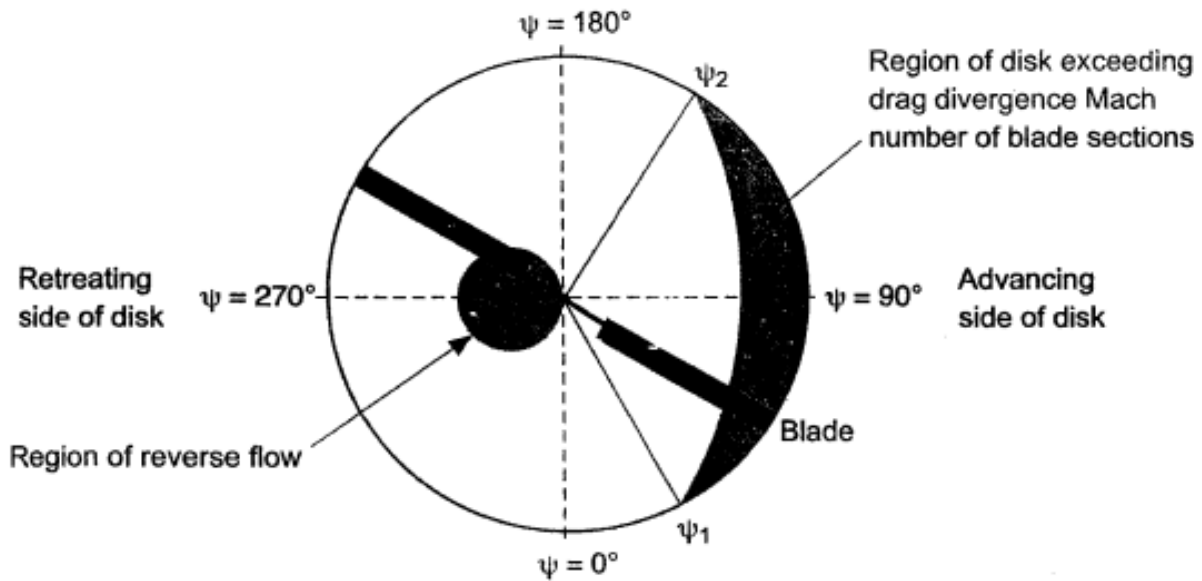


Figure 2.5 Demonstration of rotor disk with high forward speed [30, p. 221].



Figure 2.6 S-97 Raider (left) [27], X3 (center) [28], and S-72 (right) [29].

Traditional propellers are also suboptimal for this mission. As depicted in Figure 2.7, a typical propeller efficiency plot reveals that, for each pitch setting, efficiency peaks and then declines rapidly as the advance ratio increases. The advance ratio is defined as the ratio between forward speed and tip speed. Even with variable pitch propellers, the envelope of maximum efficiency is expanded, but a trend of reduced efficiency still emerges with increasing advance ratio. Since thrust is power over velocity, a constant power output leads to a reduction in thrust, and when efficiency decay is factored in, the thrust diminishes even further. Figure 2.8 illustrates the trend for a generic case. Historically, achieving the necessary speed with propeller planes has only been possible with extremely sleek, heavily modified airframes characterized by very low drag, as exemplified in *Figure A 2*. These airplanes are meticulously optimized for efficient high-speed cruising. Designing a proprotor that can perform effectively in both hover and cruise flight would inevitably compromise efficiency in either mode or both. Furthermore, cargo airplanes often have larger flat plate areas, contributed from lower fineness ratios due to cargo size constraints. Additionally, cargo doors or ramps may require further design adjustments that hinders aerodynamic efficiency.

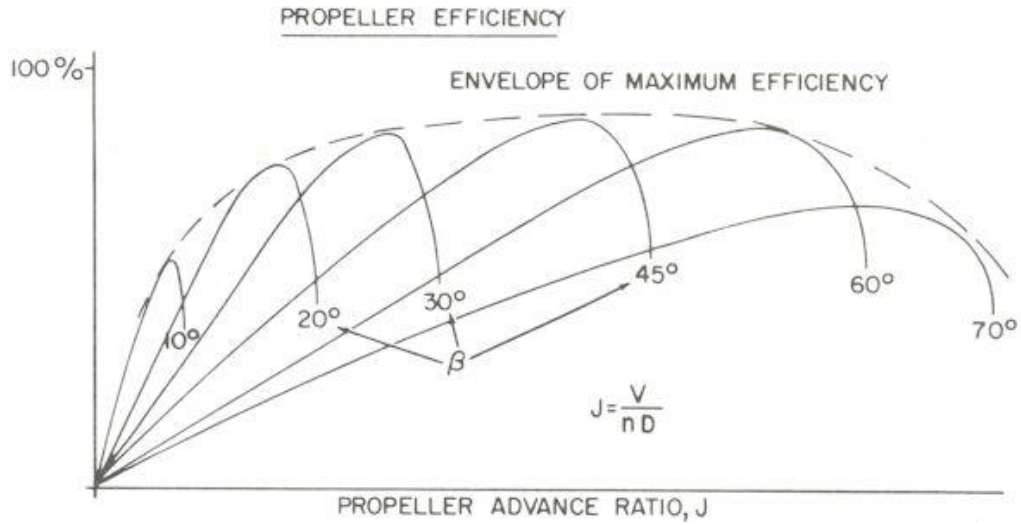


Figure 2.7 Typical propeller efficiency with specified pitch [31].

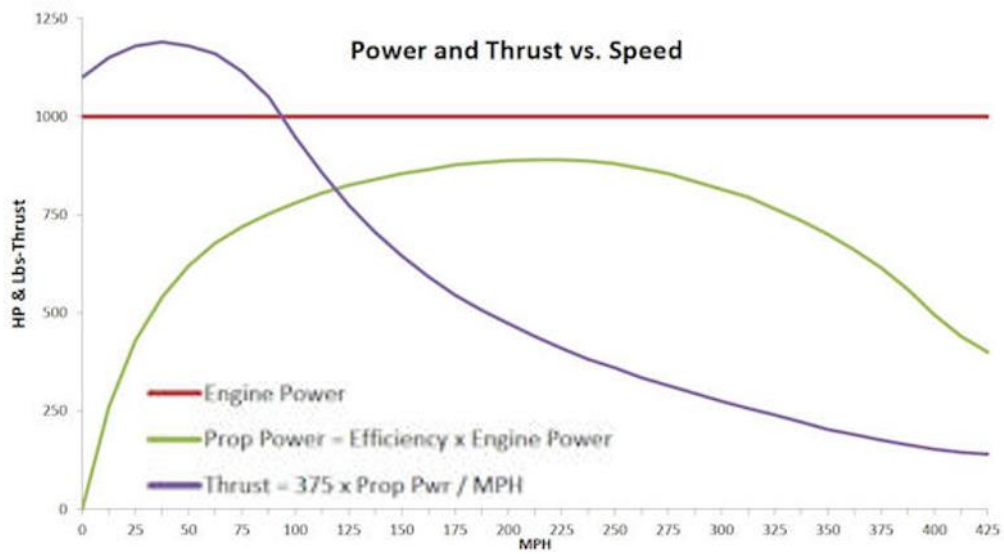


Figure 2.8 Propeller thrust trend over a range of speed with constant power [31].

The above findings are corroborated once more in [32], as illustrated in Figure 2.9, with the addition of a red line signifying the minimum required airspeed. Historically, no tiltrotor or tiltwing VTOL cargo concept has demonstrated the capability to cruise at speeds exceeding 450 knots. The plot illustrates that both the Lift fan and Stowed rotor configurations have the potential

to achieve speeds comparable to those of conventional jet transports. However, as previously discussed, it's important to note that these configurations may not be suitable for cargo lifting purposes. The visual representations of these configurations can be found in the VTOL wheel [33], and are visually presented in Figure A 1.

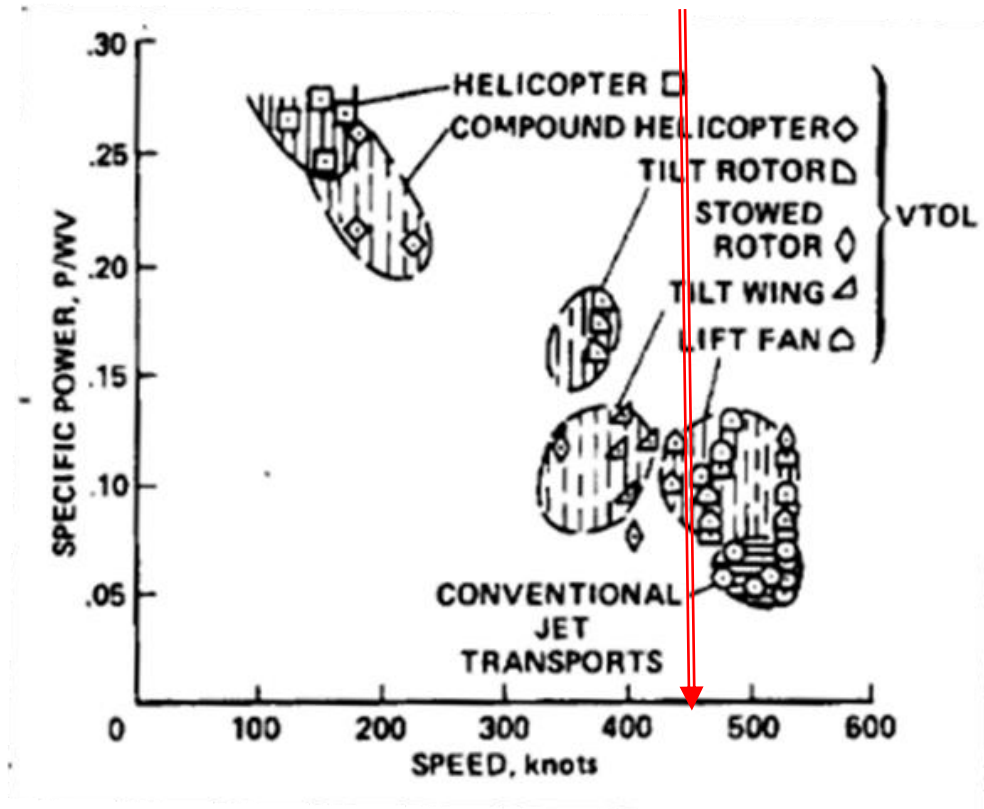


Figure 2.9 Power requirements and cruise-speed of various aircraft types [32].

The initial review of historical data played a pivotal role in the elimination of concepts with a lower probability of success. This step bears significant importance, as highlighted in Figure 1.5, not all configurations submitted for the competition can undergo in-depth analysis, primarily due to time constraints. During this review, it was observed that a channeled wing concept had also progressed to the initial round. However, upon closer examination, as detailed in [34], it became

evident that while this concept offered notable increases in payload capacity with limited ground roll, its technological differences from a tilt-wing VTOL configuration were not substantial assuming the wings were hinged. As a result, this concept was excluded from consideration in this HSVTOL study.

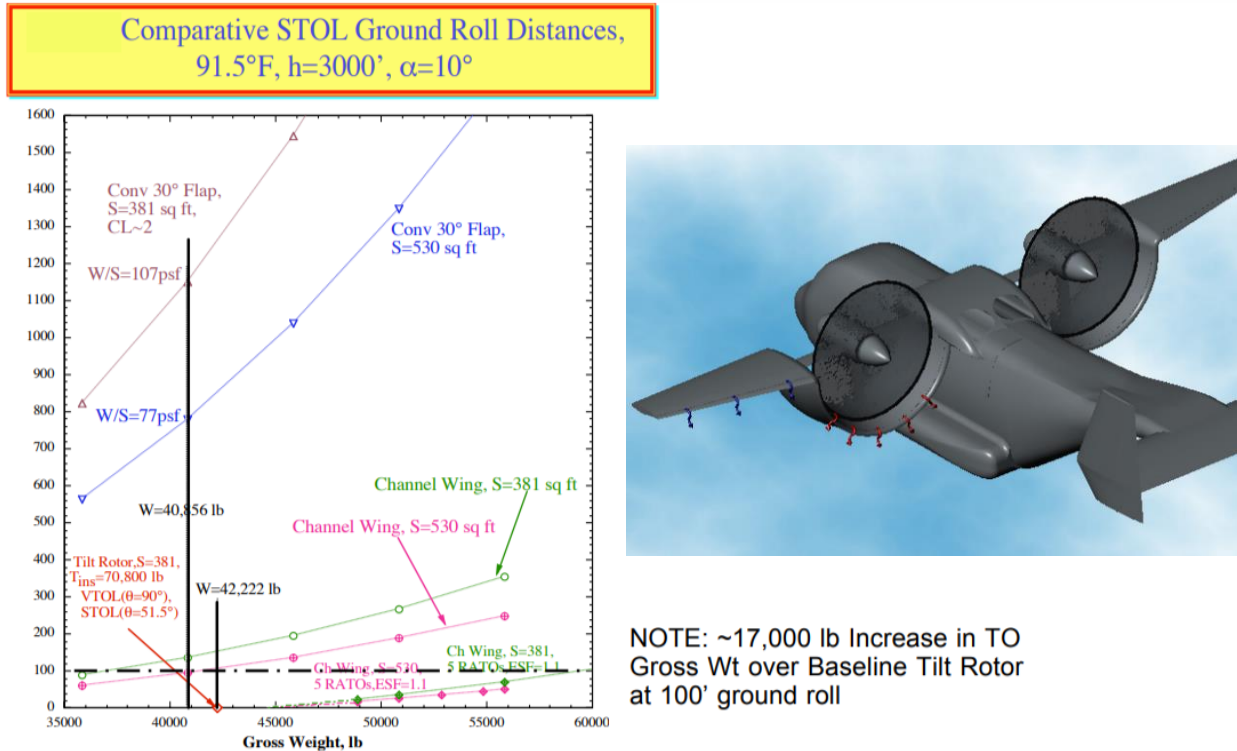


Figure 2.10 Pneumatic channel wing predicted Super-STOL takeoff performance [34].

2.2 Concept Selection

The selection of an aircraft configuration for further exploration in this study is a critical step. While recognizing that both lift fans and stowed rotors may achieve the target speed, the high disk loading and increased power consumption of lift fans may not be suitable for freighter applications. Additionally, the stowed rotor concept is yet to be realized in practical applications. While innovation in configuration is imperative, one viable approach is to build upon proven designs.

Table A 2 provides a compilation of existing VTOL aircraft and rotorcraft for reference. A comprehensive comparison of these designs, considering all essential performance aspects and comparing them with HSVTOL design requirements, expedites the identification of configurations that better align with the primary mission of HSVTOL. Figure 2.11 presented below scale the parameters relative to HSVTOL requirements, denoted by the red dotted line at a value of one across all fronts. This radar charts showcases one representative design of each type, with the MV-22 demonstrating a close alignment with the specified requirements.

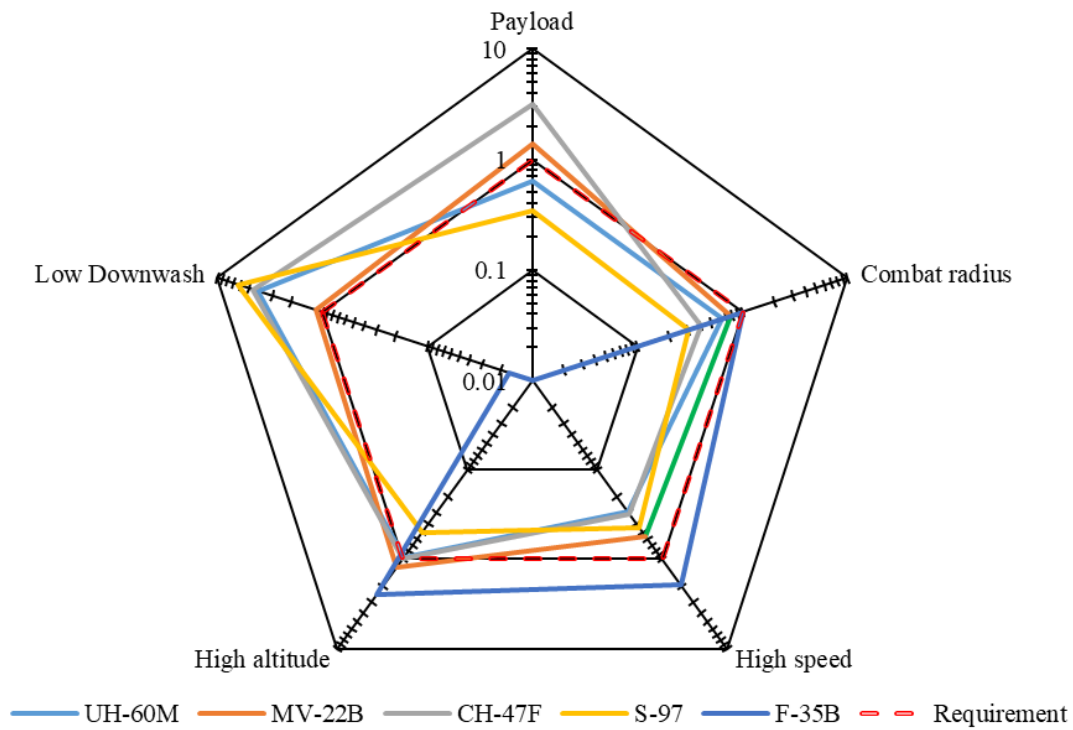


Figure 2.11 Radar plot of representing designs' performance WRT requirements.

The review of existing aircraft reveals that current tiltrotors surpass the requirements in several key aspects, with the primary deficiency being speed. It's worth noting that Figure 2.11 is in logarithmic scale, and Figure 2.12 highlights the MV-22B and the newer generation of tiltrotors, V-280, comparing them to the primary mission requirements of HSVTOL.

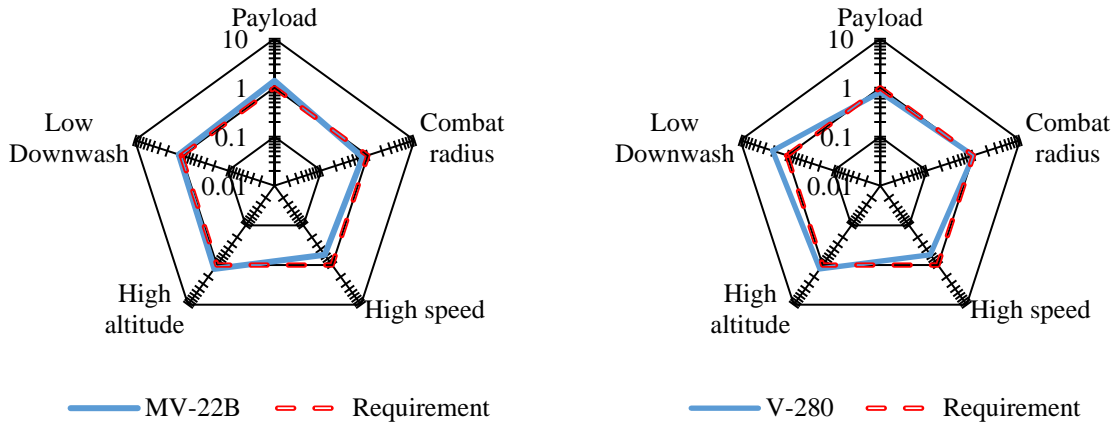


Figure 2.12 Radar plot of tiltrotor VTOL performance WRT HSVTOL requirements.

This finding is supported by the design matrix completed for the VFS HSVTOL student design competition, as presented in Table 2.2, with visual representations provided in Figure 2.13. This aligns with the design approach of Bell HSTOL, which incorporates rotors that fold after pylon tilting to achieve the desired performance characteristics, shown in Figure 2.14.

Table 2.2 HSVTOL decision matrix.

Decision Variables	Weight (1-5)	Tilt Rotor	Tilt Nacelle	Tilt Wing	Vecored Thrust	Fan in Wing	Stop-Rotor	Fold-Rotor	Stow-Rotor
Low Cruise Drag	5	1	8	5	10	9	4	7	6
Low Downwash	5	7	3	5	1	4	8	10	9
Hover Survivability	4	7	2	4	1	3	10	8	9
Cruise Survivability	3	2	6	3	9	10	1	8	7
Hover Maneuverability	2	7	3	5	1	4	9	10	8
Level of Noise	1	5	2	4	1	3	10	7	9
Transition Complexity	4	10	3	4	5	6	8	7	1
Not Susceptible to FOD	5	10	2	6	1	3	8	9	7
Structure Complexity	2	8	7	5	10	4	9	3	1
Transmission Complexity	4	2	9	10	8	1	6	3	1
Ease of Manufacturing	1	4	5	6	7	2	10	3	1
Payload Capability	5	9	2	5	1	3	8	10	6
Technology Readiness	3	10	4	8	9	5	3	2	1
Total Score		286	188	240	205	201	304	318	236

[Note: Configuration with higher score is more favorable.]

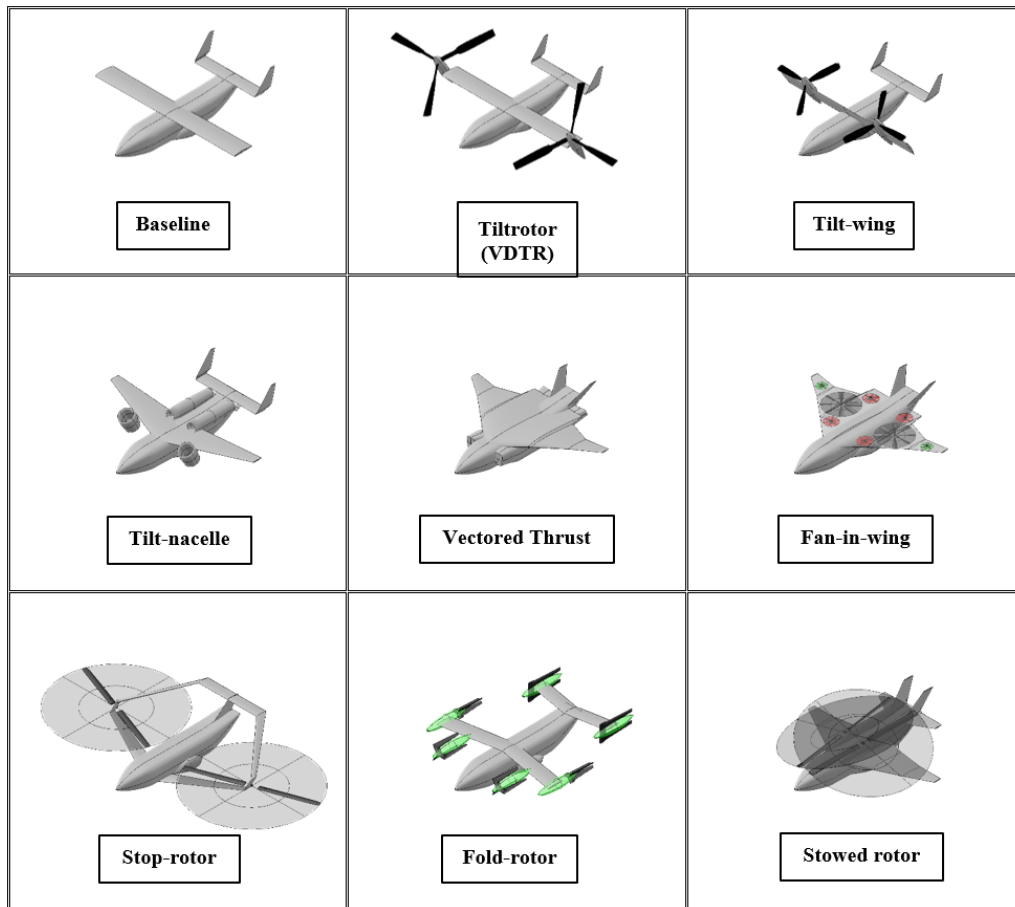


Figure 2.13 Visual representation of considered concepts.



Figure 2.14 Rendering of Bell HSVTOL concepts (Retrieved from [35]).

The Bell HSVTOL designs with novel rotor design introduces unique problems. The technologies required, and the difficulties will be discussed in the following sections.

2.3 Folding Rotor

The most prominent and visible distinction between the Bell HSVTOL and traditional tiltrotors is the folding of the rotors during level flight. Designing such a rotor system proves to be considerably more complex than the already challenging rotorhead designs. However, upon further examination, it is surprising to discover that testing on tilt-fold rotors was conducted as far back as the 1970s, as depicted in Figure 2.15. One notable issue highlighted in the research is the flapping instability of the blades during the stowing process. Nevertheless, this problem can be effectively addressed by providing sufficient constraints before stowing the rotors. It is also suggested that employing stiff blades can serve to restrict flapping freedom [36]. Additional tests are currently underway, with Bell having delivered their test stand to Holloman Air Force Base for the purpose of conducting demonstrations and technology evaluations in 2023, see Figure 2.16.

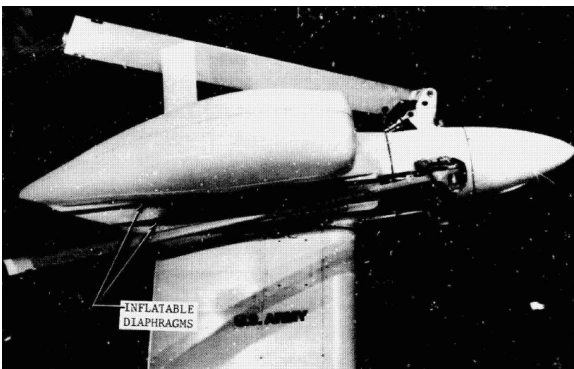


Figure 2.15 Model 627 folding proprotor pod with fold stow slots [36].

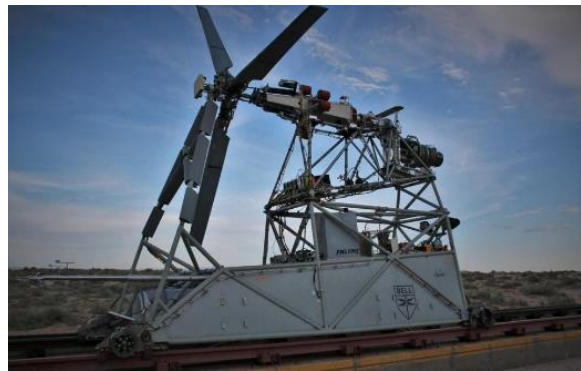


Figure 2.16 Bell's HSVTOL test article is at Holloman Air Force Base [37].

2.4 Convertible Engines

Another noteworthy challenge within this design lies in the implementation of the thrust-shaft convertible engine, which is atypical in the context of most airframes that are traditionally designed with a propulsion device covering the entire flight envelope. The installation of a convertible

design significantly amplifies complexity, increases costs, and reduces the payload fraction. However, it's important to emphasize that such a system becomes essential for HSVTOL cargo concepts with decoupled means of propulsion in hover and cruise. Extensive studies have been conducted in this regard. For instance, engines featuring Variable Inlet Guide Vanes (VIGV) were tested in the 1980s, and the experimental data can be found in [38], [39], and [40]. Furthermore, General Electric and Allison presented several concepts in the late 1980s, as listed in [41]. Managing energy loss and developing effective means to connect/disconnect power transmission in such a system pose significant challenges.

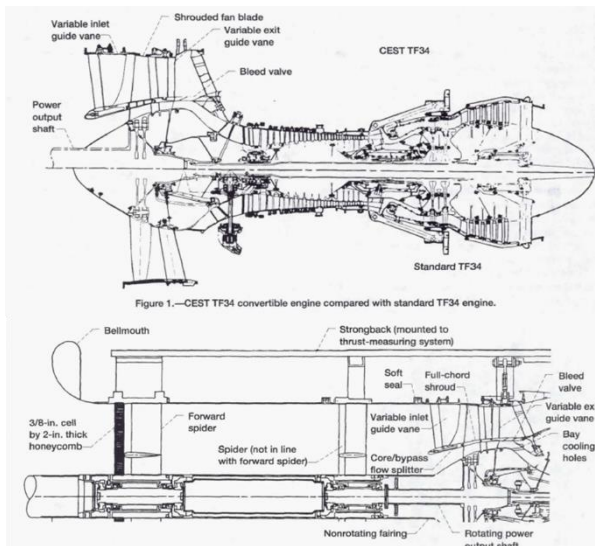


Figure 2.17 Cutaway and performance of TF34 engine with VIGV [39].

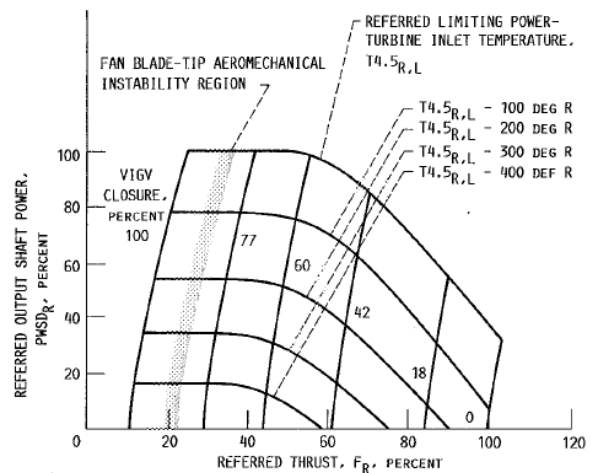


FIGURE 8. - SEA-LEVEL-STATIC PERFORMANCE OF CEST TF34 ENGINE. REFERRED FAN SPEED, N_{FR} , 90 PERCENT.

In alignment with the advancements seen in Urban Air Mobility (UAM), convertible engines designed for electricity generation are also gaining prominence. An example of this is the release of the VH-5 large-scale turbo-fan hybrid by Verdego Aero [42], capable of generating up to 1.5 MW of power and seamlessly transitioning between thrust and power-generating modes. This development has opened opportunities for employing electric motors to power lift rotors,

enhancing the flexibility of rotor placement, and reducing the complexity of mechanical transmission systems. However, it's important to note that the weight of electrical transmission components needs to be carefully evaluated in such systems.

2.5 Transmission System

The secure and reliable transfer of power is essential, whether it's from one rotor to another or from the engine to the lift fan. For safety considerations, the rotors of VTOL aircraft are physically connected, even when powered by separate power plants. As depicted in Figure 2.18, "During single engine operation, power is distributed from the remaining engine to both proprotors through the interconnecting drive shaft [43]." Consequently, when it comes to powering rotors using a distributed power source located near the rotor, there is no significant advantage in terms of weight reduction compared to splitting the power of one engine among multiple rotors. However, this approach offers a higher safety margin, which is a critical consideration in aircraft design.

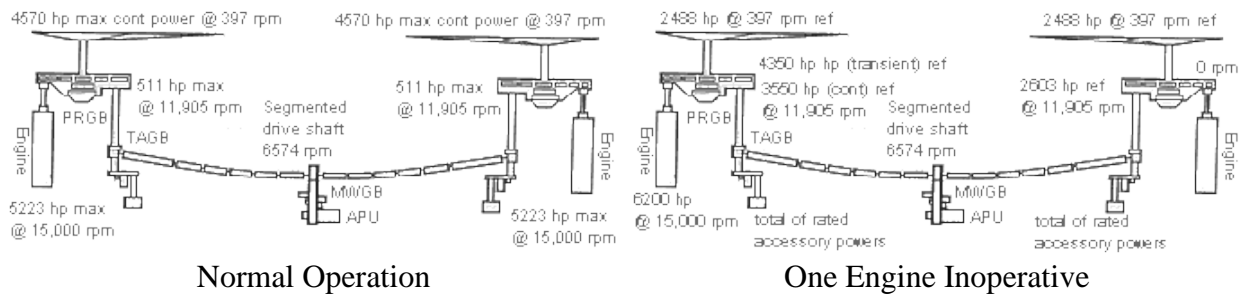


Figure 2.18 Schematics of the V-22 transmission system [43].

One of the notable sources of weight in these systems is the reduction gearbox. Many high-performance rotorcrafts are driven by turboshaft engines, in which a free (power) turbine converts the kinetic energy of the exhaust jet into shaft power. The power turbine operates at extremely high rotational speeds, typically around 23,000 RPM, and must be slowed down to approximately

400-600 RPM, depending on the requirements for rotor tip speed. Achieving this reduction necessitates a complex series of reduction gears, as illustrated in Figure 2.19. The reduction system often involves specially treated materials and advanced manufacturing methods. The reduction gears and their casing endure substantial stress and are typically heavy and bulky. Considerable efforts have been invested in reducing the weight of gear reduction systems, yet the weight of the drive system still exceeds 0.3 lb/hp, see [44, p. 19].

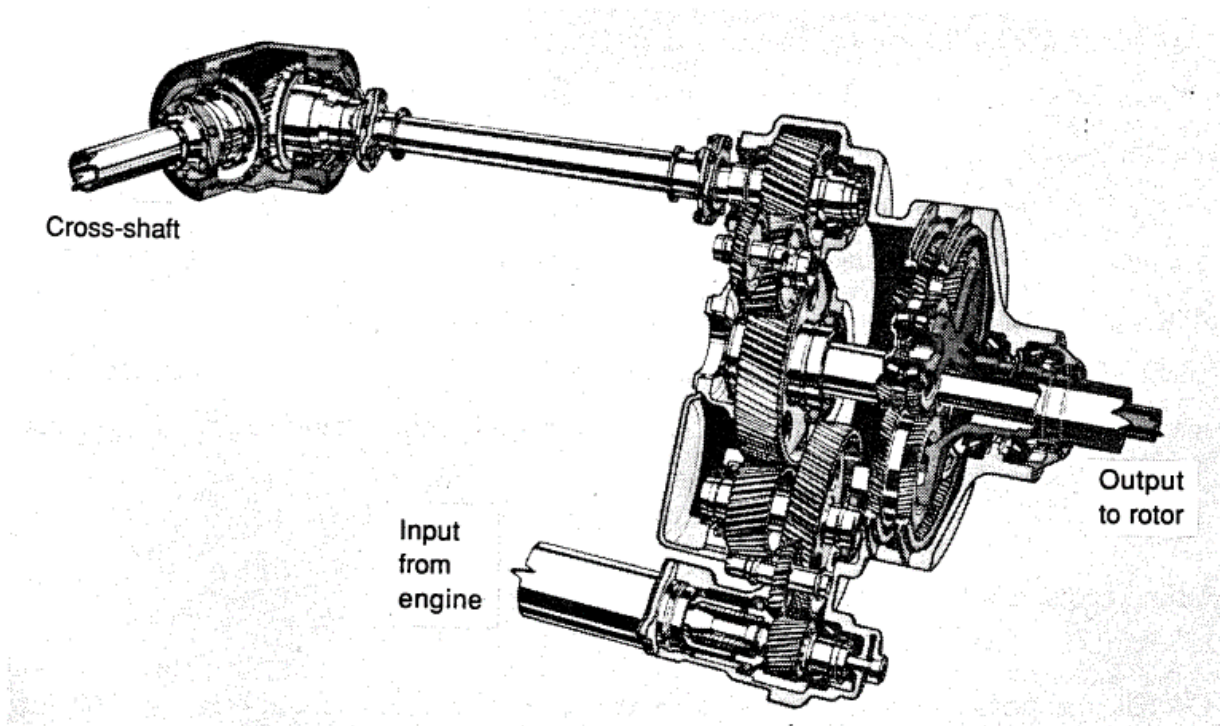


Figure 2.19 Tactical tiltrotor transmission in left nacelle [44].

The complexity of transmission systems for HSVTOL aircraft is notably amplified for tilt-fold HSVTOL configurations. This is primarily due to the engines being positioned farther from the rotors, resulting in additional discrete break points for routing within the airframe while avoiding interference with the cargo area. Placing the engines on the pylon or inside the prop wash stream

tube within the wing, although typical for some designs, can geometrically interfere with the folded blades and expose the engine intake to highly unsteady air. This configuration substantially increases the risk of engine surge or failure during flight. In Figure 2.20, the expected transmission routing for a patented HSVTOL concept with engines located near the empennage is depicted. While not necessarily the final design, it illustrates the complexity inherent in such a system. The inclusion of coupling bevel gears at each break point results in a significant weight penalty, the extent of which is contingent on the transferred torque.

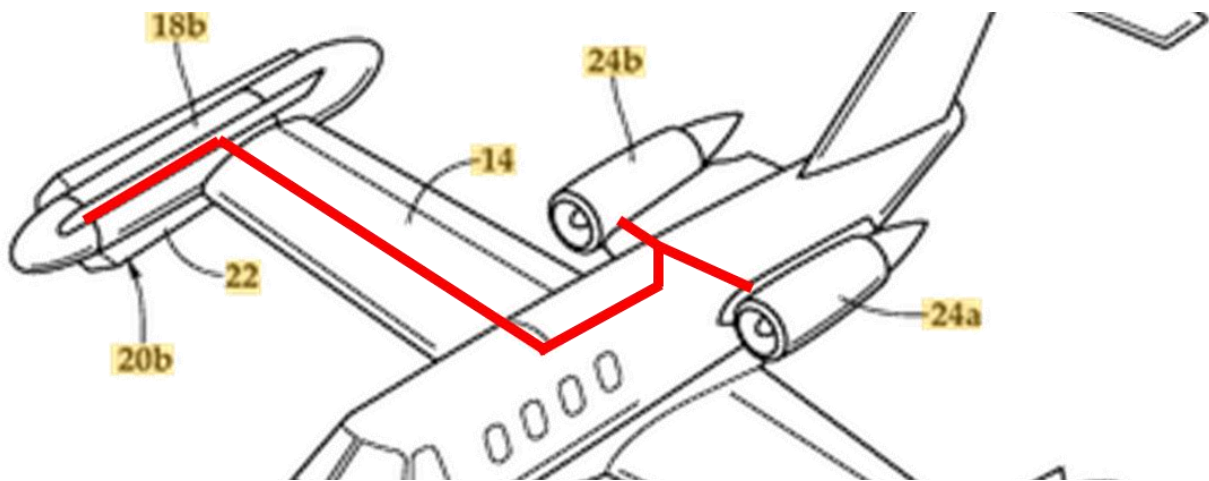


Figure 2.20 Expected route of HSVTOL transmission (Concept from [45]).

Exploring alternative power transmission methods presents an opportunity for reducing the weight of HSVTOL systems. Pneumatic transmission, which was employed in the XV-5A and mainly used in Fan-in-Wing (shown in Figure 2.21) or Tip-Jet configurations like the Canard Rotor Wing (CRW, depicted in Figure 2.22 and Figure 2.23), offers a different approach. However, these systems necessitate the redirection of air to the tips of fans or rotors, as air is highly compressible and not well-suited for applications involving high torque. While increasing the moment arm of the reaction force of air reduces the required pressure, it entails complex piping

either around or within the rotor blade. This approach is not practical for HSVTOL systems with large rotors that require stowing.

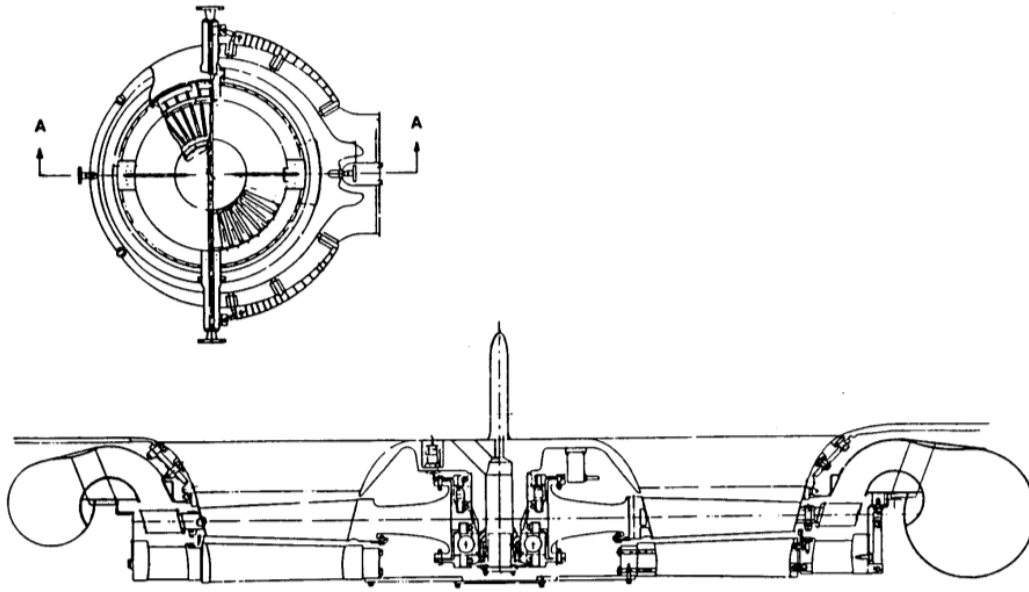


Figure 2.21 Cross section of LF-336 1.3 pressure ratio lift fan [46].

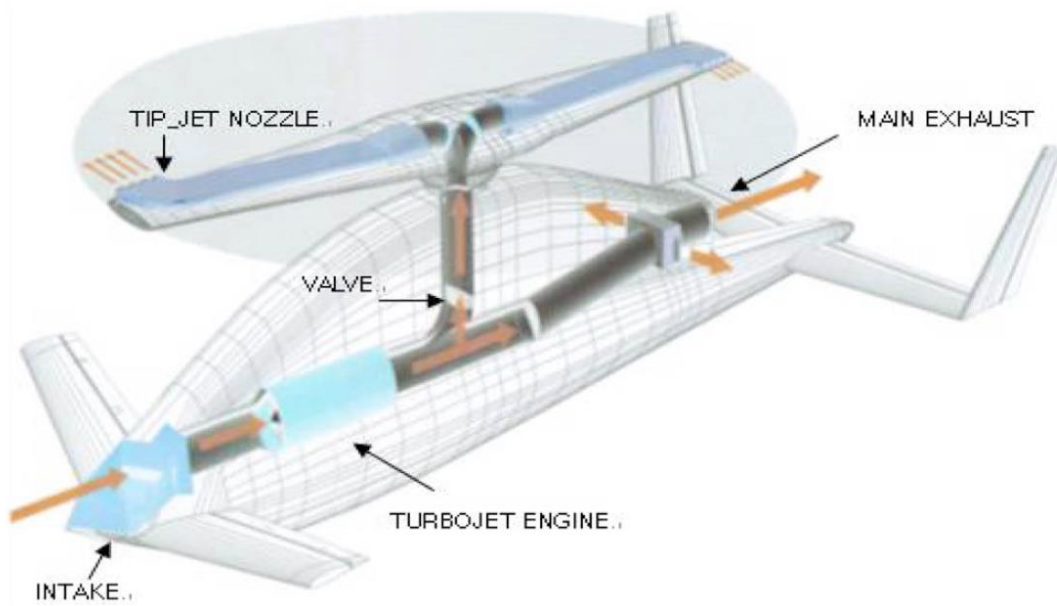


Figure 2.22 Schematic layout of smart UAV propulsion system [47].

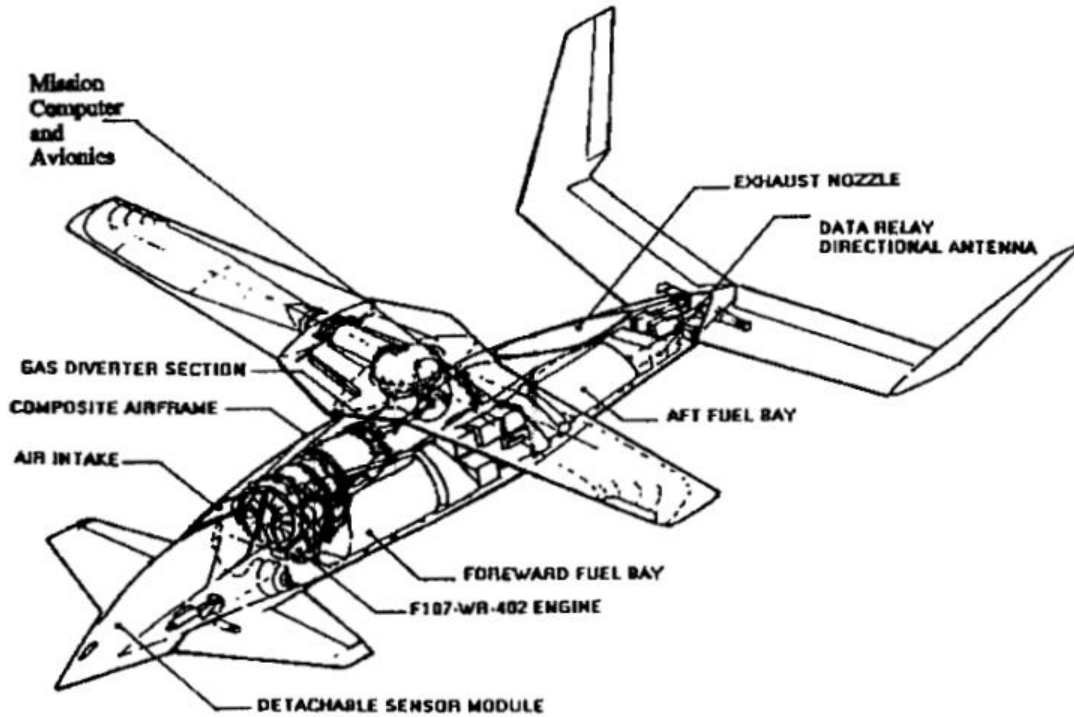


Figure 2.23 Typical CRW in UAV Configuration [48].

Another approach, which is commonly used in heavy machinery, is hydraulic transmission. However, this method is not commonly seen in aircraft in service due to its unnecessary weight for conventional aircraft. Research has been conducted on using fluid under high pressure to transmit power, but resources on this subject are extremely limited. One of the primary sources of information on hydrostatic transmission is based on the UH-1 as a baseline, as shown in Figure 2.24. This system utilizes advanced hydraulic fluid and operates under high pressure with low flow speed to minimize friction losses. It's noteworthy that this design was tested in 1967, and no follow-up studies have been found in the public domain. A more recent study, depicted in Figure 2.25, was conducted by researchers at Purdue University. The rendering of a quadcopter test vehicle shows one main motor powered by ground power, driving four pumps leading to four hydraulic motors. However, no released paper has been located on this subject.

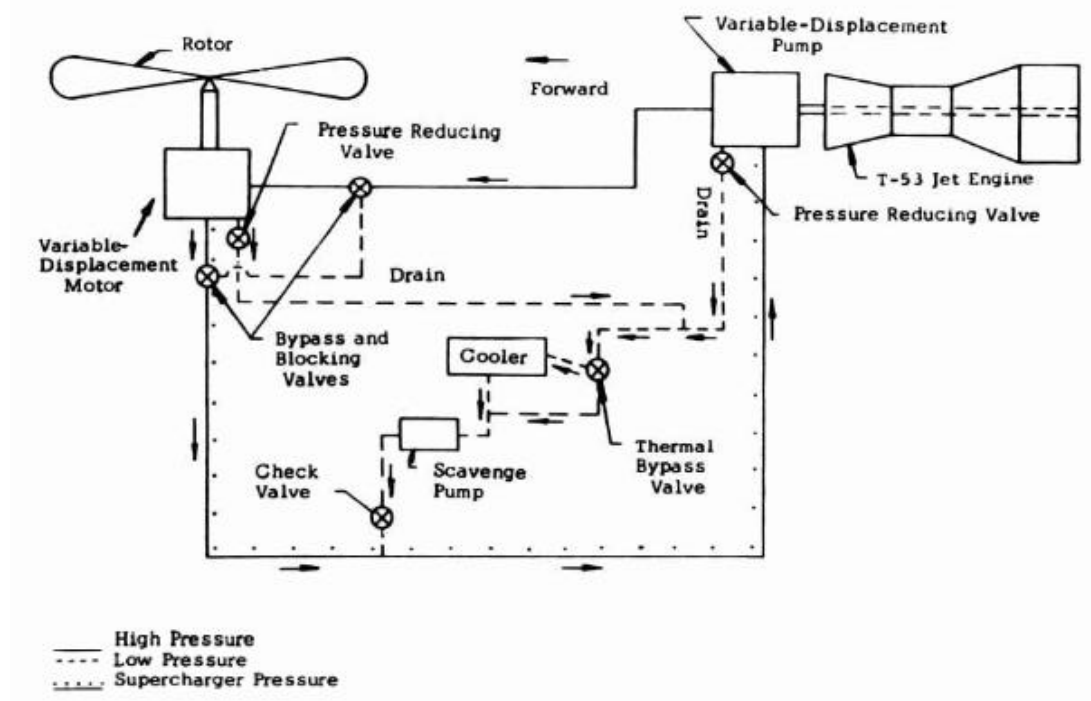


Figure 2.24 Schematic of Bell UH-1/T-53 Hydraulic Transmission System [49].

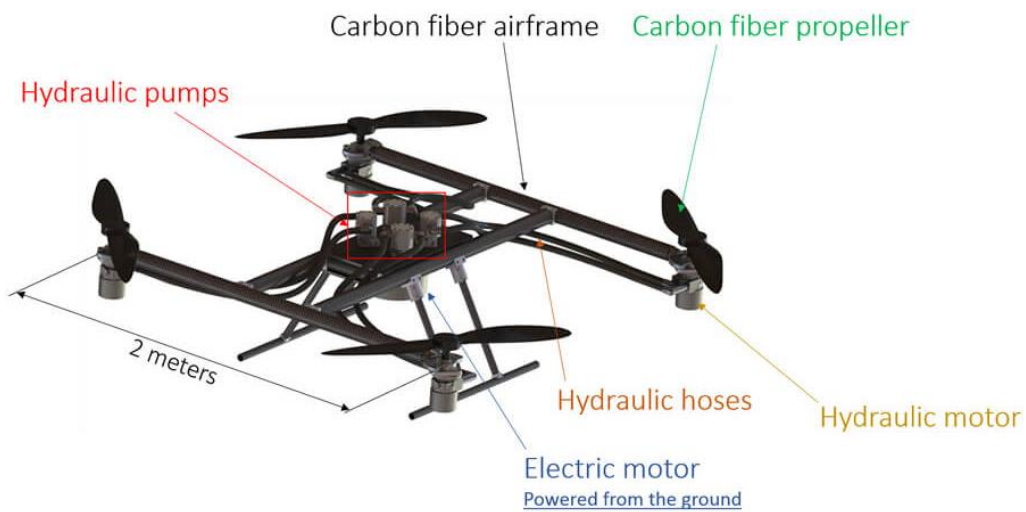


Figure 2.25 Quadcopter uses fluid for power transmission [50].

Hydrostatic transmission offers the advantage of flexible rotor placement and the potential to eliminate the need for a reduction gearbox. In one study [34], a turbine-speed hydraulic pump was

used, operating at 23,000 RPM and interfacing directly with the engine. While limited data is available on this vane pump depicted in Figure 2.26, it can operate at pressures ranging from 2,000 to 8,000 psi [51]. More information can be found in reference [52].

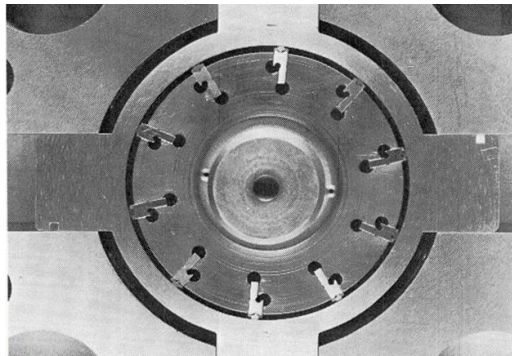


Figure 2.26 End view of turbine speed pump [51].

Publicly available research on high-power electrical transmission systems can be found in studies related to Single-aisle Turboelectric Aircraft with an Aft Boundary Layer (STARC-ABL) [53]. This concept employs under-wing engines to generate electricity, which is then used to power the electric Aft-Propulsor, reducing boundary layer thickness around the fuselage, as illustrated in Figure 2.27.

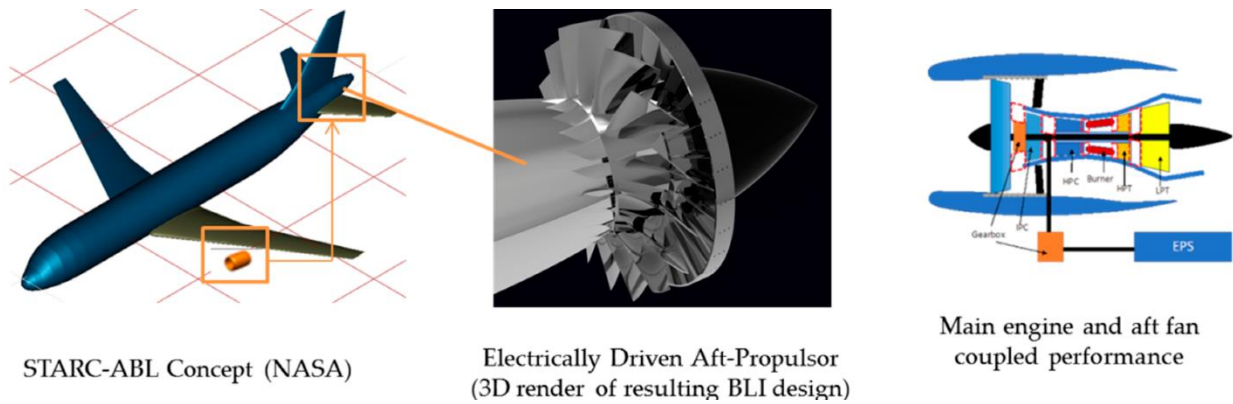


Figure 2.27 ABL concept [53](left), BLI (center) and engine layout (right) [54].

The weight of electrical transmission components was initially determined based on the specifications outlined in Table 5 of [53]. However, it's worth noting that in Section 3.4, a more detailed discussion will be provided, as certain components had to be resized using historical data from other sources. The preliminary estimation from [53] indicated that some components were significantly oversized for the specific requirements of HSVTOL.

2.6 Hypothesis

The focus of this study emerged from an examination of challenges outlined in sections 2.3 to 2.5. A survey of these challenges and existing solutions reveals that solutions have been under investigation for decades, with technology improvements progressing steadily, though marginally. While concepts such as folding rotors and convertible engines have seen limited advancements, the field of eVTOL has sparked novel approaches to power transmission. This study centers on the power transmission system of High-Speed Vertical Takeoff and Landing (HSVTOL), covering components responsible for converting energy for transmission and the mechanisms involved in transporting this energy across the airframe.

As illustrated in Figure 2.28, the weight of three major transmission systems is estimated. The widely used mechanical transmission employing gears and drive shafts serves as the baseline, while hydrostatic and turboelectric transmission components are sized to explore the impact of employing transmission lines with greater motor placement flexibility. The research suggests a potential parity in weight between hydraulic and electric transmission systems compared to traditional mechanical transmission in HSVTOL aircraft. This is achieved through the reduction of weight in components like reduction gearboxes and intermediate gearboxes, especially when the transmission line necessitates segmentation due to geometric constraints. Anticipating variations in the weight fraction of the transmission system with changes in total weight, the study

hypothesizes that the choice of the lightest transmission system will be depending upon the specific takeoff weight for different HSVTOL concepts.

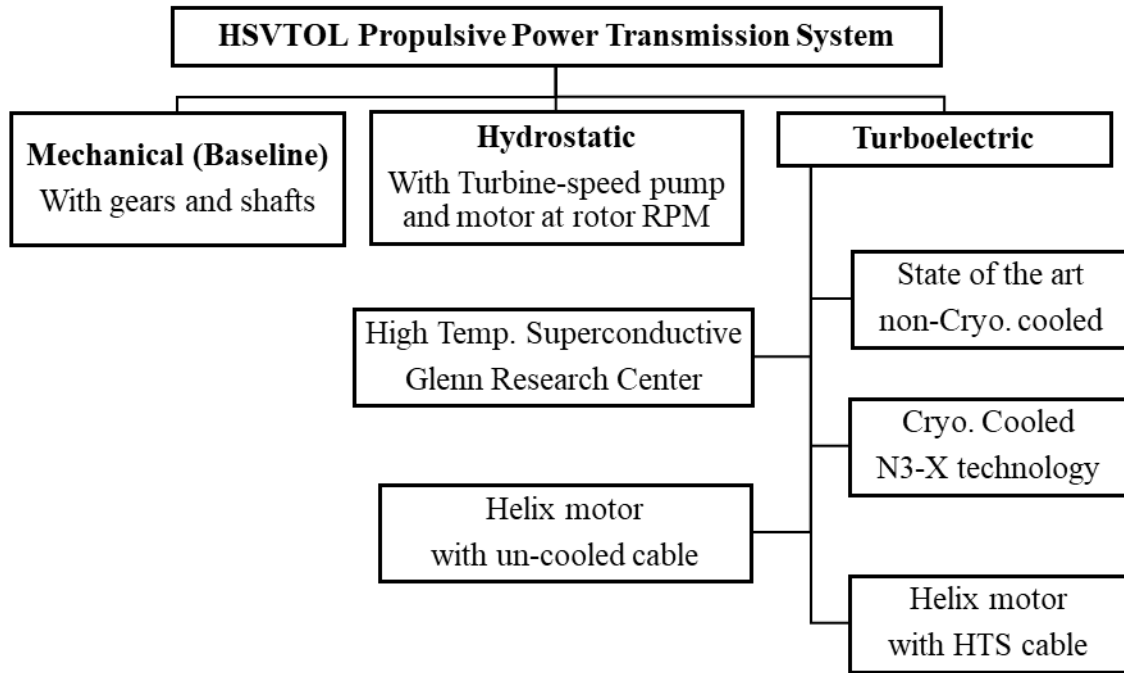


Figure 2.28 Concepts explored in this study.

3 Methodology

This section outlines the theoretical sizing of transmission components. The rationale and procedures for this research is clarified in Section 3.1, while methods for acquiring the design requirements are elaborated in Section 3.2 (Design Constraints). Further in-depth discussions on the sizing process are provided in Section 3.3 for hydraulic transmission and Section 3.4 for electric transmission.

3.1 Research Approach

The research process encompasses several key steps, including the development of hydraulic system concepts, the estimation of weight and means for weight reduction, comparisons between different transmission types at varying TRL, and drawing conclusions based on the findings. The transmission design and sizing stages are an integral part of the preliminary design process for HSVTOL components, as illustrated in Appendix Figure A 3. To estimate and compare the weight of transmission systems, equivalents to the mechanical transmission are devised for the same power output, and component weights are estimated through theoretical calculations rooted in historical data. The initial step involves compiling data on equipment used in [49] and [54], and categorizing them as counterparts to traditional mechanical systems, as depicted in Table 3.1.

Table 3.1 Counterparts of the traditional mechanical transmission systems.

Baseline Systems (Mechanical)	Hydraulic system counterpart	Electric system counterpart
Reduction gearbox	Main hydrostatic pump	Main electric generator
Transmission	Rotor hydrostatic motors	Motor electric motors
Transmission Sup.	Hydraulic Sup.	TMS
Connecting shafts, pillow blocks, freewheeling, and articulating drive	Connecting piping	Connecting cables
Oil cooling system	Oil cooling system	Oil cooling system
Oil cooling and lube pump	Scavenge pump	Oil cooling and lube pump

This study does not aim to optimize a specific design but rather focuses on the development of a collectively applicable method for estimating transmission weight across a range of power output scenarios. The primary objective is to facilitate the iterative weight estimation process within HSVTOL design. When different transmission types are employed, the aircraft's empty weight changes, while the MTOW remains constant, as the power output is unaffected. It consequently influences payload capacity, and a redesign may be required. To establish this method, the study employs the 30-passenger tilt-fold (30-TF) concept outlined in "*Technology needs for high-speed rotorcraft (3)*" [13] as the initial point and baseline design for transmission system weight estimation. Once the method is established, it is extended to concepts with varying takeoff weights, and the weights of different transmission systems are compared to the traditional mechanical system to observe trends in weight variances concerning power output.

3.2 Design Constraints

A baseline design is required for the sizing of transmission system. Although it is common for designers to use weight fraction of systems in the preliminary design phase, the historical data for novel airplane configuration and new systems are not present. The weight estimation for hydrostatic and electric transmission systems requires one or more parameters that scale with the airplane size and closely relates to the power transferred. In this case, the transmission system transfer power only when the aircraft is in rotorcraft configuration, the MTOW and several geometric parameters are required for a good estimation of the maximum continuous power required.

For this study, an existing airframe concept is selected to be modified. The gross weight of airframe is untouched at the initial stage, assuming similar structural or space constraints apply to all transmission systems, with no major change in airframe structure. Similar approach is seen in

“*Propulsion System Considerations for the Subsonic V/STOL*” [55], where number of engines are varied with basic airframe stays the same, because “for a first-order analysis typical of pre-design studies, it is possible to utilize the same basic aircraft configuration.” The 30-TF concept in NASA report [13] is selected because the mission lines up very well with the new design requirements, as explained in Section 2.2 above. For gross weight of 53,563 lbs [13], the hover thrust can be estimated assuming roto disk normal to gravity and wind calm. To use the modified momentum theorem in [30, p. 69], C_T can be obtained using (3.1) below:

$$C_T = \frac{T}{\rho \cdot A_R \cdot (\Omega \cdot R)^2} \quad (3.1)$$

Where T is thrust of each rotor, ρ is density at sea level, area A_R is 1385 ft² calculated from rotor diameter [13, p. 7], $\Omega \cdot R$ is equivalent to helicopter mode tip speed of 780 ft/s from [13, p. 21]. For further analysis, the working condition of the rotor is calculated. This design has hover tip Mach number around 0.7, rotor rotating at 354.7 RPM, and disk loading around 20 psf, representing a typical rotor. Where induced losses factor κ ranges above 1.0 (ideal) and below 1.15, and C_{D0} around 0.01 [30, p. 69]. Solidity of rotor is 0.141 given in [13, p. 8]. Power coefficient is calculated using (3.2) below:

$$C_P = C_{P_i} + C_{P_o} = \frac{\kappa \cdot C_T^{\frac{3}{2}}}{\sqrt{2}} + \frac{\sigma \cdot C_{D0}}{8} \quad (3.2)$$

Considering the paper [13] was completed in year 1991, the induced loss was be adjusted to account for improvement in rotor design. Data of an UAM concept powered by turboshaft engines is listed in [56, p. 12] with FM between 0.81-0.82, with equation given below:

$$FM = \frac{C_{P_{ideal}}}{C_P} \quad (3.3)$$

$$C_{P_{ideal}} = \frac{C_T^{\frac{3}{2}}}{\sqrt{2}} \quad (3.4)$$

By plugging in κ value of 1.075, FM of 0.809 is obtained. Now to calculate the power in hover, insert C_P value into the following equation derived from the power coefficient equation:

$$P = \frac{C_P \cdot \rho \cdot A_R \cdot (\Omega \cdot R)^3}{550} = T \cdot \sqrt{\frac{DL}{2 \times \rho}} \quad (3.5)$$

The constant 550 in (3.5) converts the value from $lbf \cdot ft/s$ to hp. For the baseline aircraft, at least 4123.04 hp of power is required to hover under MTOW. For the 30-TF concept, 10.2% of thrust is consumed by download generated by the wings, assume the continuous power can be 1.15 times the rotor-only hover power. For sizing, each main rotor requires 4741.5 hp of continuous power when first takeoff and hover under MTOW. This value is used as the baseline power so that the transmission system weight using hydraulics or electric can be compared to the traditional mechanical system.

3.3 Hydrostatic Transmission Sizing Methodology

In aircraft, hydraulic systems are primarily designed for actuating control surfaces and landing gear. While the use of hydraulics for power transmission is a common practice in heavy equipment, its application in aircraft remains relatively innovative. In most cases, hydraulic transmission may not be the optimal choice for aircraft, as it introduces unnecessary weight and complexity when applied to fans and propellers located near the powerplant. However, by utilizing pump and motors operating at the engine and rotor rotation speeds, the weight of a reduction gearbox can be eliminated.

The transmission system's components are arranged as illustrated in Figure 3.1. It is assumed that one primary pump per engine is responsible for driving all the motors through high-pressure

lines. As energy is extracted by the motor, pressure in the system is released, and the returning line maintains low pressure just sufficient to propel the fluid through the pipes. Notably, engine cooling is managed using hydraulic fluid in “*Investigation of Hydraulic Power Transmission Systems For V/STOL Aircraft*” [49], eliminating the need for an oil system and further reducing weight. For this reason, a portion of the returning fluid is diverted to a scavenge pump, which supplies the fluid to the cooling system. The system is assumed to operate at 8,000 psi, which is the highest rated power for the turbine-speed pump. Given that the actuators are powered by the same system, it's observed that the actuator weight is minimized when operates at 8,000 psi, see Figure 3.2.

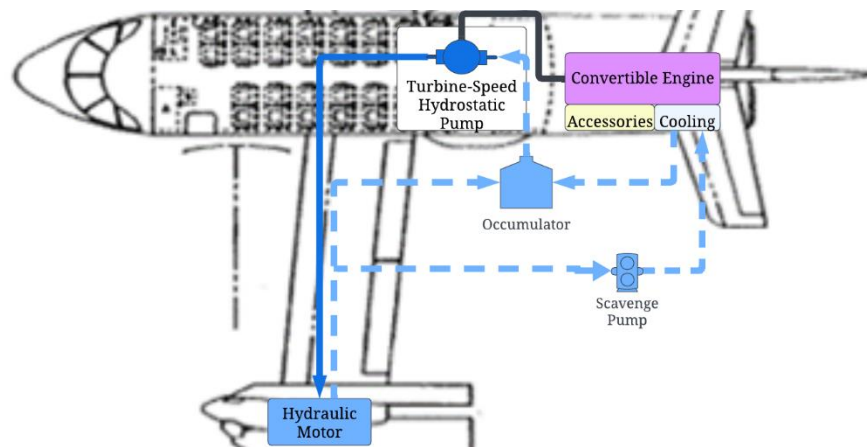


Figure 3.1 Hydrostatic transmission system components layout.

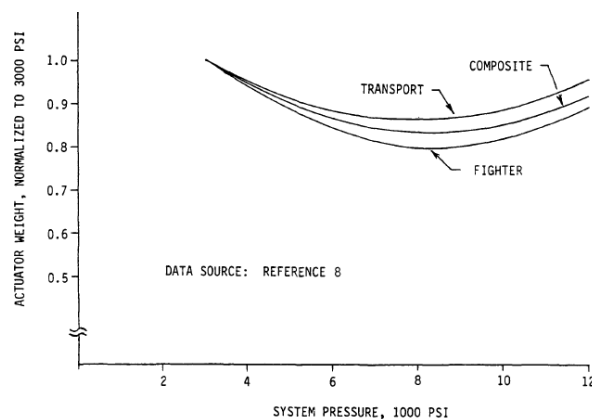


Figure 3.2 Actuator weight vs. input pressure [57].

Utilizing the highest-pressure setting aims to minimize friction losses within the hydraulic pipes, a fundamental principle of hydrostatic transmission. Operating at higher pressure allows the system to deliver the same power while requiring a lower flow rate, a topic that will be examined more thoroughly in this section. Importantly, a significant conclusion from [57] emphasizes "*Don't add weight to save energy,*" and this serves as an essential guideline for the present study.

3.3.1 Hydrostatic Pump Sizing

The process of estimating motor weight began with the collection of off-the-shelf (OTS) motor data readily available in the public domain. The collected data primarily focused on crucial parameters related to rated power, such as displacement and volumetric flow rate. All the gathered data is systematically tabulated and can be found in Table B 1. The power required to drive the pump is calculated employing a standard guideline (3.6), where P is in horsepower.

$$GPM \times PSI \times 0.007 = P \quad (3.6) [58]$$

This relationship demonstrates a linear connection between volume flow rate, pressure, and power. The constant 0.0007 in the provided equation likely incorporates a correction factor, and it would be 0.0006 in the absence of any losses, as indicated in (3.7).

$$\left[GPM \cdot \frac{1}{7.48} \left(\frac{ft^3}{gal} \right) \cdot \frac{1}{60} \left(\frac{min}{sec} \right) \right] \times \left[PSI \cdot 144 \left(\frac{in^2}{ft^2} \right) \right] \times \frac{1}{550} \left(\frac{hp}{lb \cdot \frac{ft}{s}} \right) \quad (3.7)$$

$$= GPM \times PSI \times 0.006 = P(hp)$$

Visual representations in the form of curve plots (Figure B 1 to Figure B 4) were generated to depict the relationships between these parameters and power, as well as weight. The primary objective was to identify a curve that best aligns with weight estimation, forming the basis for the power-weight scaling equation. Notably, the flow rate vs. displacement for OTS motors exhibited an excellent power fit, as demonstrated in Figure B1. In this instance, the required power was

calculated, with a linear relationship observed between power and flow rate, as depicted in Appendix Figure B 2. Moreover, both the weight-to-flow rate (Figure B 3) and weight-to-power relationships (Figure B 4) exhibited identical R^2 values with linear fits. Consequently, the power-to-weight scaling curve was selected for the sake of convenience in this study.

However, a limitation of this approach is that OTS pumps are not tailored for aircraft transmission applications, prioritizing weight reduction, which is less crucial in heavy equipment, as implied by its name. Using an OTS pump for aircraft transmission would result in excessive weight. In contrast, the turbine speed pump from [49] offers a notable advantage, reducing weight by a significant 81.0% while delivering the same power under extremely high rotation speed. Shown in Figure 3.3 is the scaling curve illustrating the relationship between turbine speed pump weight and power. This curve is derived under the assumption of following the same trend to the OTS pump, with a consistent percentage reduction in weight.

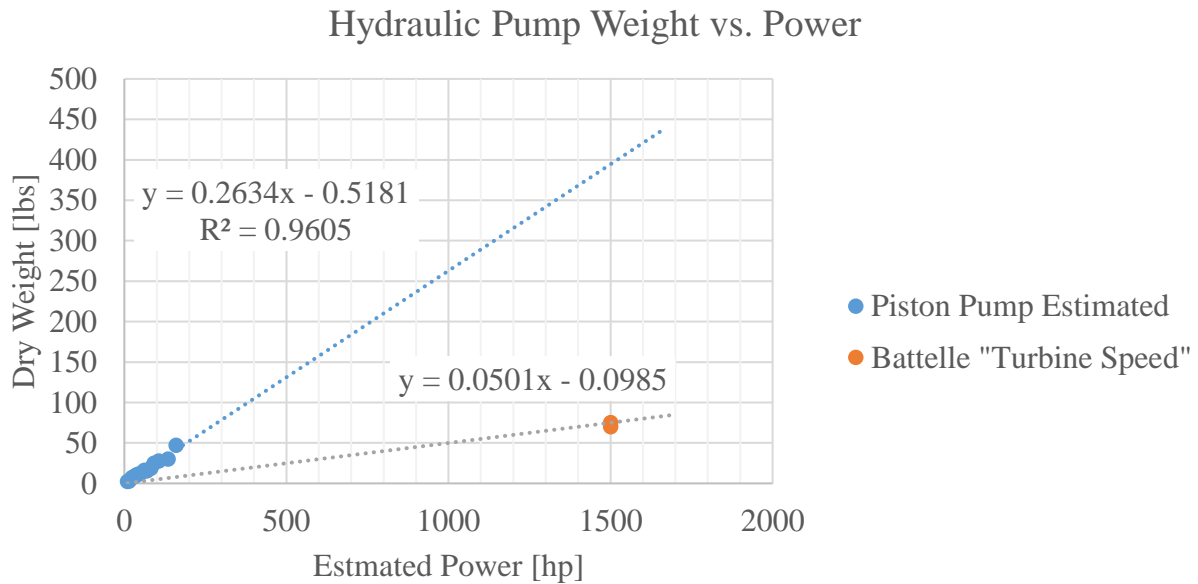


Figure 3.3 Pump weight scaling curve.

3.3.2 Hydraulic Motor Sizing

To establish an empirical equation for scaling hydraulic motors, data on OTS hydraulic motors was systematically collected, and the percentage improvement over existing products was factored in. Unlike hydraulic pumps, hydraulic motor datasheets provide direct information about their power. A comprehensive dataset, available in Appendix Table B 3 to *Table B 2*, covers a range of rated power for these motors. The trends derived from this data, as depicted in Figure B 5, reveal that the weight of hydraulic motors increases exponentially, axis in logarithmic scale. Piston hydraulic motors, widely accessible and highly optimized, operate at low RPM but are known for their exceptional torque production, making them ideal for driving main rotors. Their high torque at low RPM eliminates the necessity for reduction gears, leading to a substantially lighter and simpler design. In [49], a radial piston motor driving the UH-1 main rotor is estimated to be approximately 37.9% lighter than standard axial piston motors. Picture of both axial and radial piston motors are shown below in Figure 3.4, and the weight of OTS hydraulic motors are included in Figure 3.5.

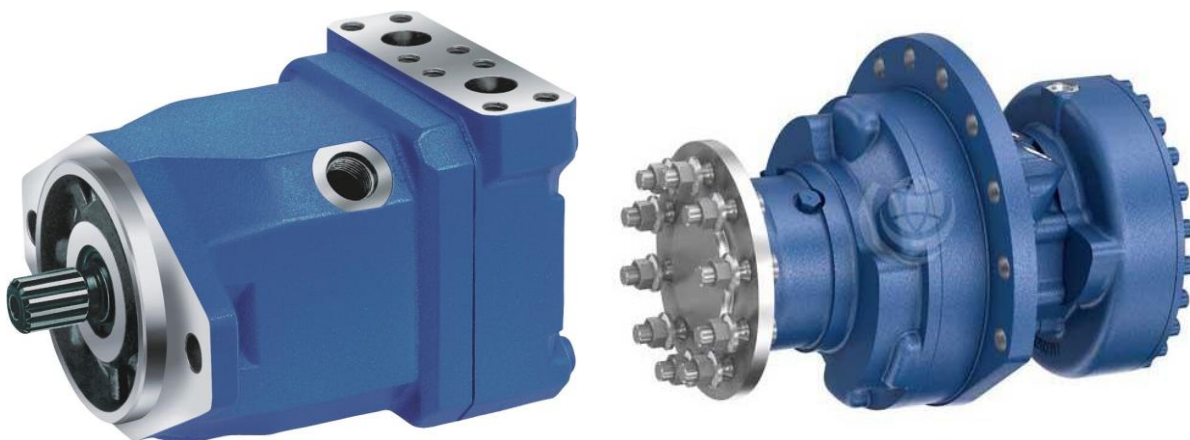


Figure 3.4 Bosch axial piston motor (left) [59], and radial piston motor (right) [60].

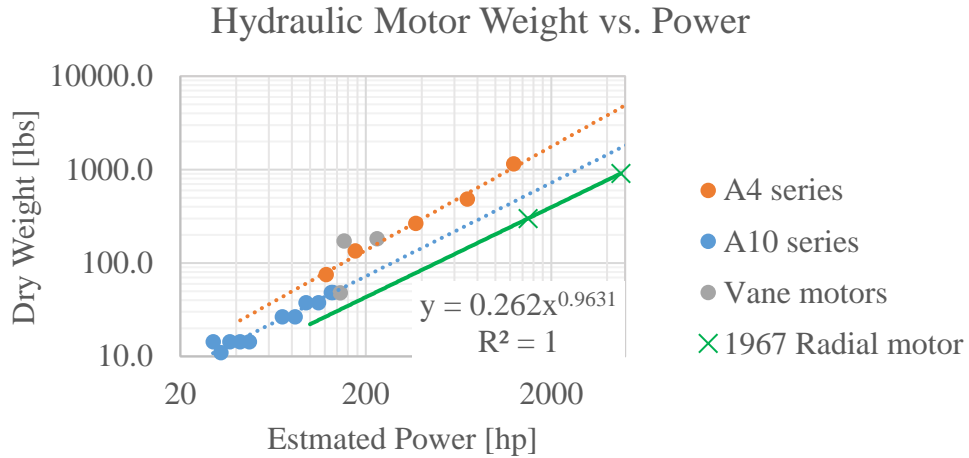


Figure 3.5 The scaling curve for hydraulic motor weight.

To validate the estimated motor weight, a comparison was made by superimposing it on historical data of similar motor types [61]. This comparison revealed a close alignment between the weight and power correlation in historical motors and the estimated weight, affirming its feasibility.

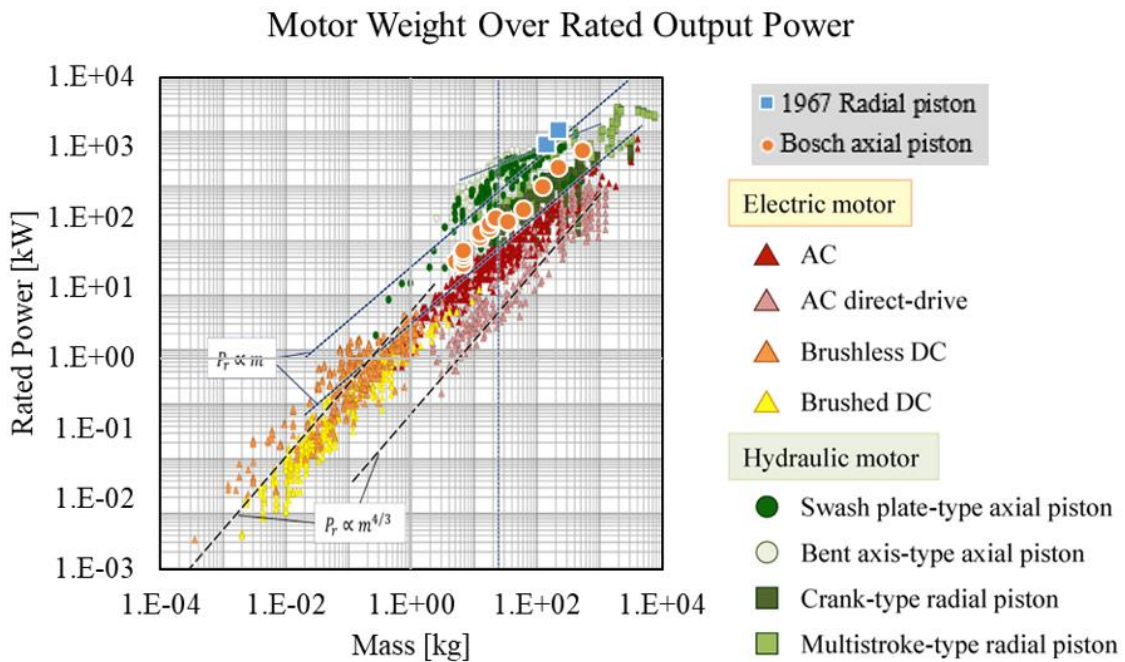


Figure 3.6 Overlaid correlation between weight and rated torque [61].

The data collected was also used in hose sizing in the following section. By plotting the outflow rate from motor against motor power in log scale, a scaling trend is obtained shown in Figure 3.7, the volumetric flow rate increases exponentially with respect to the rated motor power. Assumption needs to be made for the value to be consistent up and down stream of the motor. Specifically, the hydraulic fluid is mostly incompressible or without significant change in density by varying pressure. The experience equation obtained is (3.8), where P is in horsepower.

$$GPM = 1.2276 \cdot P^{0.812} \quad (3.8)$$

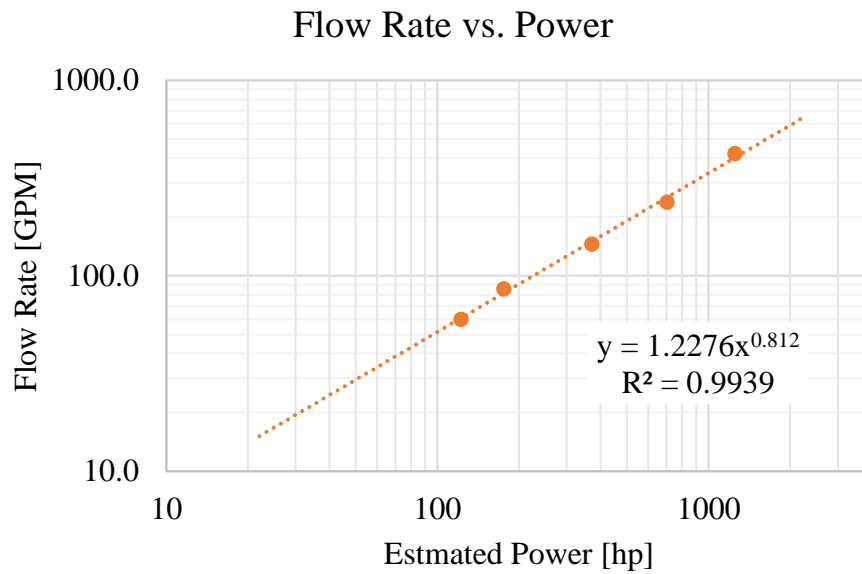


Figure 3.7 Motor outflow rate to power scaling curve.

The volumetric flow rate plays a crucial role in determining flow velocity within the constant-diameter hydraulic hoses, which is a critical aspect of pipe sizing. This will be discussed in more detail in the following subsection.

3.3.3 Hydraulic Hose Sizing

Hydraulic hoses are meticulously sized to minimize friction loss and maintain pressure integrity. The primary factor influencing pressure loss within the hose is viscosity, which varies with temperature and fluid formulation, making early-stage estimation challenging. To address this, the preliminary weight estimation focuses on controlling velocity, which can be more easily referenced by adjusting the cross-sectional area while keeping the flow velocity constant.

The hose cross-section is scaled from study [49] conducted on hydrostatic transmission for helicopter. Flow rate for HSVTOL is estimated using the relation obtained in Figure 3.7 in Section 3.3.2, with given power at design limit. The rate obtained using this method for 1500 hp motor in [49] is 465.4 GPM, equivalent to 1792 in³/s. Mentioned in the paper that stainless steel pipe is used for the 1,500 hp concept, with 2.25 inches ID, flow speed of 37.55 ft/s is obtained at location near the motor [49]. Using the same method, the 30-TF HSVTOL main motor flow rate of 1185 GPM is obtained. To keep the flow velocity u below 37.55 ft/s, the minimum cross-sectional area is 10.04 in² using (3.10) thus the minimum ID is 3.59 inches.

$$GPM \times \frac{231}{1} \left(\frac{in^3}{gal} \right) \times \frac{1}{60} \left(\frac{min}{sec} \right) = \dot{V} \left(\frac{in^3}{s} \right) \quad (3.9)$$

$$D = 2 \times \sqrt{\frac{\dot{V}}{u \cdot 12 \cdot \pi}} \quad (3.10)$$

For weight estimation, OTS hydraulic hoses rated for various pressure are collected in Table B 4 to obtain the scaling curve, the weight is substantial. To reduce the hose weight, the concept in [49], using AM 350 seamless stainless-steel tubing must be applied. Properties of the material is mentioned in AMC Spec.5584, but OTS steel provide different values and are more recent. For this study, calculations are performed using data of Condition DA precipitation hardening heat treatment AM 350. This condition provides good strength between condition H and

SCT 850, with density of 0.286 lb/in³, 0.2% yield strength 160,000 psi, and ultimate strength is 190,000 psi [62].

The thickness of AM 350 pipe is calculated with factor of safety by Code of Federal Regulations. In 14 CFR Part 25 (Airworthiness Standards: Transport Category Airplanes), the FoS requirement varies per type of element. Defined in 14 CFR 25.1435, the proof pressure (without permanent deformation, known as yielding) for tubes and fittings is 1.5×DOP, ultimate pressure is 3.0×DOP. Requirement for hose is higher with proof pressure of 2×DOP, ultimate pressure of 4.0×DOP. Considering that the vehicle’s hydraulic transmission pipes are only pressurized in rotorcraft configuration, Part 27 (Normal Category Rotorcraft) and Part 29 (Transport Category Rotorcraft) are also relevant. Defined in 14 CFR 27.1435 (a) and (b), the elements cannot yield under DOP, and no part may fail, malfunction, or experience a permanent set under 1.5×DOP. Similarly in 14 CFR 29.1435, yielding FoS is 1 with additional requirements on means to account for surge and vibration, FoS for failure is 1.5. Requirements in 14 CFR 25.1435 are used in this study to ensure the safety and practicality of the system designed.

Calculations are performed under the assumption that the atmospheric pressure between 14.696 psi at standard sea level and 4.373 psi at cruise altitude is negligible comparing to the DOP at 8,000 psi, simplify the case to cylindrical pressure vessel without external pressure. Consider the longitudinal stress and hoop stress using equations in [63] as shown below, the hoop stress will be higher under all cases. Note that σ is stress in psi, p is pressure in psi, r and t are radius and thickness in inches.

$$\text{Circumferential Stress:} \quad \sigma_1 = \frac{pr}{t} \quad (3.11)$$

$$\text{Longitudinal stress:} \quad \sigma_2 = \frac{pr}{2t} \quad (3.12)$$

From (3.11), the required thickness of pipe is obtained with (3.13) below, for AM 350 used, $\sigma_{tu} = 190,000 \text{ psi}$. Table B 5 in Appendix B lists the thickness for various pressure and diameter.

$$t = \frac{FoS_{tu} \cdot p \cdot r}{\sigma_{tu}} \quad (3.13)$$

Although it was assumed that the minimum thickness is mainly limited by ultimate strength because the FoS required is doubled from the requirement for yielding, the actual FoS must be verified. Using (3.14), FoS for the material picked is 2.53, far exceeding the requirement.

$$SOF_{0.2\%y} = \sigma_{tu} \cdot \frac{t}{p \cdot r} \quad (3.14)$$

To obtain the mass per length of piping, unit volume is obtained with cross-section area with unit length of 1ft. The unit mass can be obtained simply by multiplying volume and density ρ where AM 350 (DA) is 0.277 lb/in^3 . Equation (3.14) is given below for clarity, the constant 12 represents 12 inches per ft.

$$\frac{m}{l} = \left[\left(\frac{ID + 2 \cdot t}{2} \right)^2 - \left(\frac{ID}{2} \right)^2 \right] \cdot \pi \cdot 12 \cdot \rho \quad (3.15)$$

A list of unit weight is included in Appendix B, and plots showing the trends are listed below in Figure 3.8 and Figure 3.9. It is observable that custom seamless steel piping is lighter than OTS options. Mass of AM 350 pipes will be calculated in Section 3.3.5. Another aspect to consider is the amount of fluid in the system, which depends not only on the diameter of the pipe but also on the volume and density, as calculated in the (3.15):

$$m_{fluid} = r^2 \cdot \pi \cdot l \cdot \rho_{fluid} \quad (3.16)$$

where ρ_{fluid} varies depending on temperature, and the type of fluid used.

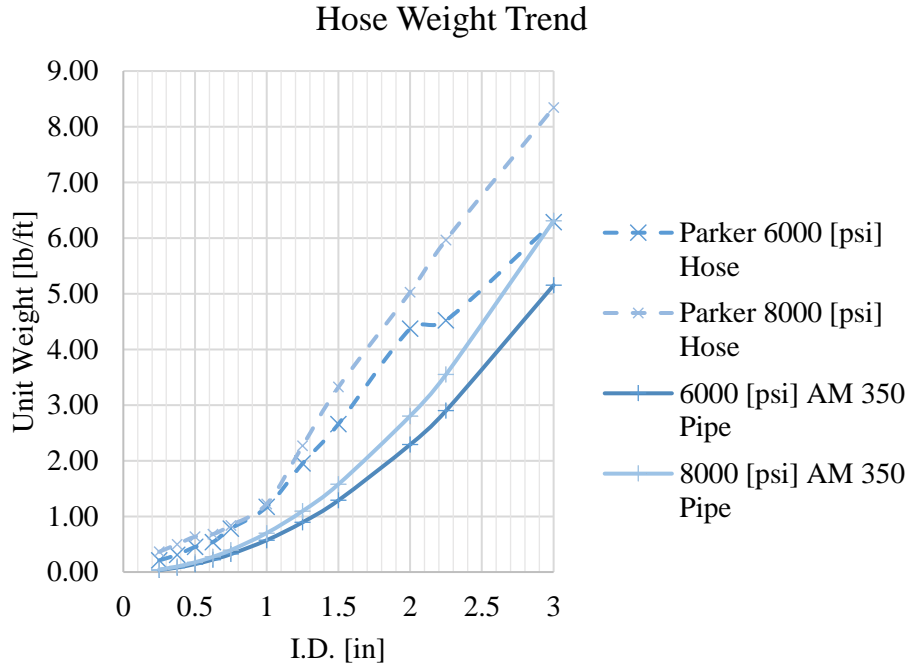


Figure 3.8 Comparison between OTS hoses and AM 350 pipes.

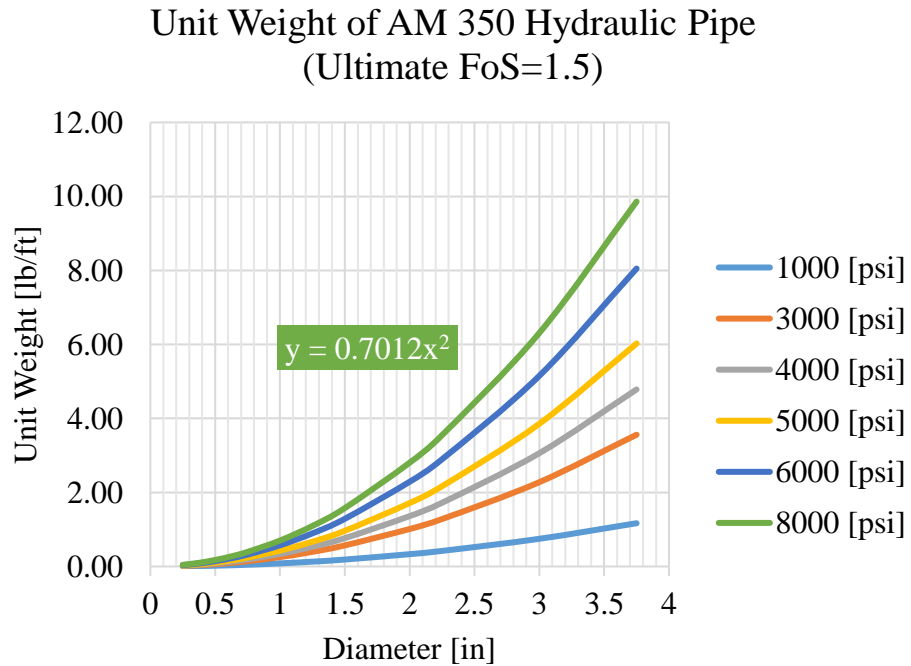


Figure 3.9 General trend of AM 350 pipe weight wrt diameter.

3.3.4 Accessory and Miscellaneous

This section outlines the sizing method for components with less substantial weight and other elements crucial for mounting and supporting the primary components. One notable exception is the power transmission component located at the joint between the wing and the tilting pylon. In this regard, two scenarios are considered, shown in Figure 3.10.

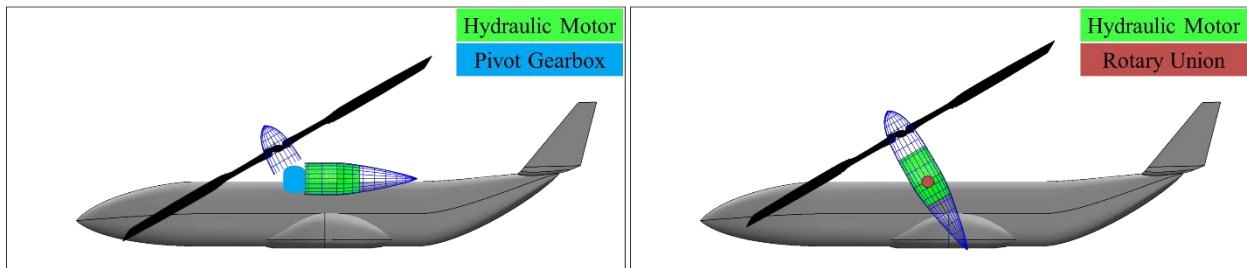


Figure 3.10 The two tilting methods considered.

In the first scenario, the setup involves the hydraulic motor remaining stationary, with only the rotor undergoing tilting, like Figure A 4. The radial piston motor operates at the same rotation speed as the main rotors, so the pivot gearbox has a reduction ratio of 1. Its primary function is to transfer torque to the rotating section of the pylon. In the second scenario, the traditional pylon tilting design is adopted, where both the hydraulic motor and the rotors tilt in unison. This configuration necessitates the inclusion of a rotary union to facilitate the transfer of fluid across the rotating joint. The weight of these components is calculated and subsequently compared.

To determine the size of the pivoting gearbox, the assumption is made that the minimum number of gears should be used to enable rotation without significant increases in weight. At a minimum, two bevel gears are necessary to transmit the rotating motion, allowing one of the gears to pivot around the axis of rotation of the other. The sizing of these gears begins with the calculation of the torque being transferred. Given a tip speed of 780 feet per second and a rotor

radius of 21 feet [13], the rotational speed is computed as 354.68 RPM in Section 3.2. The torque can be calculated using (3.17), where P is in watt and q is in Nm .

$$q = \frac{P}{RPM} \cdot 9.55 \quad (3.17)$$

Power was initially calculated in hp , and can be converted to kW bedeviling constant 1.341. In this case, the torque per rotor is 94702.96 $N \cdot m$ per rotor. Volume of the gear is then calculated using equation obtained from “*Gear Weight Equations - Gear Chain Weight Calculation Methodology*” [64], starting with the dimensions using (3.18):

$$b \cdot d_1^2 = 2000 \cdot \frac{T_1}{K} \cdot \frac{i + 1}{i} \quad (3.18) [64]$$

where b and b are the width and diameter of gears in mm, T_1 is torque on input gear in Nm , K is surface durability factor, and i is the gearbox ratio. In this case, use $K = 4$ and $i = 1$. The volume of bevel gears is calculated from (3.19):

$$V_{r1} = \frac{\pi \cdot b \cdot d_1^2}{4} \cdot \psi_1 \quad (3.19) [64]$$

where ψ is the gear volume fill factor from 0.3 to 0.7 [64], 0.3 is used for minimum volume. The resulting volume is expressed in mm^3 , and to convert to m^3 , a scaling factor of 1E-09 is applied. The typical material used for manufacturing bevel gears is S45C steel, with a density ranging from 7700 to 8030 kg/m^3 [65]. For mass calculations, an average value of 7865 kg/m^3 is used in (3.20). The number of gears n is 2 for this design, and to obtain the weight in lb , the obtained value is multiplied by 2.205. Weight of the gears are substantial due to the high input torque.

$$m = V_{r1} \cdot \rho_{S45C} \cdot n \quad (3.20) [64]$$

For the other option, rotary unions are employed for multiple fluid passes across a rotational interface, like Figure A 5. While most large OTS rotary unions do not include weight information in their sites, the MOOG Model 810 has a complete and publicly available datasheet [66].

However, this design only offers two different port sizes and two versions with either two or four passes. The limited number of data points available prevents the creation of a non-linear scaling curve, necessitating certain assumptions. Displayed in Figure 3.11 is the fluid rotary union. The ports on the flange are arranged in a circular pattern, which makes it impractical to increase the overall radius based on the area of the passages. Observing the side view, it's clear that the length of the unit is primarily determined by the diameter of the port and the spacing between the holes. Consequently, the length is chosen as the scaling factor for the rotary union.

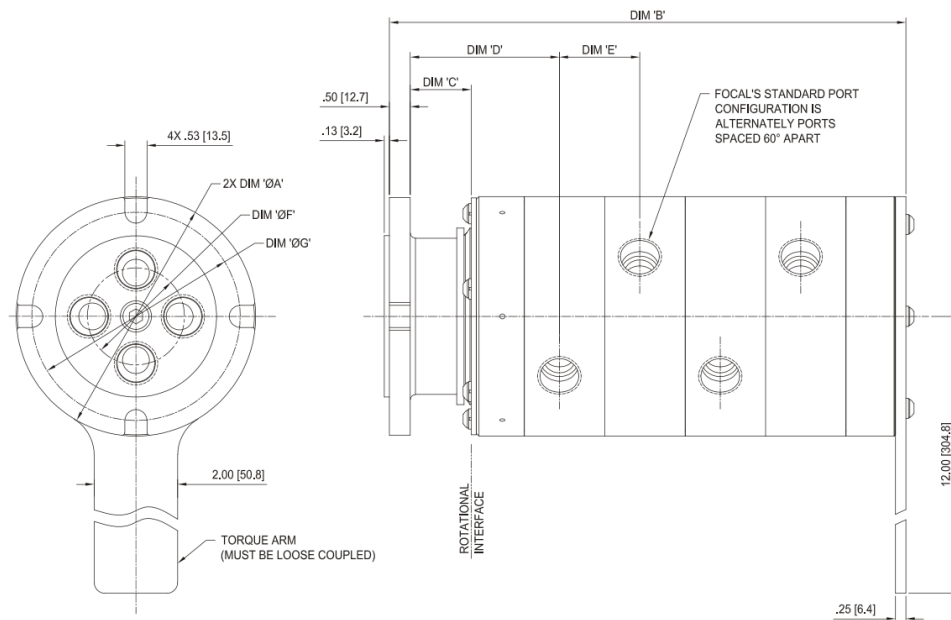


Figure 3.11 Moog Model 810 drawings [66].

Utilizing the dimensions presented in Table B 8, linear trendline for overall length concerning port size and unit weight concerning overall length is established, as depicted in Figure 3.12 and Figure 3.13. The four-pass variant features double the passage area of the two-pass variant, with a weight approximately 1.5 times that of the two-pass version. While the four-pass variant offers

advantages in terms of weight and redundancy by accommodating the splitting of two hoses for four passages, it also introduces added complexity and potential failure points.

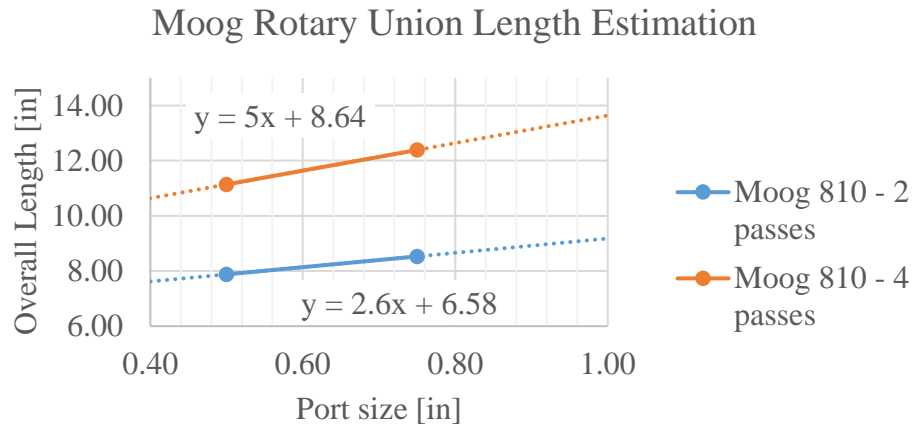


Figure 3.12 MOOG Model 810 length scaling plot.

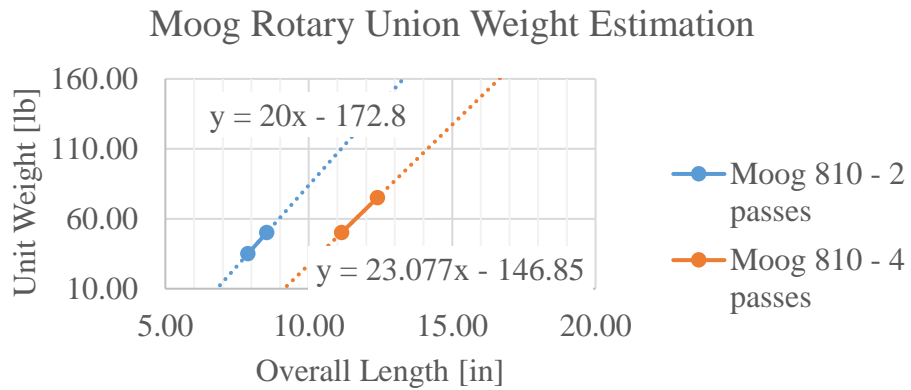


Figure 3.13 MOOG Model 810 weight scaling plot.

For the weight estimation, combining empirical equations in Figure 3.12 and Figure 3.13 yields:

$$W = (2.6 \times D_{port} + 6.58) \times 20 - 172.8 \quad (3.21)$$

where D_{port} is the diameter of connection in inches, and W is the weight in pounds. This option significantly outperforms the concept involving a stationary motor and a pivoting gearbox, provided that the tilting mechanism and actuators have a similar weight. Therefore, the concept with the entire pylon rotating is the only one taken into consideration for subsequent sizing efforts.

The weight of miscellaneous and supporting components is primarily scaled up from the system designed for the UH-1 [49], with the original weights listed in *Table B 7*. Two sets of engine-related equipment are included for redundancy, and the valve weight is estimated using the total power of the entire vehicle. This simplification does not significantly impact the study, as the total power is assumed to be the sum of power from both engines. The scaling factors are presented in *Table 3.2* below.

Table 3.2 List of scaling factor for hydrostatic transmission misc. objects.

Name of component	Scaling factor
Centerbox	$60 \times n_{engine} \times \frac{P_{engine}}{1,500 \text{ hp}}$
Oil cooler	$28 \times n_{engine} \times \frac{P_{engine}}{1,500 \text{ hp}}$
Accessory drive	$27.1 \times n_{engine} \times \frac{P_{engine}}{1,500 \text{ hp}}$
Scavenge pump drive	$0.4 \times n_{engine} \times \frac{P_{engine}}{1,500 \text{ hp}}$
Scavenge pump	$10.0 \times n_{engine} \times \frac{P_{engine}}{1,500 \text{ hp}}$
Idler gear	$0.4 \times n_{engine} \times \frac{P_{engine}}{1,500 \text{ hp}}$
Gen. drive	$0.1 \times n_{engine} \times \frac{P_{engine}}{1,500 \text{ hp}}$
Rach. Gen. drive	$0.2 \times n_{engine} \times \frac{P_{engine}}{1,500 \text{ hp}}$
Valves	$20.0 \times \frac{P_{total}}{1,500 \text{ hp}}$

3.3.5 Integration

In the hydrostatic transmission system, the main components have been sized using the methodologies described earlier in this section. One exception is the hydraulic fluid, as its volume depend on various factors and the dimensions of different components. In the reference paper [49], a specially designed additive was introduced to reduce friction loss, as depicted in Figure 3.14. While this indicates a significant improvement in efficiency, the density of the hydraulic fluid was not specified in the paper.

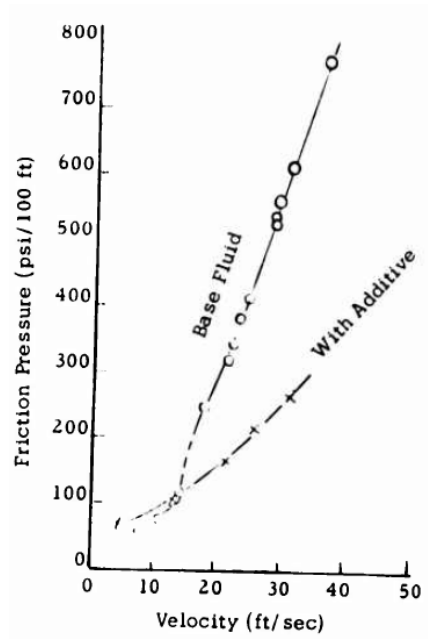


Figure 3.14 Pipe friction pressure drop versus velocity [49].

OTS low viscosity hydraulic fluids, such as Skydrol LD-4 and HyJet IV-A, exhibit comparable densities of approximately 8.35 lb/gal. Specifically, the specific gravity of LD-4 ranges from 1.003 to 1.013 at 25°C [67], which is equivalent to 8.355 to 8.438 lb/gal at 77°F. Likewise, the datasheet for HyJet IV-A indicates a density of 8.35 lb/gal at 60°F [68].

The volume calculations for the pump, motor, and pipes are determined, with an additional 10% of fluid added as a reserve. The pump and motor calculations are derived using a combination of equations from [58] and [69]. The same conversion factors as those employed in Section 3.3.1 are applied for these calculations, see (3.22) and (3.23) for volume calculations.

$$\text{Pump displacement:} \quad V_{pump} = \frac{n_{pump} \cdot P_{pump}}{0.0007 \times PSI \cdot RPM_{pump}} \quad (\text{gal}) \quad (3.22)$$

$$\text{Pump displacement:} \quad V_{motor} = \frac{63025 \times n_{motor} \cdot P_{motor}}{PSI \cdot RPM_{motor}} \times 2\pi \quad (\text{gal}) \quad (3.23)$$

The basic calculation of volume in the pipe was presented in Section 3.3.3, (3.16). In the case of the tiltrotor configuration with engines mounted on the rear of the fuselage, it is assumed that the pipe extends across the wing. Two passages meet at the wing's root and then extend $\frac{1}{4}$ of the way down the fuselage total length.

$$\text{Pipe volume:} \quad V_{pipe} = \left[(r^2 \cdot \pi) \times n_{motor} \times \left(\frac{b}{2} + \frac{l_{fus}}{4} \right) \times 12 \right] \div 231 \quad (\text{gal}) \quad (3.24)$$

The volume mentioned pertains to a one-way flow from the pump to the motor or vice versa. To determine the total volume for the complete hydraulic circuit, it's a straightforward process of doubling this volume, except when variations in length or diameter exist between the power and return pipes. By applying the calculated volumes and the given fluid density, it becomes feasible to compute the mass and, subsequently, the weight of the hydraulic fluid within the system. The total fluid weight is the aggregate of the calculated fluid volume, multiplied by 1.1 to account for a 10% reserve, unless specific variations are defined.

Using the 30-TF concept as the reference, the weights of the transmission system components are determined and presented in Table 3.3 below. The baseline weight utilizing mechanical transmission is provided, and visual representation can also be found in Figure A 5. As the turbine speed pump does not necessitate a reduction system, the centerbox now serves as a mounting point for the engine and associated accessories. Mechanical transmission components are eliminated from the system, including the wing shaft. The pylon-mounted shaft is required for the configuration with a fixed motor but becomes unnecessary when the motor tilts with the pylon. It's essential to note that the mast's weight is included for all concepts, as the weight of the motor shaft is unknown. Consequently, the weight estimation for the direct drive motor is conservative. These baseline values serve as an initial reference point for a comparative assessment against the traditional transmission system, but it's important to note that they apply specifically to the 30-TF baseline airframe.

Table 3.3 Sample transmission weight estimated for 30-TF with hydrostatic transmission.

Component	Mechanical [13]	Hydrostatic (Fixed motor)	Hydrostatic (Tilt motor)
Centerbox	603.60	379	379
Mechanical Transmission	2,225.00	-	-
Hydrostatic Pump	-	950.00	950.00
Engine Starter	113.60	114	114
Rotor Motor	-	1,818	1,818
Hose (wet) / Wire	-	900	900
Transmission Sup.	214.50	722	722
Pivot box	616.30	616	616
Pivot Gearbox	-	1,548	-
Rotary union	-	-	291
Mast	578.50	579	578
Pylon shaft	56.20	56	-
Wing Shaft	123.70	-	-
Total	4,531.40	7,682	6,369

3.4 Electric Transmission Sizing Methodology

When comparing electric transmission technology to its hydrostatic counterparts, it is evident that significant advancements have occurred in recent years. These improvements can be largely attributed to the green energy automotive industry and the more recent surge in urban air mobility (UAM). For instance, when examining motors, as depicted in the data presented in Figure 3.15, the power density of hydraulic motors reached a plateau around 1996, while the trend for electric motors continues to show growth. This figure encompasses not only traditional room temperature motors but also highlights the development of cryogenic superconducting components with even higher power density [70]. As a result of this rapid technological advancement, components at various technology levels were reviewed in this study.

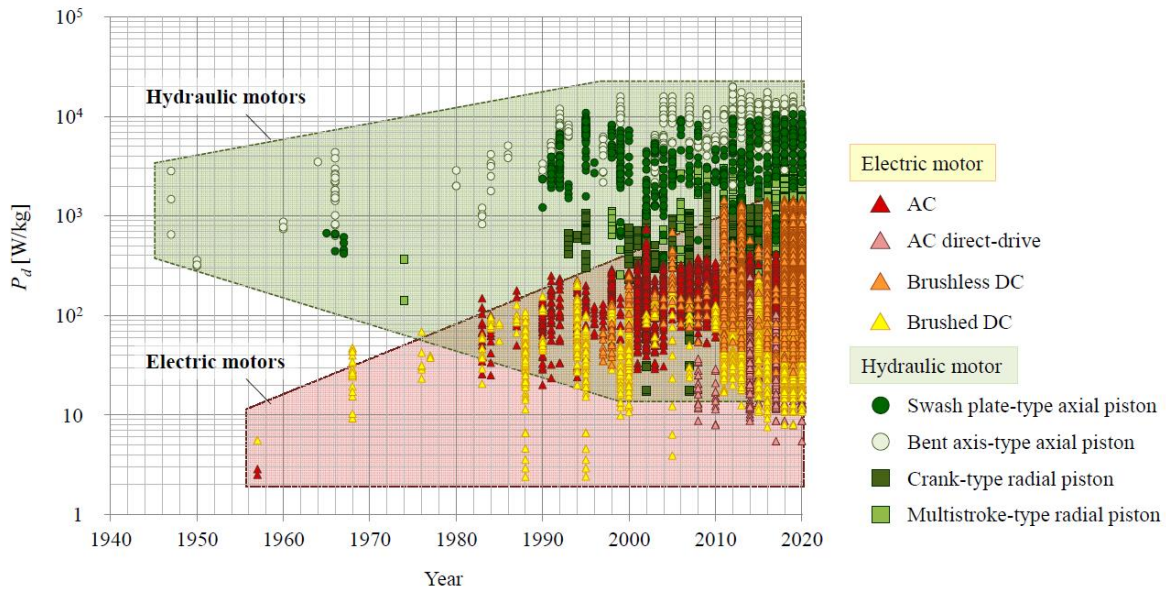


Figure 3.15 Transition of power density in electric and hydraulic motors [61].

Shown in Figure 3.16 below is the general layout of turboelectric transmission components. The is general layout remains the same despite of the technology level of components used, see

Figure 3.17. Weight power density is varied to account for the improvement in technology, but the MTOW and hover power remains the same for the comparison of transmission system weight, like the method used in Section 3.3 for hydrostatic transmission. The process of sizing component weights will be elaborated upon in the subsequent subsections.

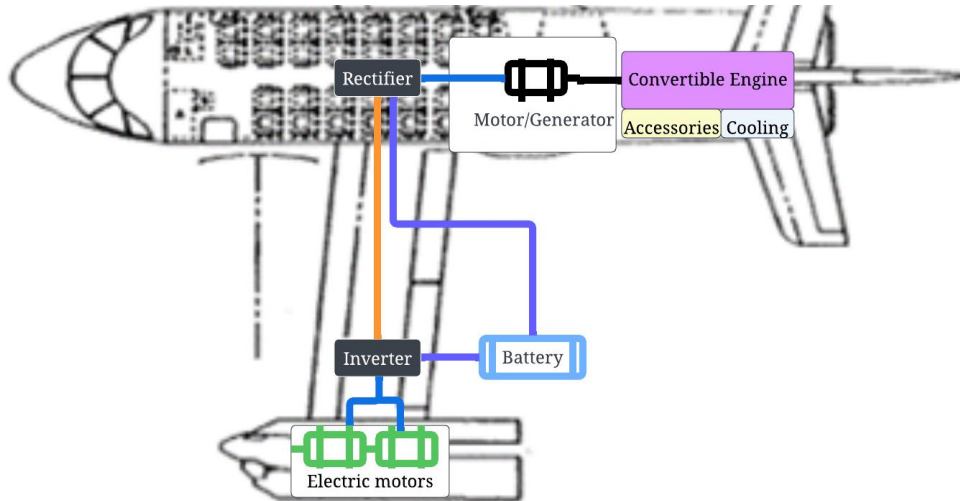


Figure 3.16 Turboelectric transmission system components layout.

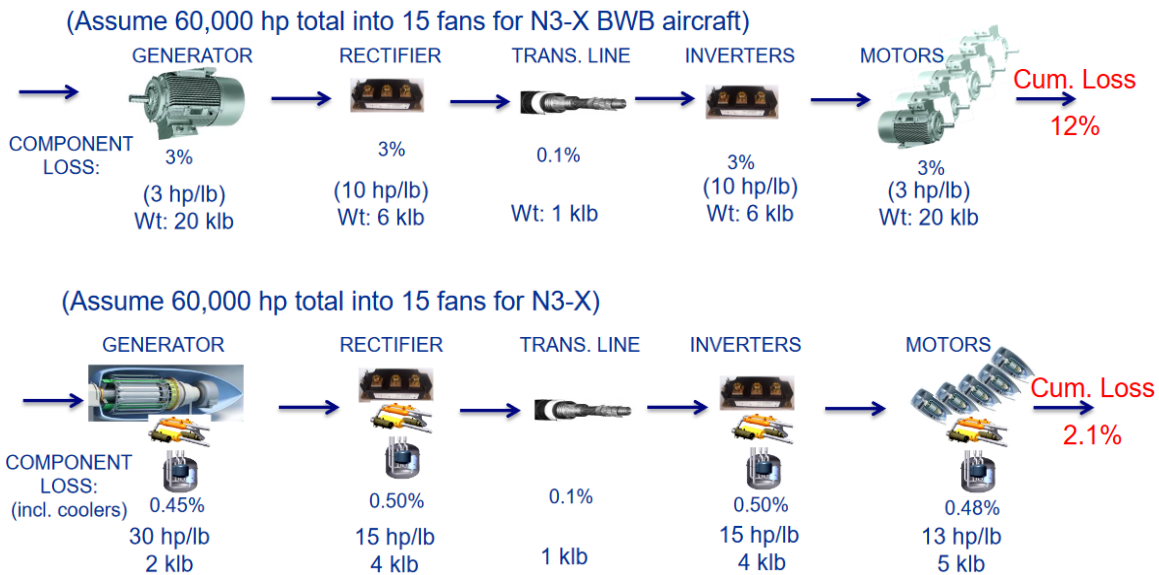


Figure 3.17 Room temp. turboelectric (top) vs. Cryo superconductor (bottom) [70].

3.4.1 Motor/Generator Sizing

The initial weights of the motor and generator are estimated based on design assumptions obtained from "*Conceptual Design of a Single-Aisle Turboelectric Commercial Transport with Fuselage Boundary Layer Ingestion*" [53], which provides specific power values. The complete table of values can be found in Appendix Table B 9. The weight can be determined using the following (3.25):

$$W = P_{motor} \cdot SP_{motor} \quad (3.25)$$

where weight is in lb, power is in hp, and specific power unit is lb/hp. The specific power for motor and generator provided in this paper is identical, both are 8 hp/lb. And using the constant specific power eliminates the difference between one component versus multiple smaller components with the same total power. While the calculation based on the assumption of a constant specific power for the motor and generator yields substantial weights, such as a combined weight of 4,741.5 pounds for the 30-TF concept, which exceeds the total weight of the traditional mechanical transmission system, a more sophisticated model is necessary to validate these weight estimates.

The exponential motor weight scaling curve is sourced from "*Air Vehicle Design and Technology Considerations for an Electric VTOL Metro-Regional Public Transportation System*" [71]. Figure B 8 displays the motor weight plotted against motor power, featuring equations for state-of-the-art (SOA) motors and High-Temperature Superconductor (HTS) motors provided in [72] by NASA Glenn Research Center (GRC). The equations denoted as (3.26) and (3.27) in this paper describe the HTS motors scaled using this curve, referred to as GRC motor in this study.

$$\text{SOA motors:} \quad W_{motor}(lb) = 1.96 \times P_{motor}^{0.8997}(kW) \quad (3.26) [71]$$

$$\text{GRC HTS:} \quad W_{motor}(lb) = 2.28 \times P_{motor}^{0.6616}(kW) \quad (3.27) [72]$$

The equations provided use power units in kW and weight in pounds. However, it's straightforward to convert from horsepower (hp) to kW using a conversion factor of 0.7457, or by dividing by 1.341. To reduce weight, we assume the use of one generator capable of generating the total power needed, along with two motors, one for each rotor. The weight for each motor or generator can be easily estimated by inserting the power into the scaling equations. It's worth noting that estimating motor weight using torque, as demonstrated in (3.28), implies that it might be more efficient to have multiple motors with low torque. However, the actual configuration exceeds the scope of this paper.

$$\text{NDARC:} \quad W_{motor}(lb) = 0.5382 \times Q_{motor}^{0.8129}(ft \cdot lb) \quad (3.28) [73]$$

Utilizing the equations for SOA and GRC motors, the estimated weight for OTS motors appears to be substantial. For the 30-TF concept, the weight of a single generator is approximately 5,697 lb, with each motor weighing around 3,054 lb. However, the high-temperature superconductor motor from GRC demonstrates much better results, with a weight of 803.11 lb for the generator and 508 lb for each motor. The results emphasize the potential weight savings achievable through advanced motor technology. Recent developments in the automotive industry have also contributed to these weight-saving efforts. For instance, in June 2023, the SPX177 [74], which features a 2x 3-phase motor capable of delivering 650 kW of power, was announced. Notably, this motor only weighs 28 kg, while the inverter weighs 13 kg, resulting in an equivalent power density of 14.12 hp/lb—approximately 196% higher than the GRC motors. The inverter also has an impressive power density of 30.41 hp/lb, which will be utilized in the following section. Assuming that this motor follows a scaling trend similar to that of the GRC motor, the scaling (3.29) can be applied to estimate its weight.

$$\text{Helix Scaled:} \quad W_{motor}(lb) = 0.8501 \times P_{motor}^{0.6616}(kW) \quad (3.29)$$

An alternative motor, also utilizes cryogenic superconducting technology, was introduced in the context of the N3-X project [70]. Specific power values for this technology are provided in Figure 3.17, with a constant value of 30 hp/lb for the generator and 13 hp/lb for the motors. When these specific power values are inserted into (3.25), the resulting estimates are a generator weight of 316 lb and 365 lb per motor. In this case, the generator proves to be the lightest among all the options. However, the motor's weight is lower than that of the GRC motor but higher than the trend scaled using the Helix motor. The specific power, a crucial parameter for sizing, is visually represented in Figure 3.18.

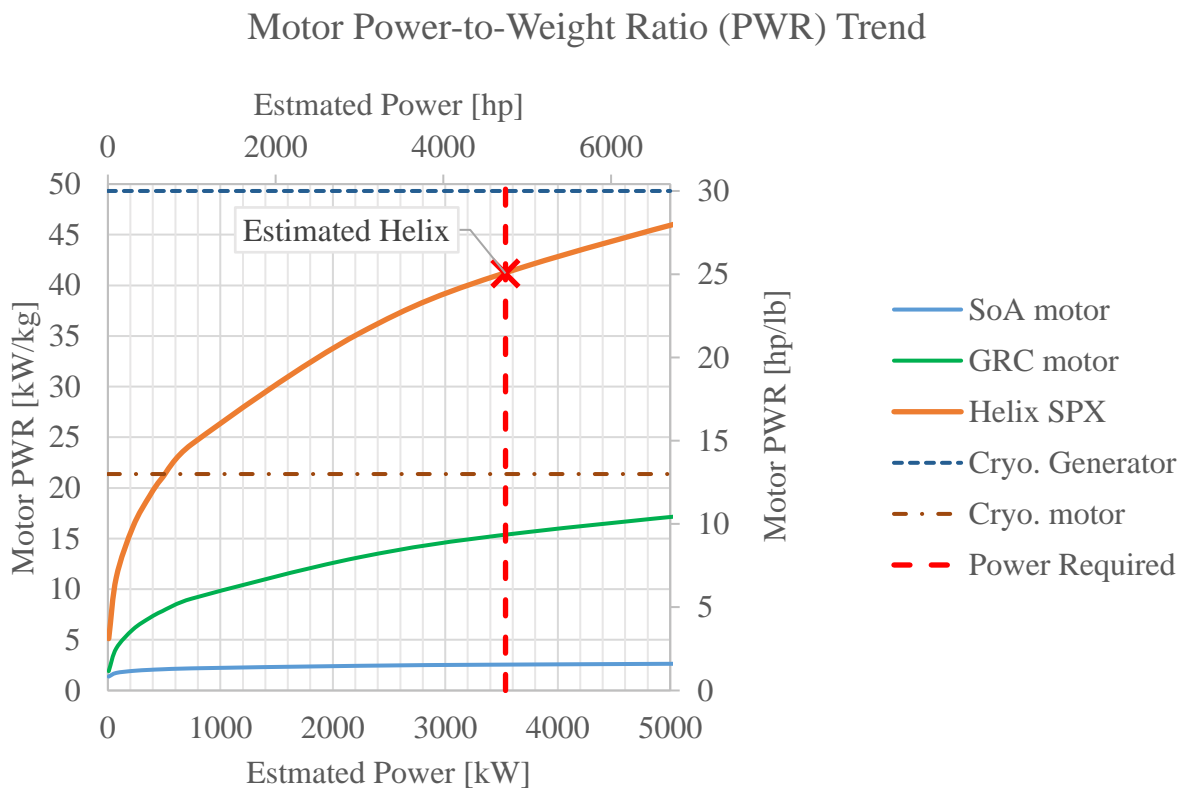


Figure 3.18 Specific power of the motor considered.

A comparison of the motor weight versus rated power, encompassing all motors is graphed in Figure B 9. It is evident that most of the motor weight curves exhibit a similar trend. However, the hydraulic motor and the N3-X assumption intersect the curves of other motors.

3.4.2 Rectifier/Inverter

Rectifiers are necessary components to convert the power before it enters the transmission wire, while inverters are required to control and drive the motors. Typically, rectifiers and inverters can be viewed as identical components, with one unit needed at each end of the transmission line. The weight calculation for inverters is relatively straightforward when compared to the process for motors since the relationship between power and weight is more linear. The baseline power is once again obtained from Table B 9, and the weight estimation can be performed using (3.30).

$$W = P_{input} \cdot SP_{inverter} \quad (3.30)$$

For the baseline design, assuming a specific power (SP) of 10 hp/lb [53], the total weight of all rectifier/inverter units (referred to as inverters for simplicity) can be calculated collectively using the formula $2 \times P_{total} \cdot SP$. In the case of the room temperature 30-TF concept, the total weight of all inverters amounts to 1,897 lb. Similarly, the GRC and N3-X concepts, employing HTS technology with an assumed SP of 15 hp/lb from reference [70]. The validity of this value is further corroborated by other cryogenically cooled inverters, as observed in a specific power of 23.3 kW/kg reported in [75], which translates to 14.17 hp/lb, result in a total weight of 1,338 lb. The inverter used by the Helix motor is notably lightweight, with SP of 30.41 hp/lb. The value used is derived from publicly available data from reference [74], also explained in previous Subsection 3.4.1. Using this value, the total inverter weight for 30-TF is 624 lb.

3.4.3 Wire Sizing

In the transmission of electrical power from the generators to the motors, a crucial consideration for wire sizing is the current capacity and permissible operating temperature. As

electrical current flows through a wire, it generates heat due to resistance, and controlling temperature is essential. Established standards and readily available data on OTS power transmission cables play a crucial role in shaping the guidelines for wire sizing.

A primary reference in this study is the FAA AC 43.13-1B [76], which provides comprehensive data on current-carrying capacity and resistance of copper wire. This dataset serves as a fundamental baseline for the research, and the relevant table is presented in Appendix Table B 10. In Figure B 10, a plot illustrating the relationship between nominal conductor area and the current carried at various temperatures is showcased. Although the 2nd order polynomial fits in this plot shows strong correlation, it's important to note that the operating current requirements for HSVTOL aircraft greatly exceed the scope of this plot. Consequently, additional sources of data concerning room temperature cables are sought to validate the extensive conductor area required for the transmission cables.

Another valuable source of information for room temperature wire sizing is the HWC 263 Cable [77] , which has a rating of 2kV and an operating temperature up to 110°C. Related parameters from this source are thoughtfully compiled in Appendix *Table B 11*, and their representation in Figure B 11 illustrates a consistent trend. In this illustration, HWC 263 cables shows significantly smaller conductor area requirements at similar temperatures, with the 110°C HWC cable nearly coinciding with the extrapolated curve for thinner wire suggested by the FAA at 200°C, as presented in Figure 3.19 below.

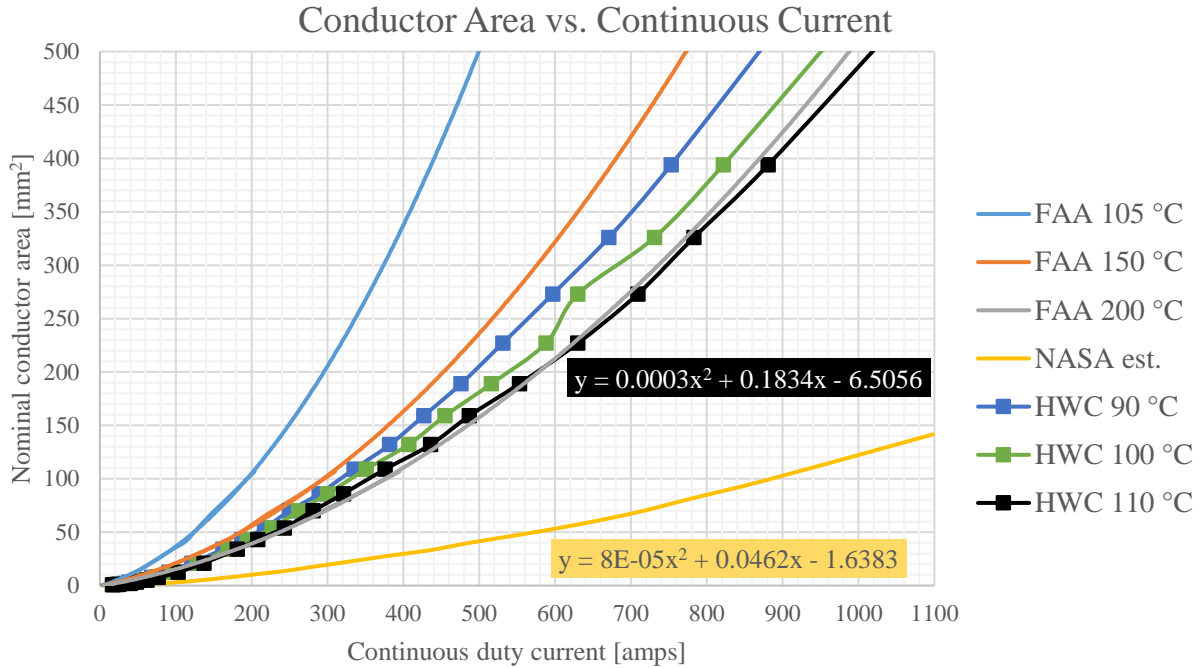


Figure 3.19 Cable conductor area with respect to the current carried.

The unit weight of room temperature cables can be determined by calculating the copper density for a given conductor area, taking into account the specific current. A fundamental current calculation for each motor is expressed as follows:

$$I(A) = P_{motor}(hp) \times 745.7 \left(\frac{W}{hp} \right) \div V_{motor} \quad (3.31)$$

where this equation allows the calculation of the current for each cable connected to a single motor. Assuming that the power transmission necessitates two cables between the rectifier and inverter, and the wire from the generator to rectifier, and inverter to motor is negligible compared to the total length of cables, the total weight of room temperature cables can be estimated using the following equations:

$$S_{conductor}(mm^2) = n_{cable}(a \cdot I^2 + b \cdot I + c) \quad (3.32)$$

[HWC @ 110°C: a=0.0003, b=0.1834, c= -6.5056, n=2]

$$\frac{m}{l} \left(\frac{g}{mm} \right) = \rho_{copper} \left(\frac{g}{mm^3} \right) \cdot S_{conductor} (mm^2) \quad (3.33)$$

[Copper density: 0.008906 g/mm³]

$$\frac{W}{l} \left(\frac{lb}{ft} \right) = \frac{m}{l} \left(\frac{g}{mm} \right) \times \frac{1}{453.6} \left(\frac{lb}{g} \right) \times 304.8 \left(\frac{mm}{ft} \right) \quad (3.34)$$

Or, for the sake of convenience, these equations can be simplified using the assumptions to (3.35) as follows:

$$\frac{W}{l} \left(\frac{lb}{ft} \right) = n_{cable} (a \cdot I^2 + b \cdot I + c) \times 0.005984 \quad (3.35)$$

Furthermore, Table B 9 assumes the cable to have a mass of 3.85 kg/m at 750V and 1926A [53]. Using the polynomial fit for HWC 263 at 110°C and equation 3.33 to calculate the area, it becomes evident that the assumed cable's cross-sectional area is only 25.18% of HWC 263, as depicted in Figure 3.19. It's worth noting that while the paper initially assumes that “*implementing a cryogenic cooling system to enable superconducting electrical components is unnecessary* [53, pp. 14-15],” this study will proceed to perform calculations for sizing the thermal management system (TMS) weight in the subsequent section. Using this method and assuming the same cable length as the hydraulic pipe, the total wire weight for the 30-TF airframe is estimated at 320 lb. This is notably less than the weight of room temperature conductors, which stands at 1,473 lb.

Another source of superconductive power transmission is detailed in “*A proposal for a lightweight, large current superconducting cable for aviation.*” [78]. This study focuses on a 20-tape cable rated for 2kA at 77K and 10kA at 20K, see Figure B 12 Figure B 12 Cross-section of the cryogenic pipe and conductor, which aligns with the temperature range of NASA's HTS technology. In Appendix Table B 13, the weight-to-current per length is documented as 0.319 kg/A/km. Converting this to weight per unit length using (3.36):

$$\frac{W}{l} \left(\frac{lb}{ft} \right) = n_{cable} \cdot I \times 0.319 \left(\frac{kg/A}{km} \right) \times 2.205 \left(\frac{lb}{kg} \right) \times \frac{1}{3281} \left(\frac{km}{ft} \right) \quad (3.36)$$

The resulting total wire weight for the 30-TF airframe is 64 lb, a significant reduction from the previous estimation.

3.4.4 Thermal Management System (TMS) Sizing

The weight of the Thermal Management System (TMS) varies significantly based on the selected motor and transmission cable technology. For room temperature TMS systems, calculations are primarily based on “*Thermal Management System Design for Electrified Aircraft Propulsion Concepts*” [79]. Two key concepts considered are STARC-ABL and RVLT, both being hybrid electric concepts with generators and loads similar to the HSVTOL concept in this study. Visual references are provided in Figure B 13 and Figure B 14. Table B 14 and Table B 15 present the component weights and sizing equations sourced from [79], which enable the estimation of rejected power based on rated power. Among the various concepts, the RVLT closely resembles the 30-TF tiltrotor concept. Power values from Table 11 in [56] (also included as Table B 16 included as in the appendix) are used for calculations. The results, including the power rejection percentage and specific weight (TMS weight divided by power rejected), are provided in Table 3.4 below. The cells are color-coded to enhance readability. Note that in this source, the rectifier/inverter are referred to as converter. Assuming converter power is identical to generator/motor power for the purpose of weight estimation.

Table 3.4 Percentage power rejected and specific weight of RVLT TMS.

	Power Rated		% Rejected [kW/kW]		Specific W [kg/kw]	
	kw	hp	Baseline	Advanced	Baseline	Advanced
Motor	545	731	6.42%	2.57%	2.03E-01	3.27E-01
Engine	3527	4730	4.90%		8.44E-02	
Converter*	2415	3239	1.99%	0.98%	2.31E-01	2.49E-01

Using the above estimation, room temperature TMS component weight of 30-TF can be calculated using the specific weight obtained above. The curve fitted value was obtained using equations in Table B 15. Delta between the two methods is minor, but the greater value is used.

Table 3.5 30-TF concept room temperature TMS component size.

Loop Type	n	Technology	Rated Power [kW]	Rejected Power [kW]	Weight [kg]	Total Required Power [kW]	Total Drag [lbf]	Total Weight [kg]	Weight Curve Fit [kg]
Engine + Generator	1	baseline	9483	465	39	49	-183	224	202
Converter*	1	baseline	9483	188	44				
Converter + Motor (HEMM)	2	baseline	4741	304	70				
Motor (HEMM)*Engine coolant loop	1	advanced	9483	93	23	15	-52	103	66
Converter + Motor (HEMM)	2	advanced	4741	122	40				

Estimating the system with HTS components differs significantly due to the substantial weight of the required cooler. The initial HTS estimation was based on the TMS sizing for the STARC-ABL in [53, p. 11]. By knowing the power ratings of the motor and generator, and power required by TMS, the percentage of TMS power required is calculated to be approximately 6.48% of the combined motor and generator rated power. The TMS weight is subsequently estimated using the provided scaling factor of 0.68 kW/kg. Using the equation:

$$W_{TMS} = \frac{1}{1.341} \left(\frac{kW}{hp} \right) \times 0.0648 (P_{m_{total}} + P_{gen_{total}}) \times \frac{1}{0.68} \left(\frac{kg}{kW} \right) \times 2.205 \left(\frac{lb}{kg} \right) \quad (3.37)$$

the simplified calculation, with a weight scaling factor of $0.157 \left(\frac{lb}{hp_{total}} \right)$, indicates that approximately 2,972 lb of TMS weight is required for the HTS components in the 30-TF.

In the N3-X assumption [70], a different value is specified for the 2009 goal, which is set at 5 lb/hp_{input}. Assuming that all losses in the transmission system are dissipated in the form of heat, with losses given in Figure 3.17, the heat rejection percentages for the generator, rectifier/inverter, transmission line, and motor are 0.45%, 0.5%, 0.1%, and 0.48%, respectively. To estimate the total rejected power, it can be calculated based on the hover power required, and subsequently, the

weight can be determined using the estimated value of 5 lb/hp_{input} or 3.04 kg/kW_{input}. Additionally, a wire-only concept is included for both room temperature motor and HTS cable applications.

Table 3.6 30-TF concept Cryogenic TMS component size.

Loop Type	n	Technology	Rated Power [kW]	Rejected Power [kW]	Weight [kg]	Total Weight [kg]
Motor & Engine coolant loop	1	Cryo. N3-X	9483	90	274	897
Converter + Motor	2	Cryo. N3-X	4741	102	311	
Cable only for Helix motor	2	Cryo. N3-X	4741	9	29	29

Table 3.7 TMS weight summary and comparison.

	Technology Level	Total Power Rejected [kW]	Required Power [kW]	Weight		Curve Fit [kg]
				[kg]	[lb]	
STARC-ABL	baseline	572	0.2	198	437	199
	advanced	106	0.31	51	112	49
RVLT-Tiltwing	baseline	361	10.54	54	119	59
	advanced	90.6	3.81	27	59	19
PEGASUS	baseline	399	0.217	196	431	164
	advanced	243	0.3	139	306	128
30-TF (estimate)	baseline	1262	49	224	493	202
	advanced	337	15	103	227	66
	Cryo. N3-X	295	-	897	1978	-

The weight of the TMS system for the 30-TF concept is presented in Table 3.7 above, alongside the NASA concepts investigated in [79] for reference. The obtained result is found to be comparable to the weights of other aircraft studied in this context.

3.4.5 Battery Sizing

Although the scope of this study does not cover full electric concepts, battery pack is required for the turboelectric concept. Battery pack is required to accommodate for surge of power when climbing at high rate, maneuvering, or under engine/generator malfunctioning conditions.

Although not strictly a part of the transmission, the weight of battery is included in this study as a necessary subsystem when electric transmission is utilized.

Compared to HSVTOL, the 15-pax RVTL tiltwing concept has very similar configuration in hover, with similar considerations for battery usage. The battery sizing criteria mentioned in [56] is considered for sizing packs for HSVTOL, reserving 2 minutes of hovering time under OEI condition. The theoretical battery packs are composed of cells with 3.7V nominal voltage, connected in series to reach the motor operating voltage. If not an integer, the cell count is rounded up. The battery capacity required was then satisfied by increasing packs connected in parallel. Assumptions are made on battery specific energy, for two technology levels with different types of cells. The estimated specific energy of cell is obtained from conference paper regarding eVTOL technology considerations [71], where specific energies estimation at year 2012, 2017, 2027 are marked in Figure 3.20 over the energy density vs. specific energy plot for multiple battery chemistries. Li-ion 18650 battery with specific energy of $0.18 \text{ kW} \cdot \text{h/kg}$ is used for baseline design, silicone anode Li-ion cell with specific energy of $0.5 \text{ kW} \cdot \text{h/kg}$ [80] for advanced room temperature concept, and Li-Po battery advanced technology level at $0.65 \text{ kW} \cdot \text{h/kg}$ is used for the future HST concept.

The battery weight is estimated in two methods for the study. For the 18650 sized cells with current TRL, the cell weight is known because the cell dimension is constant. Capacity of cell is then calculated using given specific energy, while the pack capacity is the product of cell capacity and number of legs in parallel. The number of legs is modified to provide at least 2-min of hover time with one engine inoperative, note that the C-rate is also checked for all cases. For Li-Po batteries with custom pouch size, the capacity per cell is not constant, and building the pack to the minimum required capacity is plausible. Thus, a constant C-rating giving 2-min of OEI hover time

is used to calculate the pack capacity, and the pack can be break down into reasonable cell size. Since the nominal voltage remains the same, the number of cells in series is identical to the Li-ion concept. Weight of the battery pack can then be estimated, with known capacity, number of cells in series, and the given specific energy.

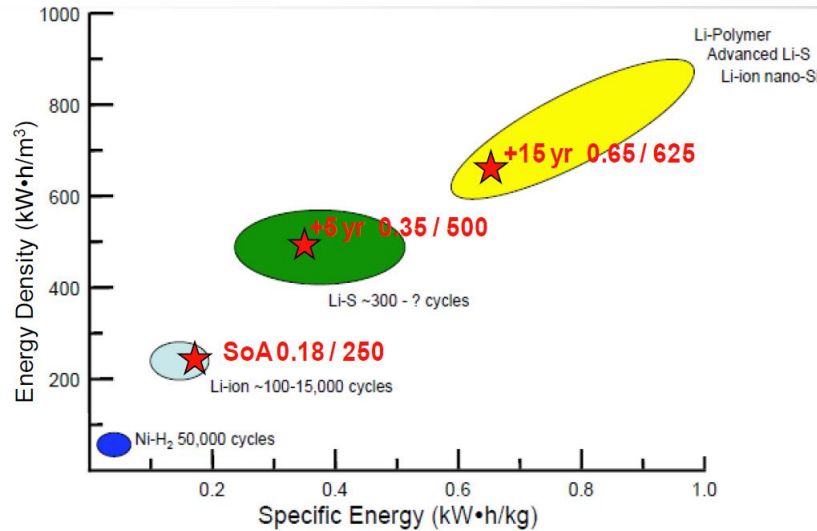


Figure 3.20 Battery specific energy and density trends [81].

Significant weight reduction can be observed by using pouch cells at any given voltage, see Section 4. The main factor of pack weight is specific energy. For smaller vehicles, the customizable size is also beneficial because the 18650 pack must be conservatively sized if total capacity is not matching with desired capacity.

3.4.6 Integration

In comparison to the relatively straightforward integration process of hydraulic transmission, sizing electric transmissions has become significantly more complex due to the rapid evolution in technology over recent years. Some concepts aimed at achieving maximum weight reduction

involve a mix of components at varying TRL. To facilitate a better understanding of the weight estimation results, Table 3.8 below provides a list of technology assumptions.

Table 3.8. Technology used for weight estimation.

	SOA DC	HTS GRC	Cryo. N3-X	Helix	Helix+ HTS
Motor Generator	OTS (Industrial)	GRC (HTS)	N3-X (Cryo. HTS)	OTS (Helix)	OTS (Helix)
Inverter	OTS (10 hp/lb)	Cryo. (14 hp/lb)	Cryo. (14 hp/lb)	Helix (30 hp/lb)	Helix (30 hp/lb)
Rotor Motor	OTS (Industrial)	GRC (HTS)	N3-X (Cryo. HTS)	OTS (Helix)	OTS (Helix)
Battery	Li-ion 18650 (.18kWh/kg)	2027 Li-Po (.65kWh/kg)	2027 Li-Po (.65kWh/kg)	2023 Li-ion (.50kWh/kg)	2023 Li-ion (.50kWh/kg)
Wire	HWC 263	HTS	Cryo. HTS	HWC 263	Cryo. HTS
Transmission Sup.	Baseline TMS	HTS TMS (linear [53])	Cryo. TMS (linear [70])	Advanced TMS	Advanced+ Cryo. TMS
Rotary union	OTS	OTS	OTS	OTS	OTS

The transmission support also encompasses the weight of circuit protection, which is estimated using 0.5 times the CableWeight from Table 5 in [53]. Another essential component for the tiltrotor is the slip ring coupling between the pylon and the wing. For the purpose of weight estimation, it is assumed that the inverter is located in the pylon, thus only two passages are required. Each ring is constructed from a segment of cable bent into a circle with a 6-inch diameter, ensuring that the brush maintains a minimum contact length of 1 inch with the ring. The width is adjusted based on the required conductor area/length in contact. This process, as described above, can be expressed in (3.38) for one slip ring unit, with the weight per length and area detailed in Section 3.4.3.

$$W_{rings}(lb) = 12\pi \times \frac{W}{l} \left(\frac{lb}{in} \right) \times 2 \frac{S(in^2)}{\sqrt{\frac{S(in^2)}{2\pi}}} \quad (3.38)$$

Table 3.9 Sample transmission weight estimated for 30-TF with hydrostatic transmission.

	Mechanical [13]	Electric (SOA DC)	Electric (HTS GRC)	Electric (Cryo. N3-X)	Electric (Helix)	Electric (Helix+HTS)
Centerbox	603.6	379	379	379	379	379
Mechanical Transmission	2,225.0	-	-	-	-	-
Motor Generator	-	5,697	803	316	599	599
Inverter	-	1,897	1,338	1,338	624	624
Engine Starter	113.6	-	-	-	-	-
Rotor Motor	-	6,107	1,015	729	599	599
Battery	-	1,260	348	348	452	452
Hose (wet) / Wire	-	1,271	320	64	1,271	64
Transmission Sup.	214.5	1,128	3,132	2,010	862	322
Pivot box	616.3	616	616	616	616	616
Rotary union	-	59	59	59	59	59
Mast	578.5	579	579	579	579	579
Pylon shaft	56.2	-	-	-	-	-
Wing Shaft	123.7	-	-	-	-	-
Total	4,531.4	18,993	8,589	6,438	6,039	4,292

By summing up the weights of all individual components, the total weight of the transmission system is determined, following a similar methodology to that of the hydraulic transmission system. As an illustrative example, Table 3.9 above presents such weight calculations, with the 30-TF HSVTOL concept serving as the baseline reference. It's important to note that certain configurations are already deemed excessively heavy and will subsequently be excluded from further analysis.

3.5 Scaling

The method presented in this paper is applied to a range of airframes with varying weights. The primary parameter affecting HSVTOL transmission is the hover power. While it is possible to estimate the power using the product of ideal power and an assumed figure of merit, a parametric sizing method is also provided. This method necessitates the provision of wing loading and disk

loading values, which may vary depending on cruise and hover conditions. For the 15-TF and 30-TF concepts, the wing loading is set at 120 pounds per square foot (psf), and the disk loading at 20 psf.

The relationship between the rotor radius (r) and half-span (b) can be calculated using the provided wing loading, disk loading, and aspect ratio (AR), derived from the fundamental equations below:

$$AR = \frac{b^2}{S}, \quad S = \frac{W}{WL}, \quad A_R = \frac{W}{n_{rotor} \cdot DL} = r^2 \cdot \pi \quad (3.39)$$

$$\frac{r}{b} = \frac{\sqrt{AR/\pi}}{\sqrt{S \cdot AR}} = \sqrt{\frac{WL}{DL} \times \frac{1}{n_{rotor} \cdot AR \cdot \pi}} \quad (3.40)$$

Conversely, the wing loading to disk loading ratio can be found using the relation below:

$$\frac{WL}{DL} = \left(\frac{r}{b}\right)^2 \times n_{rotor} \cdot AR \cdot \pi \quad (3.41)$$

When the width of the fuselage is unknown, a constant value for r/b or $r/(2b)$ is chosen as a reference. As depicted in Figure 3.21 below, this ratio for tiltrotor aircraft remains independent of takeoff weight, with an average value of around 7.81 across all collected concepts. Similarly, the aspect ratio of all tiltrotor aircraft, showing in Figure 3.22, demonstrates no dependency on aircraft weight and is likely limited by wing structure considerations. The average aspect ratio for tiltrotor aircraft is approximately 6.30, which can be utilized assuming no significant advancements in material or structural design.

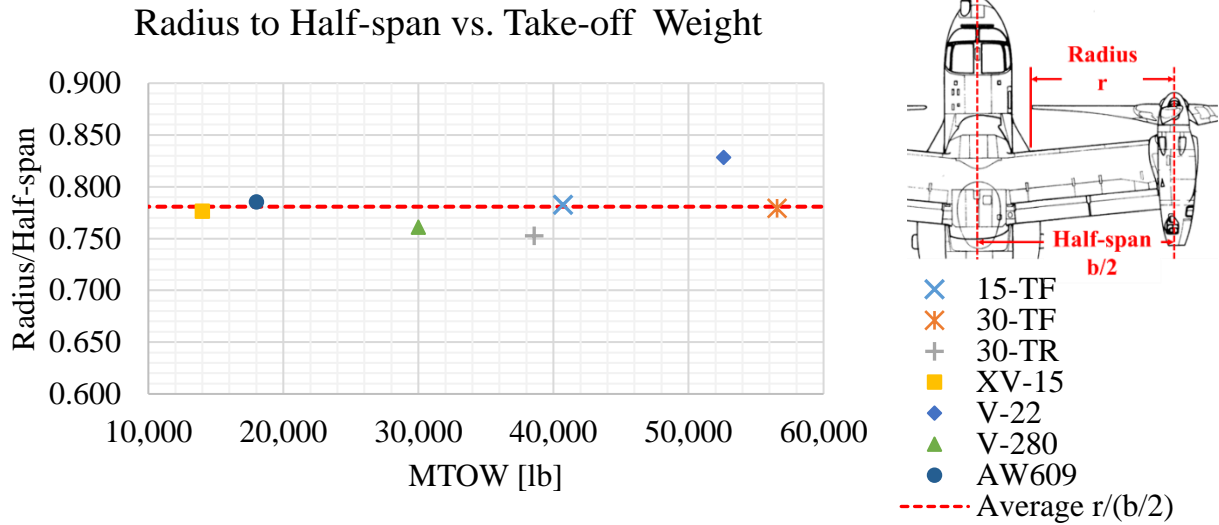


Figure 3.21 The radius to half-span ratio of various tiltrotor aircraft.

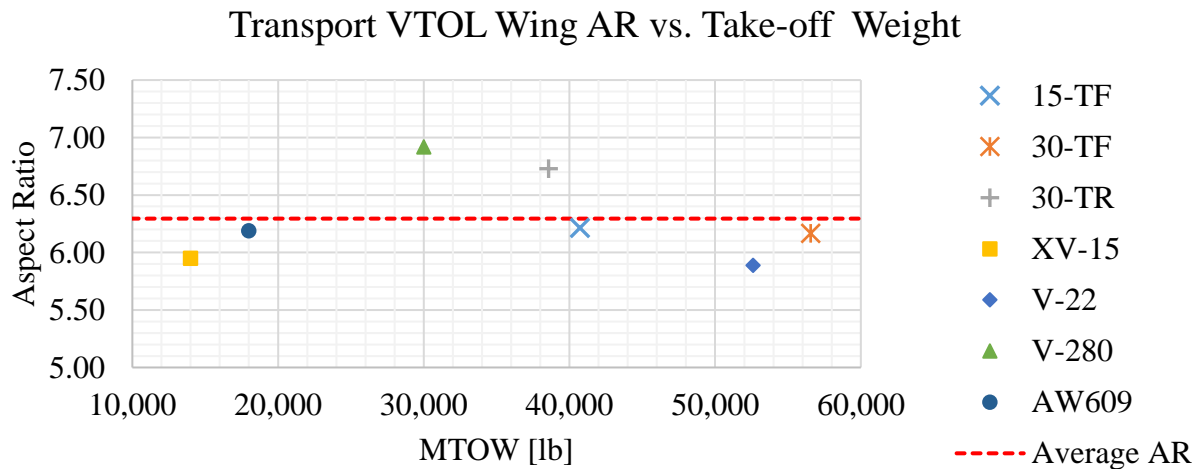


Figure 3.22 Aspect ratio of various tiltrotor aircraft (Figure A 6 - Figure A 9).

In the case of HSVTOL aircraft, especially when the application is similar to that of the V-22, the aircraft dimensions are likely to be constrained by various factors, such as operational conditions and other spatial limitations, as illustrated in Figure 3.23. This figure also indicates the clearance between the fuselage and rotor, which is 1 foot in airplane mode. To obtain a more accurate estimation, considering the cargo dimension requirements (height \times width \times length = 6.5'

$\times 8' \times 30'$ [18]), a better estimation can be made using the relationship $\frac{r}{b} = \frac{r - W_B - 2}{2b}$, where W_B represents the width of the fuselage body.

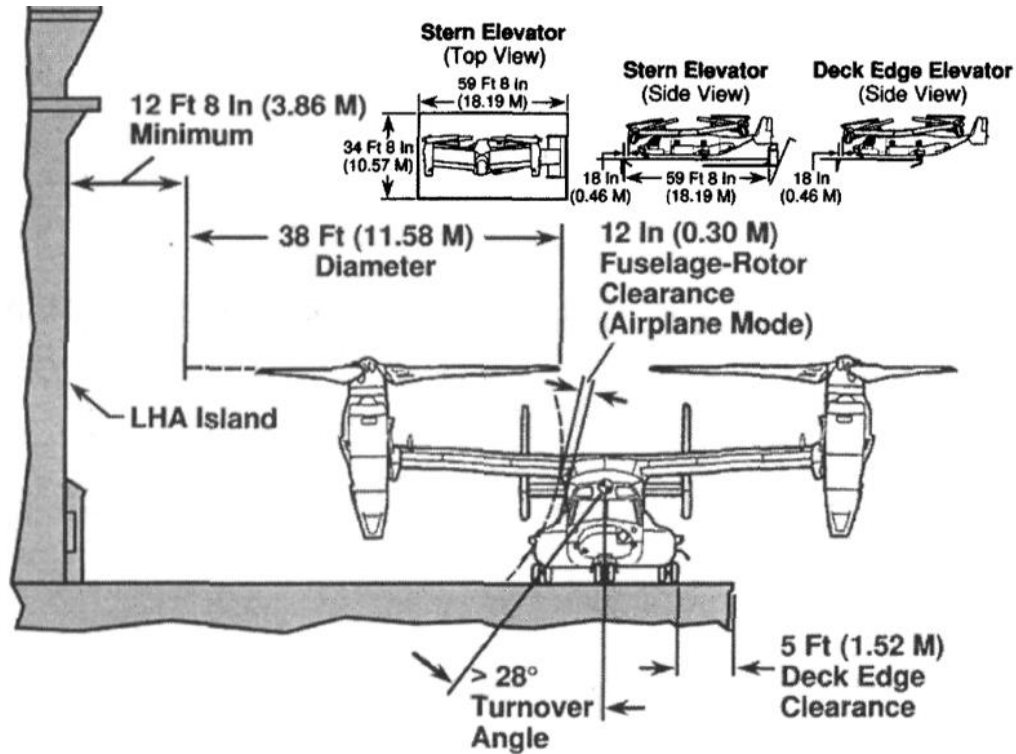


Figure 3.23 V-22 dimensions are defined by shipboard compatibility requirements [20].

This paper also examines a variety of airplane takeoff weights, and the method of calculating hover power using a constant disk loading and figure of merit is more suitable for such an analysis. In this study, it is assumed that the pump, motor, and generator are operating at the same engine, and rotor RPM, eliminating the need for a gearbox. However, in cases where torque is needed, it can be obtained by using rotor power divided by RPM, and the rotor speed can be determined by knowing the tip speed and radius, which can be calculated using Equation 3.40. The radius is provided in the results, assuming standard sea level density with a tip Mach number of 0.7, wing loading of 120 psf, and disk loading of 20 psf.

4 Results

The following section showcases the results achieved through the methodologies outlined in Section 3. The tables presented below provide the raw data for comparison against the baseline mechanical transmission, specifically the 30-TF and 15-TF concepts. The results are organized in the following sequence: weight in pounds, weight fraction relative to the Maximum Takeoff Weight (MTOW), component percentage weight relative to the transmission system weight, and the battery configurations for the electrical transmission.

4.1 30-TF Transmission Weight Results

The weight breakdown for 30 and 15-TF are provided in Table 4.1 and Table 4.5. All concepts are included, with the components labeled to the left of the table.

Table 4.1 Weight of various transmission comparing to 30-TF HSVTOL baseline.

30-TF Drive System Weight (lb) Comparison								
	Baseline [13]	Hyd. (Fixed motor)	Hyd. (Tilt motor)	Electric (SOA DC)	Electric (HTS GRC)	Electric (Cryo. N3-X)	Electric (Helix)	Electric (Helix+ HTS)
Centerbox	603.6	379	379	379	379	379	379	379
Mechanical Transmission	2,225.0	-	-	-	-	-	-	-
Hydrostatic Pump	-	950	950	-	-	-	-	-
Motor Generator	-	-	-	5,697	803	316	599	599
Inverter	-	-	-	1,897	1,338	1,338	624	624
Engine Starter	113.6	114	114	-	-	-	-	-
Rotor Motor	-	1,818	1,818	6,107	1,015	729	599	599
Battery	-	-	-	1,260	348	348	452	452
Hose (wet) / Wire	-	900	900	1,271	320	64	1,271	64
Transmission Sup.	214.5	722	722	1,128	3,132	2,010	862	322
Pivot box	616.3	616	616	616	616	616	616	616
Pivot Gearbox	-	1,548	-	-	-	-	-	-
Rotary union	-	-	291	59	59	59	59	59
Mast	578.5	579	579	579	579	579	579	579
Pylon shaft	56.2	56	-	-	-	-	-	-
Wing Shaft	123.7	-	-	-	-	-	-	-
Total	4,531.4	7,682	6,369	18,993	8,589	6,438	6,039	4,292

The total transmission system weight is color-coded in ascending order from green to red, with green representing the lightest and red the heaviest. The weight fraction of components and the total transmission system is provided below in Table 4.2. The same table is generated for 15-TF, provided in Table 4.6.

Table 4.2 Weight fraction of various transmission system comparing to 30-TF baseline.

30-TF Drive System Overall Weight Fraction (Component/MTOW)								
	Baseline	Hyd. (Fixed motor)	Hyd. (Tilt motor)	Electric (SOA DC)	Electric (HTS GRC)	Electric (Cryo. N3-X)	Electric (Helix)	Electric (Helix+ HTS)
Centerbox	0.0107	0.0067	0.0067	0.0067	0.0067	0.0067	0.0067	0.0067
Mechanical Transmission	0.0393	-	-	-	-	-	-	-
Hydrostatic Pump	-	0.0168	0.0168	-	-	-	-	-
Motor Generator	-	-	-	0.1007	0.0142	0.0056	0.0106	0.0106
Inverter	-	-	-	0.0335	0.0237	0.0237	0.0110	0.0110
Engine Starter	0.0020	0.0020	0.0020	-	-	-	-	-
Rotor Motor	-	0.0321	0.0321	0.1080	0.0180	0.0129	0.0106	0.0106
Battery	-	-	-	0.0223	0.0062	0.0062	0.0080	0.0080
Hose (wet) / Wire	-	0.0159	0.0159	0.0225	0.0057	0.0011	0.0225	0.0011
Transmission Sup.	0.0038	0.0128	0.0128	0.0199	0.0554	0.0355	0.0152	0.0057
Pivot box	0.0109	0.0109	0.0109	0.0109	0.0109	0.0109	0.0109	0.0109
Pivot Gearbox	-	0.0274	-	-	-	-	-	-
Rotary union	-	-	0.0051	0.0010	0.0010	0.0010	0.0010	0.0010
Mast	0.0102	0.0102	0.0102	0.0102	0.0102	0.0102	0.0102	0.0102
Pylon shaft	0.0010	0.0010	-	-	-	-	-	-
Wing Shaft	0.0022	-	-	-	-	-	-	-
Total	0.0801	0.1358	0.1126	0.3358	0.1518	0.1138	0.1068	0.0759

The percentage weight of each component over the transmission system helps identify the parts with major weight impact, as shown in Table 4.3 and Table 4.7. The battery specifications are also listed in Table 4.4 and Table 4.8 for 30 and 15-TF HSVTOL.

Table 4.3 Percentage component weight of transmission for 30-TF HSVTOL.

30-TF Drive System Component Percentage Weight (Component/Transmission system)								
	Baseline	Hyd. (Fixed motor)	Hyd. (Tilt motor)	Electric (SOA DC)	Electric (HTS GRC)	Electric (Cryo. N3-X)	Electric (Helix)	Electric (Helix+ HTS)
Centerbox	13.32%	4.94%	5.96%	2.00%	4.42%	5.89%	6.28%	8.84%
Mechanical Transmission	49.10%	0.00%	0.00%	0.00%	0.00%	0.00%	0.00%	0.00%
Hydrostatic Pump	0.00%	12.37%	14.92%	0.00%	0.00%	0.00%	0.00%	0.00%
Motor Generator	0.00%	0.00%	0.00%	30.00%	9.35%	4.91%	9.92%	13.95%
Inverter	0.00%	0.00%	0.00%	9.99%	15.58%	20.79%	10.33%	14.53%
Engine Starter	2.51%	1.48%	1.78%	0.00%	0.00%	0.00%	0.00%	0.00%
Rotor Motor	0.00%	23.66%	28.54%	32.16%	11.82%	11.33%	9.92%	13.95%
Battery	0.00%	0.00%	0.00%	6.63%	4.05%	5.40%	7.49%	10.54%
Hose (wet) / Wire	0.00%	11.72%	14.14%	6.69%	3.73%	0.99%	21.04%	1.48%
Transmission Sup.	4.73%	9.40%	11.34%	5.94%	36.46%	31.22%	14.27%	7.51%
Pivot box	13.60%	8.02%	9.68%	3.24%	7.18%	9.57%	10.21%	14.36%
Pivot Gearbox	0.00%	20.15%	0.00%	0.00%	0.00%	0.00%	0.00%	0.00%
Rotary union	0.00%	0.00%	4.57%	0.31%	0.68%	0.91%	0.97%	1.37%
Mast	12.77%	7.53%	9.08%	3.05%	6.74%	8.99%	9.58%	13.48%
Pylon shaft	1.24%	0.73%	0.00%	0.00%	0.00%	0.00%	0.00%	0.00%
Wing Shaft	2.73%	0.00%	0.00%	0.00%	0.00%	0.00%	0.00%	0.00%

Table 4.4 Different types of batteries sized for the 30-TF concept.

24P 18650 @Nominal 3.7V, 0.18 kW · h/kg		
# of Cell Per Leg	Total # of Cells	Mass per cell [g]
541	12984	44
Total mass [lb]	1259.71	
Battery Cap [Ah]	51.37	
Hover C rating	29.92	
W _{battery} /GW (ref 0.026)	0.022	
Battery Hover Time [min]	2.01	
10P pouch Li-ion @Nominal 3.7V, 0.5 kW · h/kg		
# of Cell Per Leg	Total # of Cells	Cell Capacity [Ah]
541	5410	5.12
Total mass [lb]	452.34	
Battery Cap [Ah]	51.24	
Hover C rating	30.00	
W _{battery} /GW (ref 0.026)	0.008	
Battery Hover Time [min]	2.00	
10P advanced Li-Po @Nominal 3.7V, 0.65 kW · h/kg		
# of Cell Per Leg	Total # of Cells	Cell Capacity [Ah]
541	5410	5.12
Total mass [lb]	347.96	
Battery Cap [Ah]	51.24	
Hover C rating	30.00	
W _{battery} /GW (ref 0.026)	0.006	
Battery Hover Time [min]	2.00	

4.2 15-TF Transmission Weight

Table 4.5 Weight of various transmission comparing to 15-TF HSVTOL baseline.

15-TF Drive System Weight (lb) Comparison								
	Baseline [13]	Hyd. (Fixed motor)	Hyd. (Tilt motor)	Electric (SOA DC)	Electric (HTS GRC)	Electric (Cryo. N3-X)	Electric (Helix)	Electric (Helix+ HTS)
Centerbox	525.5	271	271	271	271	271	271	271
Mechanical Transmission	1,533.1	-	-	-	-	-	-	-
Hydrostatic Pump	-	679	679	-	-	-	-	-
Motor Generator	-	-	-	4,214	643	226	480	480
Inverter	-	-	-	1,356	957	957	446	446
Engine Starter	104.3	104	104	-	-	-	-	-
Rotor Motor	-	1,316	1,316	4,517	813	522	480	480
Battery	-	-	-	945	249	249	323	323
Hose (wet) / Wire	-	587	587	612	154	39	612	39
Transmission Sup.	137.8	516	516	659	2,202	1,434	468	227
Pivot box	536.5	537	537	537	537	537	537	537
Pivot Gearbox	-	949	-	-	-	-	-	-
Rotary union	-	-	243	25	25	25	25	25
Mast	370.6	371	371	371	371	371	371	371
Pylon shaft	48.7	49	-	-	-	-	-	-
Wing Shaft	107.0	-	-	-	-	-	-	-
Total	3,363.5	5,378	4,624	13,506	6,222	4,630	4,013	3,198

Table 4.6 Weight fraction of various transmission system comparing to 15-TF baseline.

15-TF Drive System Overall Weight Fraction (Component/MTOW)								
	Baseline	Hyd. (Fixed motor)	Hyd. (Tilt motor)	Electric (SOA DC)	Electric (HTS GRC)	Electric (Cryo. N3-X)	Electric (Helix)	Electric (Helix+ HTS)
Centerbox	0.0129	0.0067	0.0067	0.0067	0.0067	0.0067	0.0067	0.0067
Mechanical Transmission	0.0377	-	-	-	-	-	-	-
Hydrostatic Pump	-	0.0167	0.0167	-	-	-	-	-
Motor Generator	-	-	-	0.1035	0.0158	0.0056	0.0118	0.0118
Inverter	-	-	-	0.0333	0.0235	0.0235	0.0110	0.0110
Engine Starter	0.0026	0.0026	0.0026	-	-	-	-	-
Rotor Motor	-	0.0323	0.0323	0.1109	0.0200	0.0128	0.0118	0.0118
Battery	-	-	-	0.0232	0.0061	0.0061	0.0079	0.0079
Hose (wet) / Wire	-	0.0144	0.0144	0.0150	0.0038	0.0010	0.0150	0.0010
Transmission Sup.	0.0034	0.0127	0.0127	0.0162	0.0541	0.0352	0.0115	0.0056
Pivot box	0.0132	0.0132	0.0132	0.0132	0.0132	0.0132	0.0132	0.0132
Pivot Gearbox	-	0.0233	-	-	-	-	-	-
Rotary union	-	-	0.0060	0.0006	0.0006	0.0006	0.0006	0.0006
Mast	0.0091	0.0091	0.0091	0.0091	0.0091	0.0091	0.0091	0.0091
Pylon shaft	0.0012	0.0012	-	-	-	-	-	-
Wing Shaft	0.0026	-	-	-	-	-	-	-
Total	0.0826	0.1321	0.1136	0.3317	0.1528	0.1137	0.0986	0.0786

Table 4.7 Percentage component weight of transmission for 15-TF HSVTOL.

15-TF Drive System Component Percentage Weight (Component/Transmission system)								
	Baseline	Hyd. (Fixed motor)	Hyd. (Tilt motor)	Electric (SOA DC)	Electric (HTS GRC)	Electric (Cryo. N3-X)	Electric (Helix)	Electric (Helix+ HTS)
Centerbox	15.62%	5.04%	5.87%	2.01%	4.36%	5.86%	6.76%	8.48%
Mechanical Transmission	45.58%	0.00%	0.00%	0.00%	0.00%	0.00%	0.00%	0.00%
Hydrostatic Pump	0.00%	12.63%	14.69%	0.00%	0.00%	0.00%	0.00%	0.00%
Motor Generator	0.00%	0.00%	0.00%	31.20%	10.34%	4.88%	11.96%	15.00%
Inverter	0.00%	0.00%	0.00%	10.04%	15.38%	20.67%	11.11%	13.94%
Engine Starter	3.10%	1.94%	2.26%	0.00%	0.00%	0.00%	0.00%	0.00%
Rotor Motor	0.00%	24.47%	28.46%	33.44%	13.07%	11.27%	11.96%	15.00%
Battery	0.00%	0.00%	0.00%	7.00%	4.00%	5.37%	8.06%	10.11%
Hose (wet) / Wire	0.00%	10.90%	12.68%	4.53%	2.48%	0.84%	15.26%	1.22%
Transmission Sup.	4.10%	9.60%	11.16%	4.88%	35.39%	30.97%	11.67%	7.10%
Pivot box	15.95%	9.97%	11.60%	3.97%	8.62%	11.59%	13.37%	16.77%
Pivot Gearbox	0.00%	17.64%	0.00%	0.00%	0.00%	0.00%	0.00%	0.00%
Rotary union	0.00%	0.00%	5.26%	0.18%	0.40%	0.53%	0.62%	0.77%
Mast	11.02%	6.89%	8.01%	2.74%	5.96%	8.00%	9.24%	11.59%
Pylon shaft	1.45%	0.91%	0.00%	0.00%	0.00%	0.00%	0.00%	0.00%
Wing Shaft	3.18%	0.00%	0.00%	0.00%	0.00%	0.00%	0.00%	0.00%

Table 4.8 Different types of batteries sized for the 15-TF concept.

18P 18650 @Nominal 3.7V, 0.18 kW · h/kg		
# of Cell Per Leg	Total # of Cells	Mass per cell [g]
541	9738	44
Total mass [lb]	944.78	
Battery Cap [Ah]	38.53	
Hover C rating	28.53	
W _{battery} /GW (ref 0.026)	0.023	
Battery Hover Time [min]	2.10	
7P pouch Li-ion @Nominal 3.7V, 0.5 kW · h/kg		
# of Cell Per Leg	Total # of Cells	Cell Capacity [Ah]
541	3787	5.24
Total mass [lb]	323.49	
Battery Cap [Ah]	36.65	
Hover C rating	30.00	
W _{battery} /GW (ref 0.026)	0.008	
Battery Hover Time [min]	2.00	
7P advanced Li-Po @Nominal 3.7V, 0.65 kW · h/kg		
# of Cell Per Leg	Total # of Cells	Cell Capacity [Ah]
541	3787	5.24
Total mass [lb]	248.84	
Battery Cap [Ah]	36.65	
Hover C rating	30.00	
W _{battery} /GW (ref 0.026)	0.006	
Battery Hover Time [min]	2.00	

4.3 Trend of Transmission Weight

The trend of transmission weight is graphically represented below in relation to the takeoff weight. Given the constant values of DL and FM, the relationship between power and weight can be approximated as linear using (3.5). Therefore, plotting the transmission weight in relation to power is unnecessary. The parameters utilized for weight estimation are listed in Table 4.9 below. It is worth noting that all designs feature two rotors, and the listed values for radius and torque pertain to each individual rotor, while the power value represents the total power.

Table 4.9 The design parameter used for a range of MTOW in pounds.

MTOW	5000	10000	20000	40000	60000	80000
Span [ft]	16.19	22.90	32.39	45.81	56.10	64.78
Length [ft]	18.41	26.04	36.83	52.08	63.78	73.65
Power [hp]	8.37E+02	1.67E+03	3.35E+03	6.70E+03	1.00E+04	1.34E+04
Radius [ft]	6.31	8.92	12.62	17.84	21.85	25.23
RPM	1183	837	592	418	342	296
Torque [lbft]	1.85E+03	5.23E+03	1.48E+04	4.18E+04	7.68E+04	1.18E+05

As illustrated in Figure 4.1, the transmission weight trend in relation to the takeoff weight is depicted, along with the curve-fitted equations provided within the plot. In Figure 4.2, the weight fractions are plotted to assist in understanding the overall curvature of the transmission system weight concerning the maximum vertical takeoff weight. These figures will be further analyzed in the subsequent section.

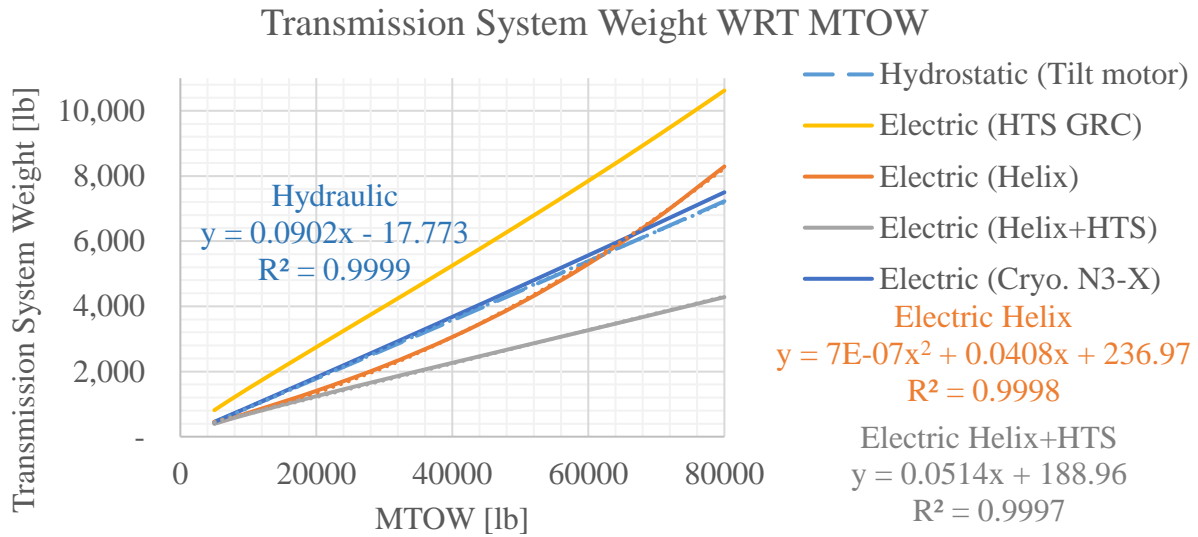


Figure 4.1 The transmission weight versus maximum vertical takeoff weight.

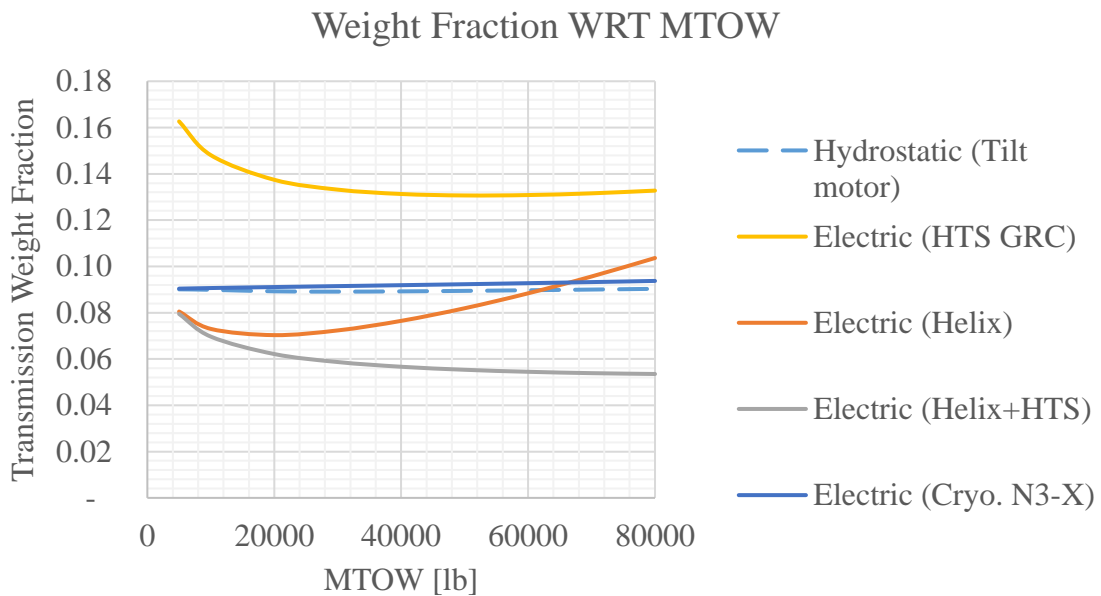


Figure 4.2 The transmission weight fraction versus maximum vertical takeoff weight.

The study also delves into the influence of individual component weights on the overall weight. Presented below are tables displaying the percentage weight of all components relative to the transmission system weight across a range of takeoff weights. These tables employ color-coding

based on magnitude, where red indicates higher values and green represents lower values. Table 4.10 through Table 4.13 provides the values for transmission system using hydrostatic, HTS GRC, Cryogenic N3-X, non-Cryogenic Helix, and HTS Helix. The corresponding plots are Figure 4.3 to Figure 4.7. The change in color signifies the shift in the dominance of components as the weight varies. The plots are also presented along with the tables for a visual representation of the data.

Table 4.10 The hydraulic component weight out of the total system weight.

Hydrostatic (Tilt motor)									
MTOW	5000	10000	20000	30000	40000	50000	60000	70000	80000
Centerbox	7%	7%	8%	8%	8%	7%	7%	7%	7%
Pump	19%	19%	19%	19%	19%	19%	19%	19%	19%
Rotor Motor	39%	38%	37%	37%	36%	36%	36%	35%	35%
Hose (wet) / Wire	8%	10%	13%	15%	16%	17%	18%	19%	20%
Support	14%	14%	14%	14%	14%	14%	14%	14%	14%
Rotary union	13%	11%	9%	8%	7%	6%	6%	5%	5%

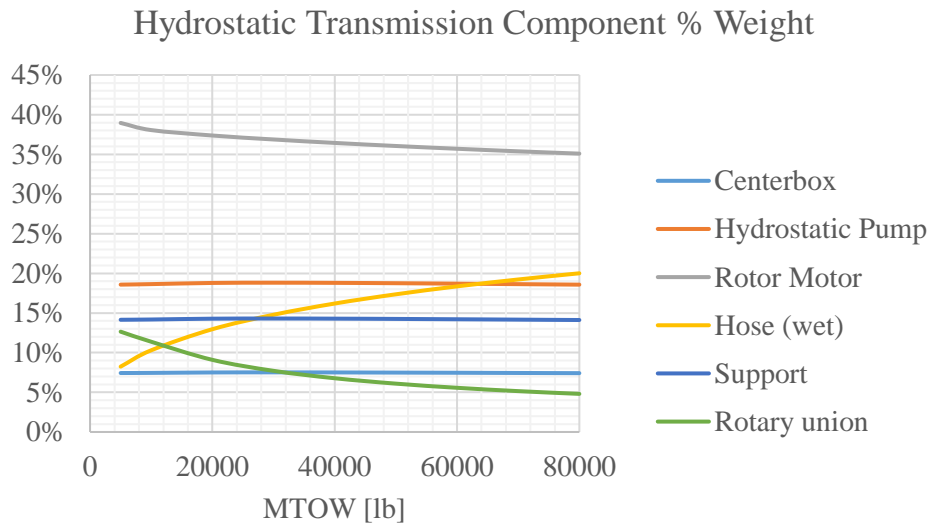


Figure 4.3 Trend of hydrostatic transmission component percentage weight.

Table 4.11 The percentage transmission component weight using HTS GRC components.

Electric (HTS GRC)									
MTOW	5000	10000	20000	30000	40000	50000	60000	70000	80000
Centerbox	4%	5%	5%	5%	5%	5%	5%	5%	5%
Motor Generator	20%	17%	15%	13%	12%	11%	11%	10%	10%
Inverter	15%	16%	17%	18%	18%	18%	18%	18%	18%
Rotor Motor	25%	22%	19%	17%	15%	14%	13%	13%	12%
Battery	4%	4%	4%	5%	5%	5%	5%	5%	5%
Hose (wet) / Wire	0%	1%	1%	2%	3%	4%	5%	6%	7%
Support	32%	36%	39%	40%	41%	42%	42%	43%	43%
Rotary union	0%	0%	0%	0%	0%	1%	1%	1%	1%

HTC GRC Transmission Component % Weight

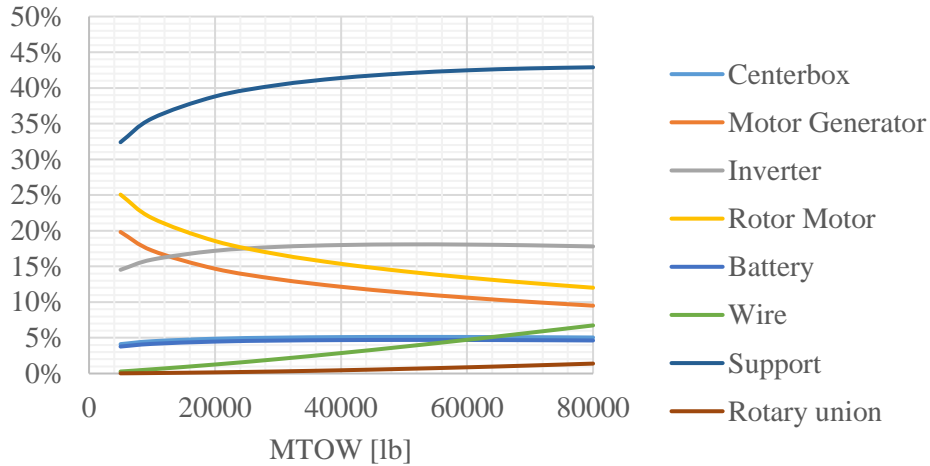


Figure 4.4 Trend of HTC GRC transmission component percentage weight.

Table 4.12 The percentage transmission component weight using N3-X assumption.

Electric (Cryo. N3-X)									
MTOW	5000	10000	20000	30000	40000	50000	60000	70000	80000
Centerbox	7%	7%	7%	7%	7%	7%	7%	7%	7%
Motor Generator	6%	6%	6%	6%	6%	6%	6%	6%	6%
Inverter	26%	26%	26%	26%	26%	26%	25%	25%	25%
Rotor Motor	14%	14%	14%	14%	14%	14%	14%	14%	14%
Battery	7%	7%	7%	7%	7%	7%	7%	7%	7%
Hose (wet) / Wire	0%	1%	1%	1%	1%	1%	1%	1%	1%
Support	39%	39%	39%	39%	39%	38%	38%	38%	38%
Rotary union	0%	0%	0%	0%	1%	1%	1%	2%	2%

Cryo. N3-X Transmission Component % Weight

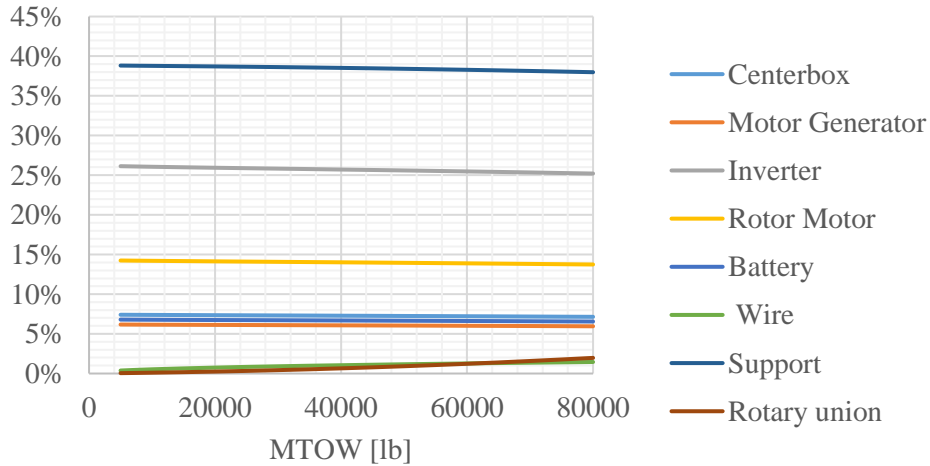


Figure 4.5 Trend of transmission component percentage weight with N3-X assumption.

Table 4.13 The percentage transmission component weight using Helix motor.

Electric (Helix)									
MTOW	5000	10000	20000	30000	40000	50000	60000	70000	80000
Centerbox	8%	9%	10%	9%	9%	8%	8%	7%	6%
Motor Generator	30%	26%	21%	18%	16%	13%	12%	10%	9%
Inverter	14%	15%	16%	15%	14%	13%	12%	12%	11%
Rotor Motor	30%	26%	21%	18%	16%	13%	12%	10%	9%
Battery	10%	11%	11%	11%	10%	10%	9%	8%	8%
Hose (wet) / Wire	2%	5%	10%	15%	20%	24%	28%	31%	34%
Support	6%	8%	11%	13%	15%	17%	18%	20%	21%
Rotary union	0%	0%	0%	1%	1%	1%	1%	2%	2%

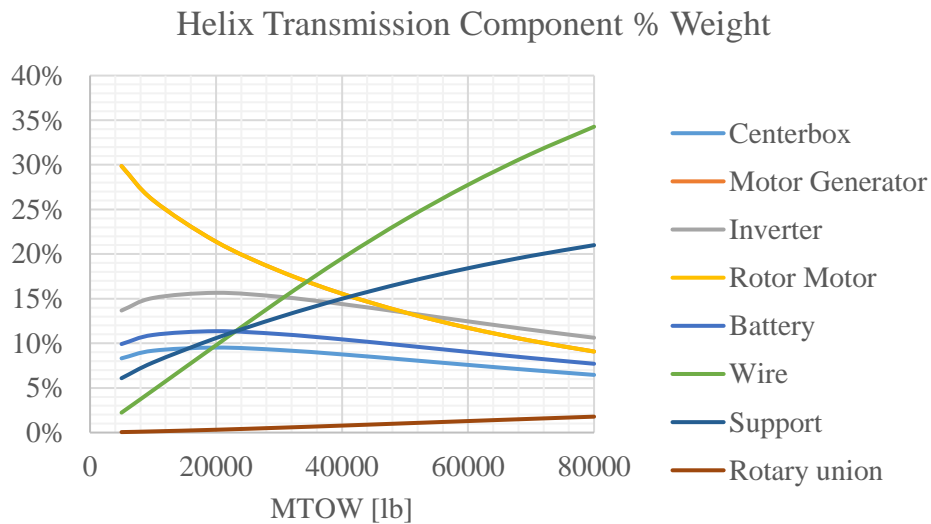


Figure 4.6 Trend of transmission component percentage weight using Helix motor.

Table 4.14 The percentage component weight using Helix motor + HTS wire.

Electric (Helix + HTS)									
MTOW	5000	10000	20000	30000	40000	50000	60000	70000	80000
Centerbox	8%	10%	11%	11%	12%	12%	12%	12%	13%
Motor Generator	30%	27%	24%	22%	21%	20%	19%	18%	18%
Inverter	14%	16%	18%	19%	19%	20%	20%	20%	21%
Rotor Motor	30%	27%	24%	22%	21%	20%	19%	18%	18%
Battery	10%	11%	13%	14%	14%	14%	15%	15%	15%
Hose (wet) / Wire	0%	1%	1%	1%	2%	2%	2%	2%	3%
Support	7%	8%	9%	9%	10%	10%	10%	11%	11%
Rotary union	0%	0%	0%	1%	1%	2%	2%	3%	3%

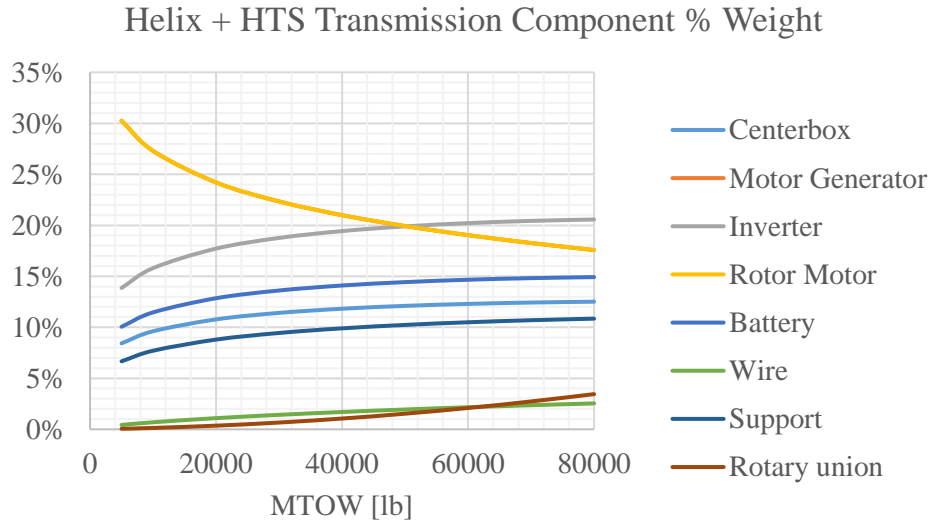


Figure 4.7 Trend of transmission component percentage weight using Helix & HTS.

4.4 Comparison

The results are compared against the transmission weight trends of the HSVTOL baseline design and helicopter transmission systems. The weight of the helicopter transmission system is obtained from [82].

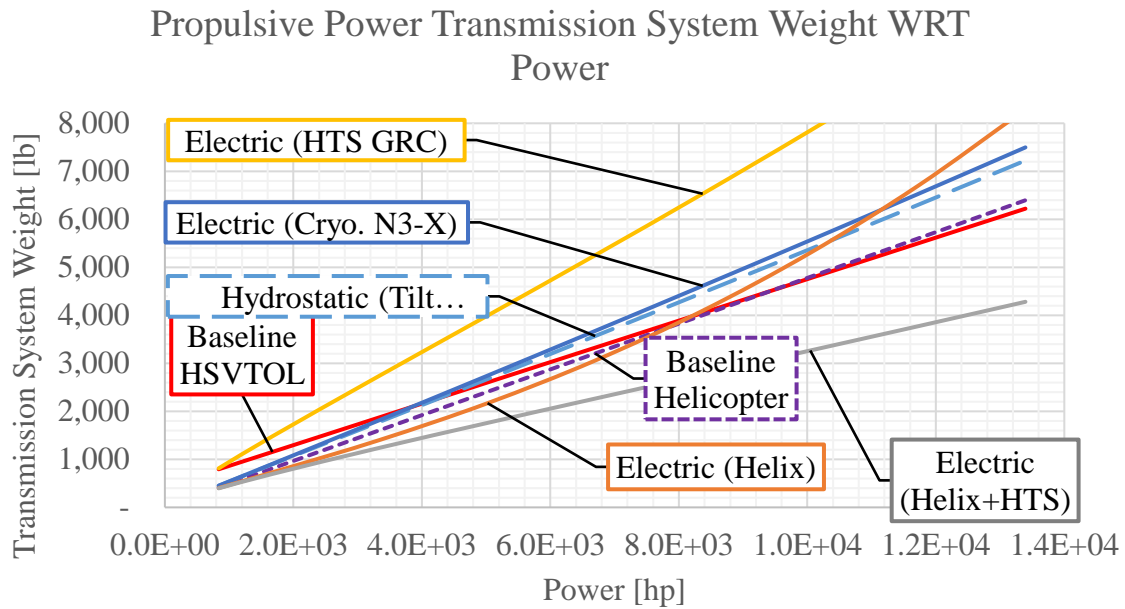


Figure 4.8 Transmission weight trend WRT total power.

Table 4.15 Power transmission weight scaling equation WRT power.

Power Transmission Concept	Transmission Weight WRT Power
Mechanical Baseline HSVTOL	$W_{PT} = 0.4323 \cdot P_{total} + 431.48$
Mechanical Baseline Helicopters	$W_{PT} = 0.4765 \cdot P_{total} + 14.697$
Hydrostatic	$W_{PT} = 0.4765 \cdot P_{total} + 14.697$
GRC HTS Electric	$W_{PT} = 0.7741 \cdot P_{total} + 132.72$
N3-X Cryo. Electric	$W_{PT} = 0.5604 \cdot P_{total} - 48.898$
Helix Motor with Un-cooled Cable	$W_{PT} = 3E - 05 \cdot P_{total}^2 + 0.2438 \cdot P_{total} + 236.97$
Helix Motor with HTS Cable	$W_{PT} = 0.3068 \cdot P_{total} + 188.96$

5 Discussions, Conclusions, and Recommendations

This section analyzes the results obtained in the previous section and utilizes the findings to draw conclusions. The main focus is on the impact on weight of the transmission components using various groups of technologies.

5.1 Discussion

The mechanical transmission system for High-Speed Vertical Takeoff and Landing (HSVTOL) aircraft accounts for approximately 8% of the maximum takeoff weight and roughly 11% of the empty weight. This close relationship between the weight of the transmission system and the power required forms a design loop where changes in takeoff weight affect power, power alterations impact transmission weight, and the transmission weight, in turn, adds to the takeoff weight.

In this study, by assuming that the available power remains constant, different technologies are explored to assess their impact on the transmission weight. The implementation of hydrostatic transmission utilizing a turbine-speed pump and radial piston motor eliminates the need for a reduction gearbox in the system. Additionally, the use of electric motors and generators offers greater flexibility in motor placement. These concepts are compared against HSVTOL designs employing traditional mechanical transmission technology.

The scaling curves for mechanical, hydraulic, and electric transmission systems intersect as the MTOW varies. Based on the assumptions detailed in the methodology, it becomes evident that the hydraulic transmission system is approximately 40.5% heavier than the baseline mechanical transmission system for the 30-TF concept and 37.5% heavier for the 15-TF concept. The mechanical transmission system exhibits lower weight for MTOW values below 23,114 lb, specifically at 4,226 hp.

In contrast, the electric transmission system employing the Helix motor and room temperature cable is 33.3% heavier for the 30-TF concept and 19.3% heavier for the 15-TF concept. The electrical transmission at 2kV with room temperature components is lighter when the MTOW is under 50,577 lb and requires 7,186 hp. However, with cryogenic cooling and superconductive cables, the configuration utilizing the Helix motor consistently maintains a lighter weight compared to the baseline, with the gap increasing as MTOW varies.

The trend of the transmission system concerning weight or power required is generally linear for most concepts, as depicted in Figure 5.1 and Table 5.1. The only exception arises with the electrical transmission employing room temperature cables, where the cable weight increases exponentially and begins to dominate the overall system weight. The contribution of each component varies as weight increases. In the case of hydraulic transmission, the motor consistently holds the heaviest weight and remains the most substantial component. The weight of the rotary union has a diminishing influence as weight increases, while the hoses contribute a larger fraction to the overall weight.

In contrast, the cryogenically cooled electrical transmission exhibits different characteristics, with the motor, generator, and cables being relatively light, while the cooling components are notably heavy. Across a range of takeoff weights, the fraction of transmission support, inverter, and cable increases, whereas the motor and generator fractions decrease. A similar trend is observed for room temperature electrical transmission, where the motor and generator fractions are identical and decrease as weight increases. However, in this case, the cable weight eventually dominates the overall weight. Notably, this does not occur when only the cables are cryogenically cooled using HTS technology, and the other components remain uncooled.

Propulsive Power Transmission System Weight WRT MTOW

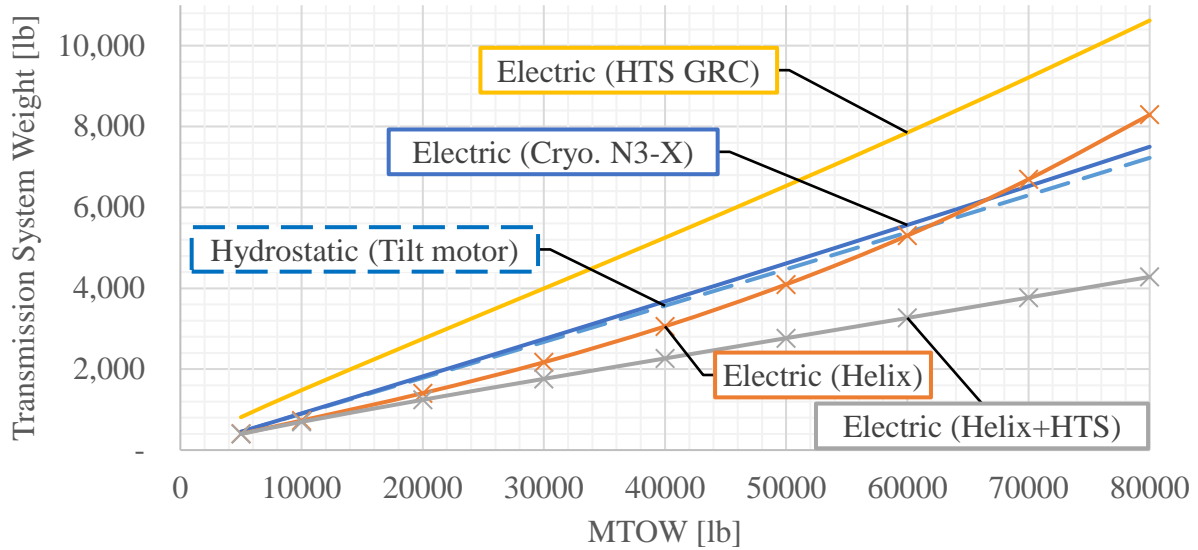


Figure 5.1 Power transmission weight trend of all the reviewed concepts.

Table 5.1 Scaling equation of HSVTOL power transmission weight.

Power Transmission Concept	Transmission Weight Scaling Equation
Mechanical Baseline	$W_{PT} = 0.0737 \cdot MTOW + 363.6$
Hydrostatic	$W_{PT} = 0.0902 \cdot MTOW - 17.773$
GRC HTS Electric	$W_{PT} = 0.1296 \cdot MTOW + 132.72$
N3-X Cryo. Electric	$W_{PT} = 0.0938 \cdot MTOW - 48.898$
Helix Motor with Un-cooled Cable	$W_{PT} = 7E - 07 \cdot MTOW^2 + 0.0408 \cdot MTOW - 0.048$
Helix Motor with HTS Cable	$W_{PT} = 0.0514 \cdot MTOW + 188.96$

5.2 Conclusions

The study's results indicate that, despite notable advancements in hydraulic and electric transmission technologies, mechanical transmission systems remain the most favorable choice in terms of weight-to-power ratios for heavy High-Speed Vertical Takeoff and Landing (HSVTOL)

aircraft. While hydraulic and electric transmission systems may be suitable for smaller vehicles with lower hover power requirements, offering benefits such as reduced mechanical complexity and enhanced rotor placement flexibility, the decision between mechanical, hydraulic, and electric transmission depends on specific mission requirements.

It is important to note that the tipping point at which one transmission technology becomes more advantageous than another is contingent upon the precise demands of the mission. The study primarily focused on the HSVTOL concept, maintaining constant wing loading and disc loading for the specified mission. However, the equations presented in the methodology extend beyond this specific context and can be applied to any airframe with distinct design requirements. Additionally, as technology continues to advance, these equations can be adapted to incorporate future developments in convertible transmission systems.

In summary, the weight and power considerations explored in this study provide valuable insights for optimizing transmission systems of convertible aircraft design. These findings have relevance for a wide range of concepts and missions. The pursuit of more efficient, lighter, and technologically advanced transmission systems remains an ongoing endeavor, and this research serves as a valuable step toward achieving these objectives.

REFERENCES

- [1] M. Maisel, "Lincoln EAA Chapter 1541: A Brief History of the Tilt Rotor Aircraft – Part 1 – The Beginning," April 2017. [Online]. Available: <https://eaa1541.org/members/newsletters/april-2017/a-brief-history-of-the-tilt-rotor-aircraft-part-1-the-beginning/>. [Accessed October 2023].
- [2] M. Maisel, "A Brief History of the Tilt Rotor Aircraft – Part 2 – The XV-3," May 2017. [Online]. Available: <https://eaa1541.org/members/newsletters/may-2017/a-brief-history-of-the-tilt-rotor-aircraft-part-2-the-xv-3/>. [Accessed 2023].
- [3] The Vertical Flight Society, "V/STOL Aircraft and Propulsion Concepts - Lockheed XFV-1," [Online]. Available: <https://vtol.org/vstol/VSTOLWheel/LockheedXFV-1.htm>. [Accessed 2023].
- [4] D. Gibbings, Fairey Rotodyne, Dublin, Ireland: The History Press, 2011.
- [5] The Vertical Flight Society, "V/STOL Aircraft and Propulsion Concepts - Ryan X-13 Vertijet," [Online]. Available: <https://vtol.org/vstol/VSTOLWheel/RyanX-13Vertijet.htm>. [Accessed 2023].
- [6] The Vertical Flight Society, "V/STOL Aircraft and Propulsion Concepts - Short SC.1," [Online]. Available: <https://vtol.org/vstol/VSTOLWheel/ShortSC-1.htm>. [Accessed 2023].
- [7] The Vertical Flight Society, "V/STOL Aircraft and Propulsion Concepts - GE-Ryan XV-5A," [Online]. Available: <https://vtol.org/vstol/VSTOLWheel/GE-RyanXV-5A.htm>. [Accessed 2023].
- [8] The Vertical Flight Society, "V/STOL Aircraft and Propulsion Concepts - Bell XV-3," [Online]. Available: <https://vtol.org/vstol/VSTOLWheel/BellXV-3.htm>. [Accessed 2023].
- [9] The Vertical Flight Society, "V/STOL Aircraft and Propulsion Concepts - Canadair CL-84 Dynavert," [Online]. Available: <https://vtol.org/vstol/VSTOLWheel/CanadairCL-84Dynavert.htm>. [Accessed 2023].
- [10] The Vertical Flight Society, "V/STOL Aircraft and Propulsion Concepts - Dornier Do 31," [Online]. Available: <https://vtol.org/vstol/VSTOLWheel/DornierDo31.htm>. [Accessed 2023].
- [11] S. Magnuson, "Air Force Special Ops Wants Runway Independence, More Speed (UPDATED)," National Defense Industrial Association, 14 July 2023. [Online]. Available: <https://www.nationaldefensemagazine.org/articles/2023/7/14/air-force-special-ops-wants-runway--independence-more-speed>. [Accessed 2023].
- [12] J. Reed, "Avionics International: The Benefits of eVTOL Aircraft for Military Applications," February 2023. [Online]. Available: <https://interactive.aviationtoday.com/avionicsmagazine/january-february-2023/the-benefits-of-evtol-aircraft-for-military-applications/>. [Accessed October 2023].

- [13] J. DeTore and S. Conway, "Technology needs for high speed rotorcraft (3) NAS2-13072," NASA Ames Research Center, Moffett Field, 1991.
- [14] D. Gettinger, "Air Force Picks 11 Companies for High-Speed VTOL Program," Vertical Flight Society, 28 February 2022. [Online]. Available: <https://evtol.news/news/air-force-picks-11-companies-for-high-speed-vtol-program>. [Accessed October 2023].
- [15] VFS Staff, "Air Force Challenges Industry for High-Speed VTOL," Vertical Flight Society, 25 August 2021. [Online]. Available: <https://evtol.news/news/air-force-challenges-industry-for-high-speed-vtol>. [Accessed October 2023].
- [16] A. Baker, "Special Notice (SN) DARPA-SN-23-43: SPRINT Proposers Day," 23 March 2023. [Online]. Available: <https://sam.gov/api/prod/opps/v3/opportunities/resources/files/4c62118138284a13a655c2ce07e074d2/download?&token=> . [Accessed May 2023].
- [17] Air Force Research Laboratory (AFRL), "AFWERX CHALLENGE High-Speed VTOL Market Research Recipients," 2021. [Online]. Available: <https://afwerxchallenge.com/hsvtolmr>. [Accessed July 2022].
- [18] "40 th Annual Student Design Competition 2022-2023 Request for Proposals (RFP) High-Speed Vertical Takeoff," 2022. [Online]. Available: https://vtol.org/files/dmfile/rfp_sikorskyhvstol_40thdc_2022-23_final.pdf. [Accessed 22 May 2023].
- [19] C. G. Manning, "Technology Readiness Levels," The National Aeronautics and Space Administration, 27 September 2023. [Online]. Available: <https://www.nasa.gov/directorates/somd/space-communications-navigation-program/technology-readiness-levels/>. [Accessed October 2323].
- [20] M. A. McVeigh, J. Liu, S. J. O'Toole and S. Woods, "V-22 Osprey aerodynamic development a progress review," *The Aeronautical Journal*, no. June/July 1997, p. 242, 1997.
- [21] M. Flemming, "Structural Aspects of the Do 31 Jet-Lift VTOL Aircraft," *The Aeronautical Journal*, vol. 72, no. 692, pp. 719-734, 1968.
- [22] L. Mark, "Study of Aerodynamic Technology For Single-Cruise-Engine V/STOL Fighter/Attack Aircraft (NAS2-11002)," NASA Ames Research Center, Moffett Field, 1982.
- [23] M. Maisel, D. Giulianetti and D. Dugan, *The History of the XV-15 Tilt Rotor Research Aircraft from Concept to Flight*, Moffett Field: NASA Ames Research Center, 2000.
- [24] M. C. True, "Advanced Lift Fan System (LFX) Study Continuation," U.S. ARMY Aviation Material Laboratory, Fort Eustis, 1967.
- [25] R. Murphy and I. Wilken, "The North American Rockwell XFV-12A - Reflections and some lessons," in *American Institute of Aeronautics and Astronautics (AIAA)*, 1990.

- [26] M. R. Dudley, "Large-Scale V/STOL Experimental Investigations of an Ejector-Lift Fighter and a Twin Tilt-Nacelle Transport," in *AIAA International*, Hartford, 2016.
- [27] M. Chadwick, "S-97 RAIDER - Expanding the Envelope for Future Vertical Lift," Lockheed Martin Corporation, 2023. [Online]. Available: <https://www.lockheedmartin.com/en-us/products/s-97-raider.html>.
- [28] "X3 - Celebrating a game-changing high-speed demonstrator," AIRBUS, [Online]. Available: <https://www.airbus.com/en/who-we-are/our-history/helicopters-history/x3>. [Accessed 2023].
- [29] F. Colucci, J. Bulakowski and J. Buckley., Sikorsky Archives News, Stratford: Igor I. Sikorsky Historical Archives, 2021.
- [30] J. G. Leishman, *Principles of Helicopter Aerodynamics*, New York: Cambridge University Press, 2006.
- [31] "Propeller Performance Factors," EPI Inc., January 2020. [Online]. Available: http://www.epi-eng.com/propeller_technology/selecting_a_propeller.htm. [Accessed 2023].
- [32] S. B. Anderson, "Historical Overview of V/STOL Aircraft Technology. NASA-TM-81280," NASA Ames Research Center, Moffett Field, 1981.
- [33] M. Hirschberg, "The wheel of V/STOL Aircraft and Propulsion Concepts," March/April 1997. [Online]. Available: <https://vtol.org/vstol/wheel.htm>. [Accessed 23 May 2023].
- [34] R. J. Englar and B. A. Campbell, "Experimental Development and Evaluation of Pneumatic Powered-Lift," Proceedings of the 2004 NASA/ONR Circulation Control Workshop, Part 1, 2005.
- [35] "High-Speed Vertical Takeoff and Landing (HSVTOL)," Bell Textron Inc., 2023. [Online]. Available: <https://www.bellflight.com/experience/innovation/hsvtol>. [Accessed 2023].
- [36] "LARGE SCALE WIND TUNNEL INVESTIGATION OF A FOLDING TILT ROTOR [NASA-CR-114464]," Bell Helicopter Company, Fort Worth, 1972.
- [37] E. Tegler, "Know when to fold 'em - Bell tests its HSVTOL folding rotors," Forbes Magazine, 15 September 2023. [Online]. Available: <https://www.forbes.com/sites/erictegler/2023/09/14/know-when-to-fold-embell-tests-its-hsvtol-folding-rotors/?sh=2496c138170d>. [Accessed October 2023].
- [38] D. P. Edkins, "Convertible Fan/Shaft Engines Incorporating Variable-Pitch Fan Rotors (AD0859275)," U.S. ARMY Aviation Material Laboratories, Fort Eustis, 1969.
- [39] J. G. Mcardel, "The convertible engine: A dual-mode propulsion system (N88-16639)," NASA (Army Rotorcraft Technology.), Washington, 1988.

- [40] J. G. McArdle, R. L. Barth, L. M. Wenzel and T. J. Biesiadny, "Dynamic and Transient Performance of Turbofan/Turboshaft Convertible Engine With Variable Inlet Guide Vanes," NASA Lewis Research Center, Cleveland, 1996.
- [41] J. D. Eisenberg, "The Selection of Convertible Engines With Current Gas Generator Technology for High Speed Rotorcraft," in *Vertical Lift Aircraft Design Conference*, San Francisco, 1990.
- [42] "The VH-5 makes a new class of ultra high-performance electrified aircraft possible.," VERDEGO AERO, 2023. [Online]. Available: <https://verdegoaero.com/product/vh5/>. [Accessed 2023].
- [43] J. Pike, "V-22 Osprey Propulsion System," GlobalSecurity.org, 15 June 2016. [Online]. Available: <https://www.globalsecurity.org/military/systems/aircraft/v-22-propulsion.htm>. [Accessed 2023].
- [44] J. W. J. Lenski, "Advanced Rotorcraft Transmission Program (ART). ADA303528," NASA Lewis Research Center, Cleveland, 1995.
- [45] T. C. Schank, C. A. Fenny, A. Maresh and C.-S. Tzeng., "Tiltrotor Aircraft having Rotary and Non Rotary Flight Modes". United States of America Patent US20170144746A1, 09 February 2017.
- [46] D. H. Hichkey and J. V. Kirk., "Survey of lift-fan aerodynamic technology (NASA-CR-177615)," NASA Ames Research Center, Moffett Field, 1993.
- [47] C. Kong, J. Park and M. Kang, "A Study on Transient Performance Characteristics of the Canard Rotor Wing Type Unmanned Aerial Vehicle Propulsion System During Flight Mode Transition," *Journal of Engineering for Gas Turbines and Power*, vol. 128, p. 573, 2006.
- [48] S. Osder, "Integrated navigation, guidance, and control for Canard rotor/wing (CRW) aircraft," in *AIAA/IEEE Digital Avionics Systems Conference. 13th DASC*, Phoenix, 2002.
- [49] J. L. Overfield and H. R. Crawford, "Investigation Of Hydraulic Power Transmission Systems For V/STOL Aircraft. AD0661311," U.S. Army Aviation Material Laboratories, Fort Eustis, 1967.
- [50] C. Adam, "Advancement in driverless aircraft could direct the future of drones, flight," Purdue University, 9 May 2019. [Online]. Available: https://www.purdue.edu/newsroom/releases/2019/Q2/using-the-power-of-fluid-for-the-future-of-drones,-flight.html?_ga=2.108437122.1292534280.1698033641-2083967665.1698033641. [Accessed 2023].
- [51] J. C. Swain, D. L. Thomas, W. Slabiak and H. A. Santo., "A Turbine-Speed Pump for Vehicle Transmission Use," SAE International, Warrendale, 1967.
- [52] D. L. Thomas, R. K. Mitchell and J. P. Wilcox, " INVESTIGATION OF A 30,000-RPM TURBINE-SPEED HYDRAULIC PUMP. (AD0834312)," 1968.

- [53] J. R. Welstead and J. R. Welstead, "Conceptual Design of a Single-Aisle Turboelectric Commercial Transport with Fuselage Boundary Layer Ingestion," American Institute of Aeronautics and Astronautics, San Diego, 2016.
- [54] R. Schnell, X. Zhao, E. Rallis, M. D. Kavvalos, S. Sahoo, M. Schnoes and K. Kyprianidis, "Assessment of a Turbo-Electric Aircraft Configuration with Aft-Propulsion Using Boundary Layer Ingestion," *Aerospace*, vol. 6, no. 12, p. 134, 2019.
- [55] J. D. Cyrus, J. M. DeVillier and J. Kaminski, "Propulsion System Considerations for the Subsonic V/STOL," Naval Air Development Center, Warminster, Pa., 1979.
- [56] W. Johnson, C. Silva and E. Solis, "Concept Vehicles for VTOL Air Taxi Operations," in *American Helicopter Society (AHS)*, San Francisco, 2018.
- [57] R. V. Hupp and R. K. Haning, "Power Efficient Hydraulic Systems. Volume 1. Study Phase. ADA203899," Naval Air Development Center, Warminster, 1988.
- [58] "Hydraulic Pump Calculations," Womack Machine Supply Company, [Online]. Available: <https://www.womackmachine.com/engineering-toolbox/formulas-and-calculations/hydraulic-pump-calculations/>. [Accessed 2023].
- [59] "AXIAL-PISTON MOTOR A A10F M 45 /52W-VRC66N000-SO481," Bosch Rexroth Corporation, [Online]. Available: https://store.boschrexroth.com/Hydraulics_1_1181981/Motors_2_1182000/Axial-piston-motors_3_279264/Fixed-displacement_4_279265/Axial-Piston-Motor_R902406027?cclcl=en_US. [Accessed 2023].
- [60] "Bosch Rexroth MCR-F Radial Piston Motor," Hydraulics Online, [Online]. Available: <https://hydraulicsonline.com/product/bosch-rexroth-mcr-f-radial-piston-motor/>. [Accessed 2023].
- [61] S. Sakama, Y. Tanaka and A. Kamimura, "Characteristics of Hydraulic and Electric Servo Motors. doi: 10.3390/act11010011," *Actuators*, vol. 11, 2022.
- [62] A. T. Incorporated, "AM 350 Technical Data Sheet," 9 3 2012. [Online]. Available: https://www.atimaterials.com/Products/Documents/datasheets/stainless-specialty-steel/precipitationhardening/am_350_tds_en_v2.pdf. [Accessed 2023].
- [63] A. Ibrahim, Y. Ryu and M. Saidpour, "Stress Analysis of Thin-Walled Pressure," *Modern Mechanical Engineering*, pp. 1-9, 2015.
- [64] R. E. and R. M., "Gear Weight Equations - Gear Chain Weight Calculation Methodology," Rzeszów University of Technology, Rzeszów, Poland, 2011.
- [65] "JIS G4051 S45C Steel For Machine Structural Use," OTAI, [Online]. Available: <https://www.astmsteel.com/product/jis-s45c-steel-machine-structural/>. [Accessed 2023].
- [66] Moog Inc., "Hydraulic Fluid Rotary Union Model 810," 2018. [Online]. Available: https://www.macartney.com/media/6870/2_fru_model-810.pdf.

- [67] EASTMAN, "Technical Data Sheet - Skydrol® LD4 Fire Resistant Hydraulic Fluid," [Online]. Available: https://productcatalog.eastman.com/tds/ProdDatasheet.aspx?product=71093409&pn=Skydrol+LD-4#_ga=2.84039001.1579565228.1695688248-427987166.1695687005. [Accessed 2023].
- [68] Exxon Mobil Co., "HyJet™ IV-A Plus Page 1," [Online]. Available: <https://pdfgenerator-west.exxonmobil.com/PDFHandlers/PdfGeneratorHandler.ashx?component=PDS&downloadUrl=https://www.exxonmobil.com/en-US/Aviation/pdsdownload/GL-XX-HyJet-IV-A-Plus?p=1>. [Accessed 2023].
- [69] "Hydraulic Motor Calculations," Womack Machine Supply Co., [Online]. Available: <https://www.womackmachine.com/engineering-toolbox/formulas-and-calculations/hydraulic-motor-calculations/>. [Accessed 2023].
- [70] G. V. Brown, "Efficient Flight-Weight Electric Systems," NTRS - NASA Technical Reports Server, 13 March 2012. [Online]. Available: <https://ntrs.nasa.gov/citations/20150010194>. [Accessed 2023].
- [71] J. Sinsay, J. Alonso, D. Kontinos, J. Melton and S. Grabbe, "Air Vehicle Design and Technology Considerations for an Electric VTOL Metro-Regional Public Transportation System," in *12th AIAA Aviation Technology, Integration, and Operations (ATIO)*, Indianapolis, 2012.
- [72] C. e. a. Synder, "Propulsion Investigation for Zero and Near-Zero Emissions Aircraft," NASA Glenn Research Center, Cleveland, 2009.
- [73] W. Johnson, "NDARC. NASA Design and Analysis of Rotorcraft (TP 2015-218751)," April 2015.
- [74] S. Jaycocks, "Helix develops revolutionary 650kW electric motor," Integral Powertrain Limited, 07 June 2023. [Online]. Available: <https://www.ehelix.com/communication/helix-develops-revolutionary-650kw-electric-motor/>. [Accessed 2023].
- [75] H. Gui et al., "Development of High-Power High Switching Frequency Cryogenically Cooled Inverter for Aircraft Applications," *IEEE Transactions on Power Electronics*, vol. 35, no. 6, pp. 5670-5682, 2020.
- [76] Federal Aviation Administration, "Advisory Circular 43.13-1B - Acceptable Methods, Techniques, and Practices - Aircraft Inspection and Repair," 08 September 1998. [Online]. Available: https://www.faa.gov/documentLibrary/media/Advisory_Circular/AC_43.13-1B_w-chg1.pdf. [Accessed 2023].
- [77] Houston Wire & Cable Company, "Specification HW363 Single Conductor Power Cable - 2kV," [Online]. Available: <https://www.houwire.com/pdf/HW263.pdf?r=false>. [Accessed 2023].
- [78] S. Yamaguchi and M. Kanda., "A proposal for a lightweight, large current superconducting cable for aviation," *upercond. Sci. Technol.*, vol. 34, 2021.

- [79] J. W. Chapman, H. Haseeb and S. Schnulo., "Thermal Management System Design for Electrified Aircraft Propulsion Concepts (NASA/TM-20205011477)," in *AIAA Propulsion and Energy 2020 Forum*, Virtual Event, 2020.
- [80] "The All-New Amprius 500 Wh/kg Battery Platform is Here," Amprius Technologies, Inc., 23 March 2023. [Online]. Available: <https://amprius.com/the-all-new-amprius-500-wh-kg-battery-platform-is-here/>. [Accessed 2023].
- [81] M. Dudley, "Promising Electric Aircraft Drive Systems," in *EAA Electric Aircraft World Symposium*, Oshkosh, 2010.
- [82] J. J. C. Gilbert J. Weden, "Summary of Drive-Train Component Technology in Helicopters (TR 84-30294)," AVSCOM Research and Technology Laboratories, NASA Lewis Research Center, Cleveland, 1984.
- [83] C. Acree, "EFFECTS OF ROTOR DESIGN VARIATIONS ON TILTROTOR WHIRL-MODE STABILITY," NASA Ames Research Center, Moffett Field, 2000.
- [84] "Bell Boeing V-22 Osprey Blueprint," [Online]. Available: <https://drawingdatabase.com/bell-boeing-v-22-osprey/>. [Accessed 2023].
- [85] B. Sunick, "AW609: Tiltrotor Technology for Business Aviation," 11 October 2017. [Online]. Available: <https://nbaa.org/wp-content/uploads/2018/02/152715061-AW609-NBAA-9OCT2017-Agustawestland.pdf>. [Accessed 2023].
- [86] "BELL V-280 VALOR," Bell Textron Inc., [Online]. Available: <https://www.bellflight.com/products/bell-v-280>. [Accessed 2023].
- [87] CiTrus90, "Bell V-280 Valor," 16 January 2015. [Online]. Available: <https://www.secretprojects.co.uk/attachments/1-jpg.646813/>. [Accessed 2023].
- [88] W. Tan, Y. Li, Y. Miao and H. Lv., "The Analysis of Airworthiness Issues Influence to the Development of Tiltrotor Aircraft," in *3rd International Symposium on Aircraft Airworthiness*, 2013.
- [89] B. C. Ross, D. R. Bockmiller, M. L. Isaac and B. J. Cox., "SPINDLE MOUNTED TILTROTOR PYLON WITH FIXED ENGINE ARRANGEMENT". United States of America Patent 9,126,678 B2, 08 September 2015.

APPENDIX A – Design of HSVTOL Airframe

Table A 1 Public domain peed records of aircraft using various propulsion types.

Type	Name	Altitude [ft]	KIAS (max)
Tiltrotor	Bell HSVTOL	30,000	480.00
	V-22 Osprey (SL)	0.00	266.00
Fixed Wing	P-51 Voodoo	4,655	430.57
	Tu-95	39,370	499.66
	P. 180 Avanti	41,000	475.17
Helicopter	S-72	4,000	300.00
	S-97	10,000	220.00
	Eurocopter X ³	10,000	255.00
Jet+ Lift Fan	Ryan XV-5	40,000	475.00

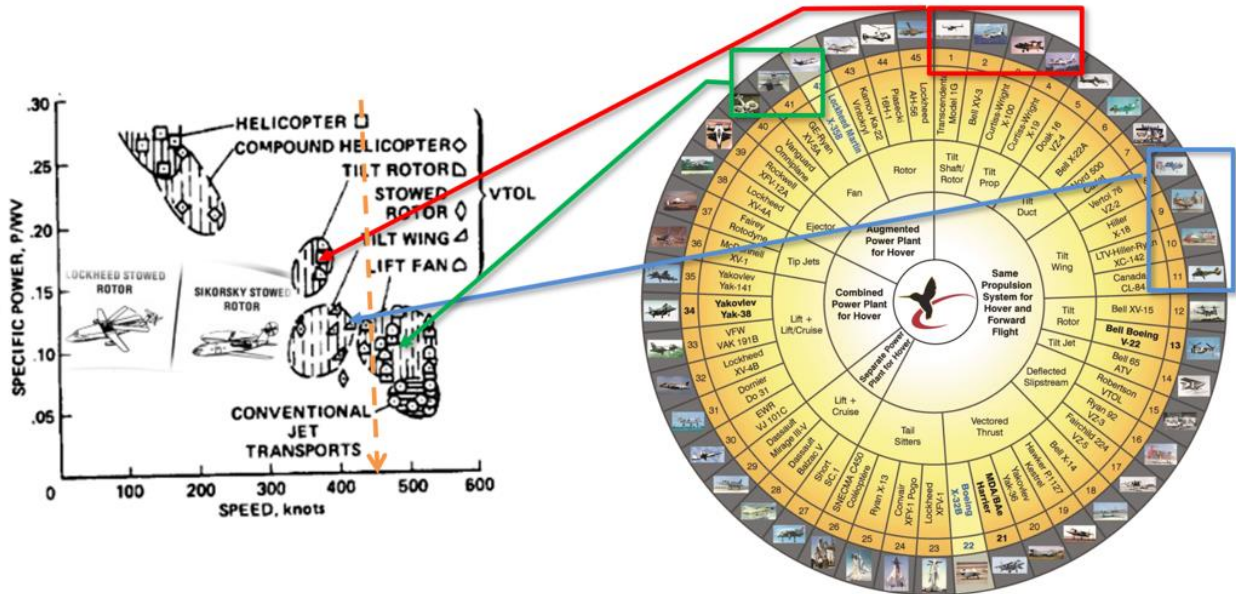


Figure A 1 VTOL with existing prototype (VTOL wheel is from [33]).

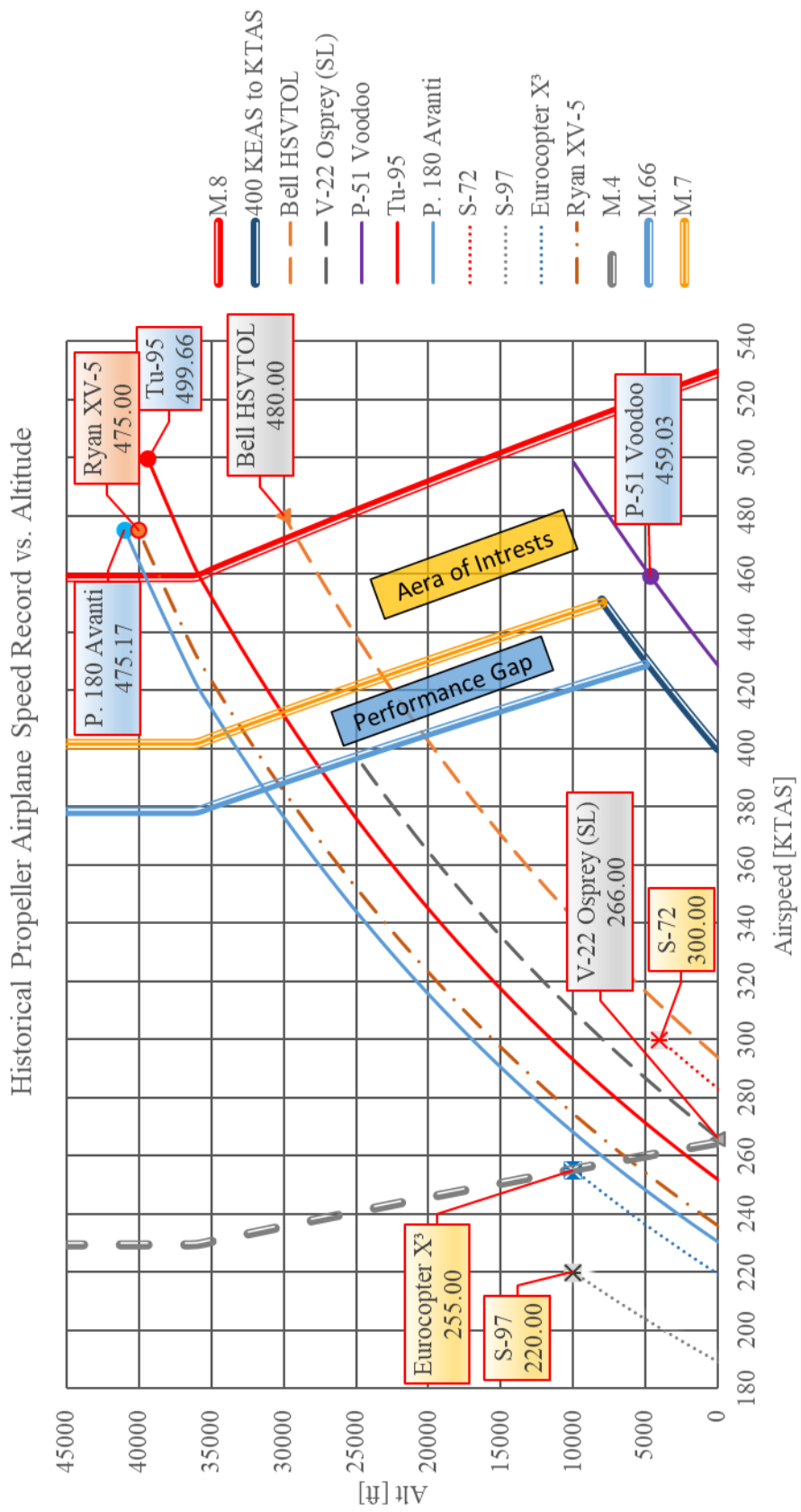
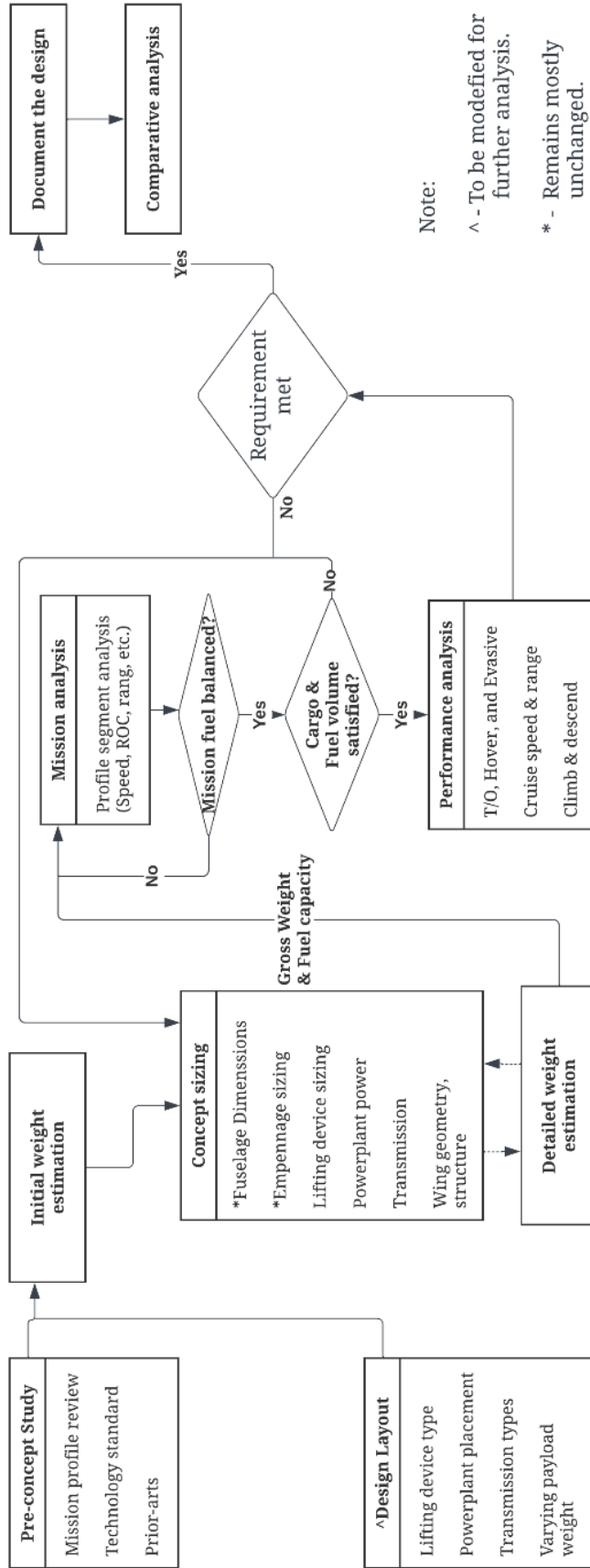


Figure A 2 Aircraft indicated speed records (constant) in KTAS at different altitude.

Table A 2 Public domain data of existing VTOL vs. VFS design requirements.

Aircraft	We [lb]	W _{to} [lb]	Payload [lb]	Combat radius [nm]	u_Cruise [kts]	u_Max [kts]	Ceiling [ft]	DL _{MTO} [lbft ²]	P _{tot} [shp]
UH-60M	12511	19398	3190	320	151	159	19000	9.73	3988
V-280	18078	37999	4060	500	280	300	25000	19.75	9500
MV-22B	31800	42712	6960	390	250	305	25000	35.2	12300
AW609	10505	16799	1740	350	N/A	275	37283	9.95	4026
CH-47F	24578	45000	15950	200	160	170	20000	8.84	9466
X2	5300	6000	N/A	N/A	N/A	250	19000	5.47	1800
S-97	N/A	11400	1740	155	220	240	10000	6.28	3351
S-69	N/A	11000	N/A	N/A	109	263	25000	5.4	1825
XV-5	7541	12300	N/A	435	N/A	470	40000	247.59	20000
F-35B	32472	60000	N/A	505	N/A	1067	50000	2383.19	<u>58000</u>
Goal		25000	5000	500	450	549	20000	40	



Note:
 ^ - To be modified for further analysis.
 * - Remains mostly unchanged.

Figure A 3 Design process of HSVTOL based on common aircraft design process.

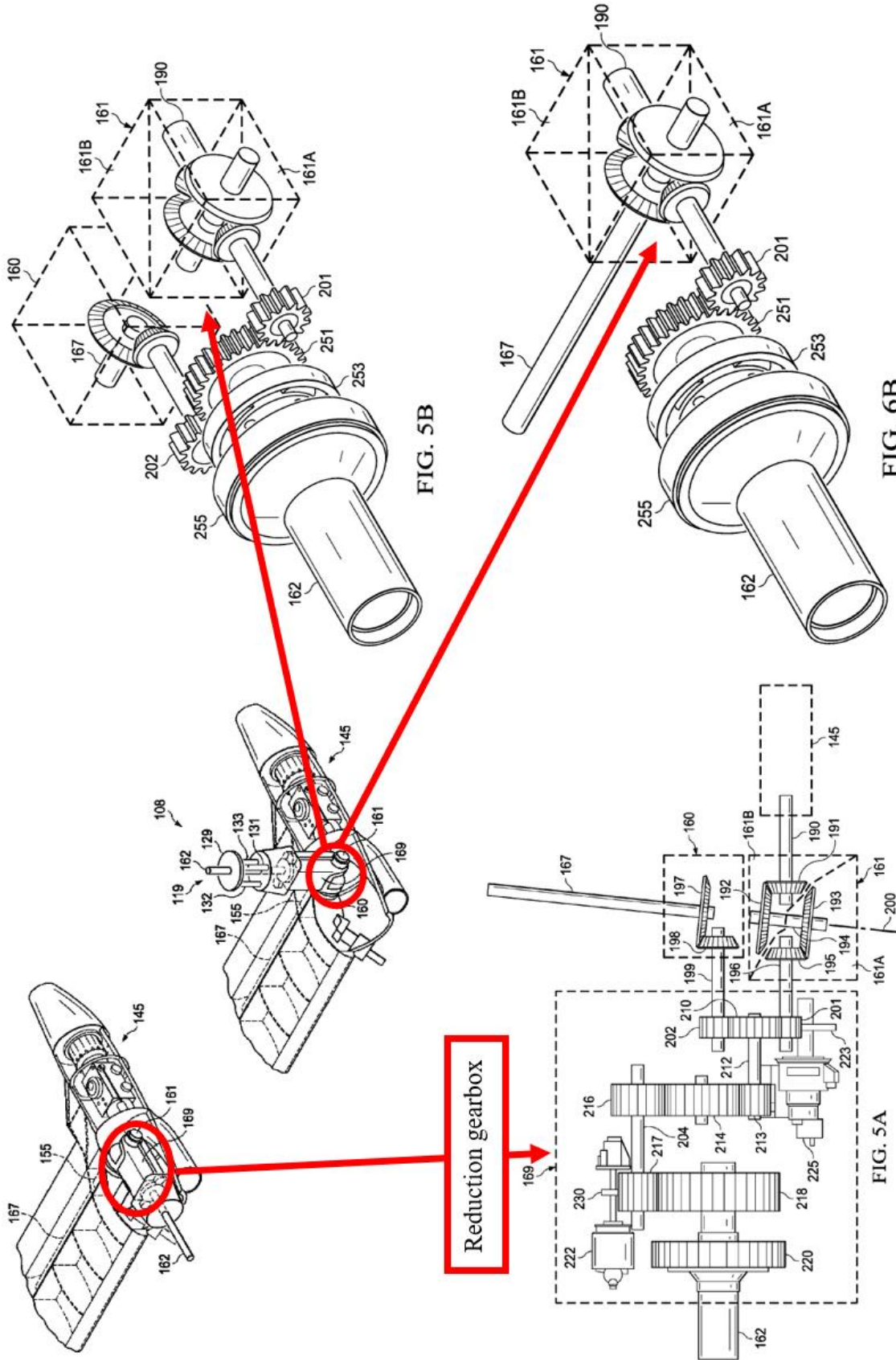


Figure A 4 Schematics of tiltrotor pylon with fixed engine arrangement [89].

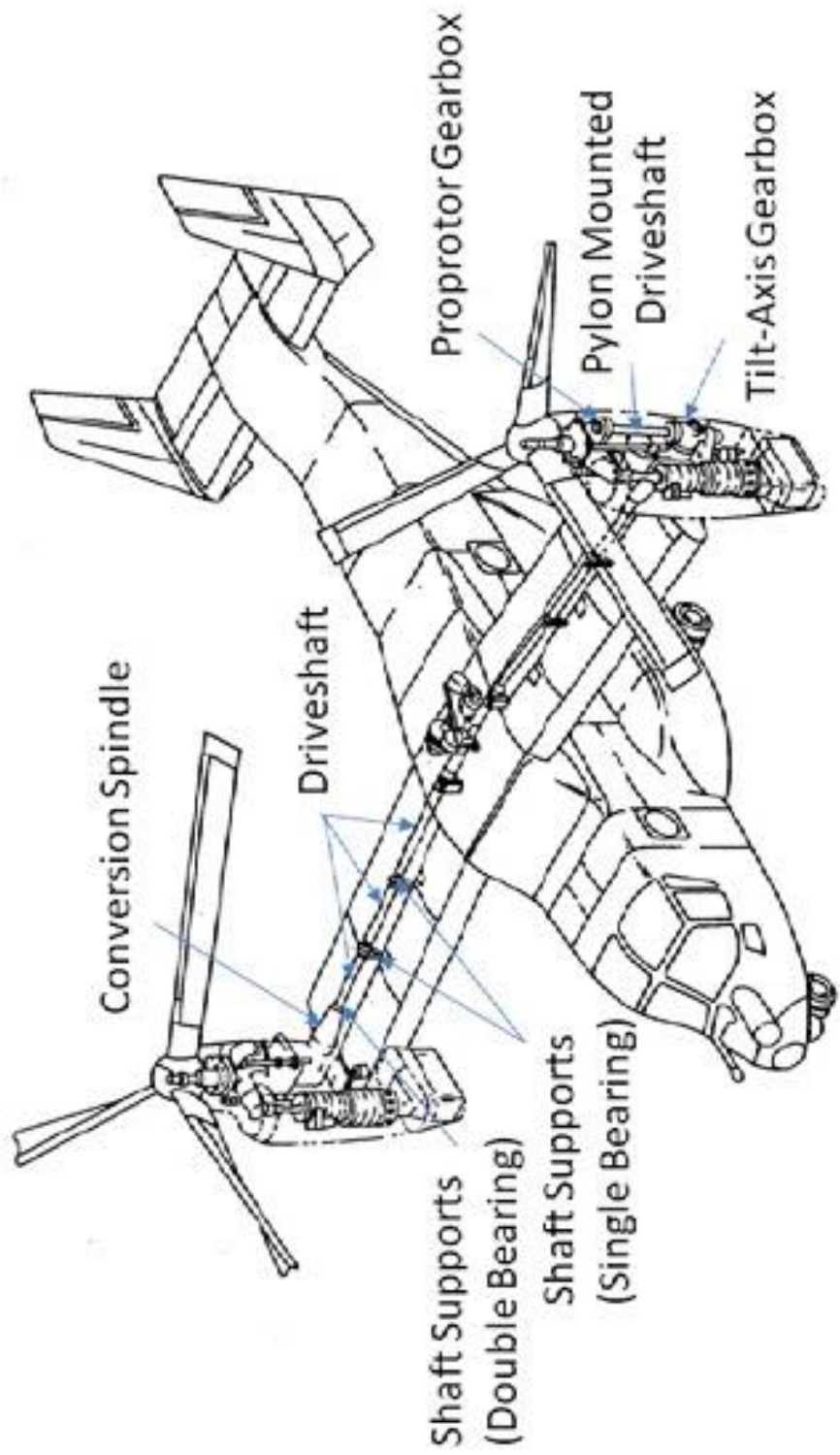


Figure A 5 A representative tiltrotor aircraft configuration [88].

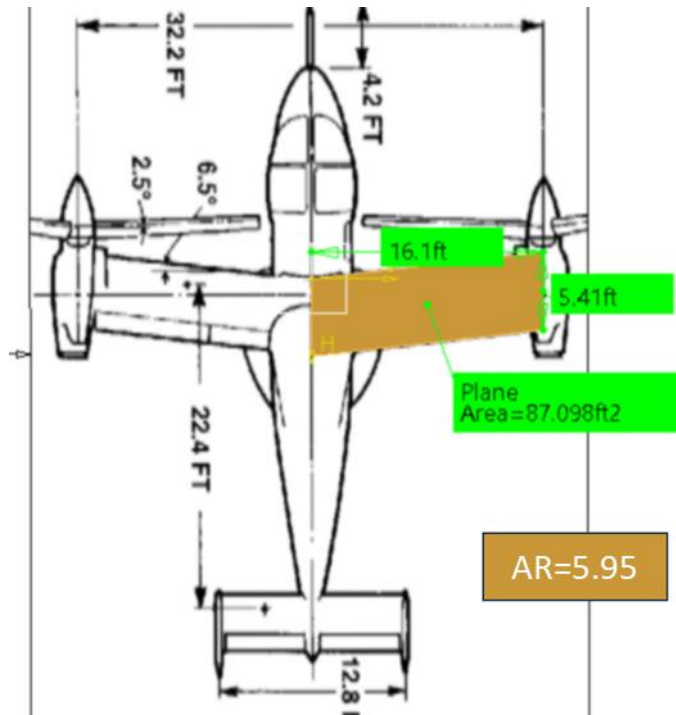


Figure A 6 XV-15 aspect ratio (Drawing from [83]).

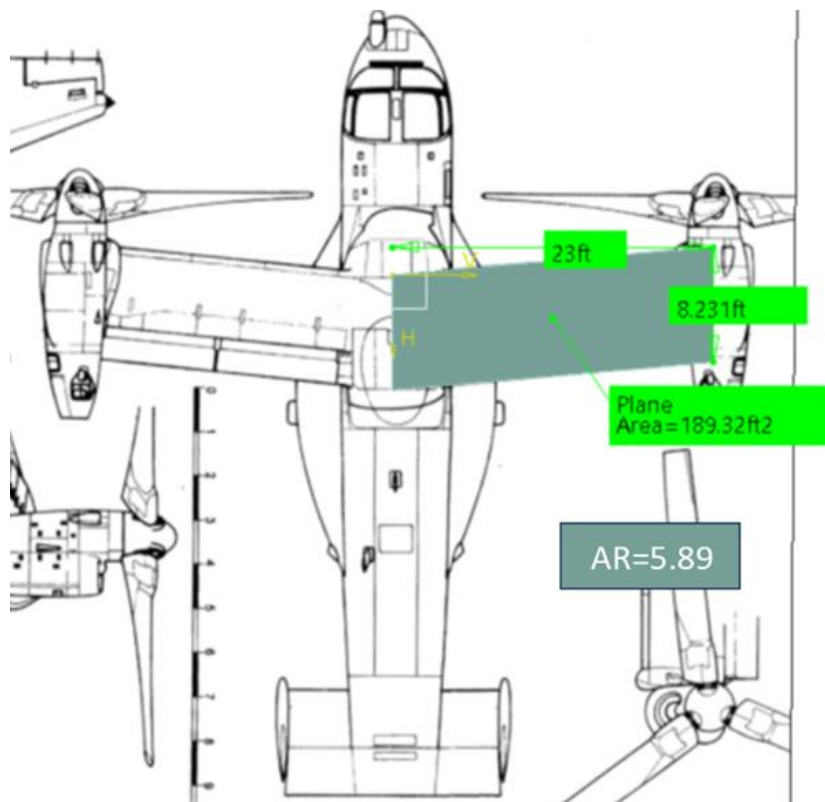


Figure A 7 V-22 aspect ratio (Drawing from [84]).

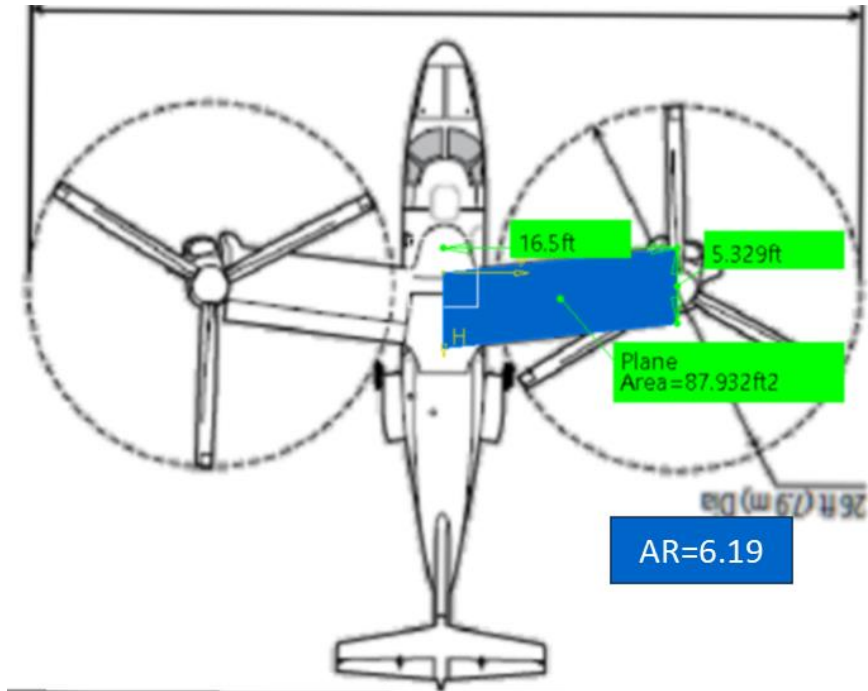


Figure A 8 AW609 aspect ratio (Drawing from [85]).

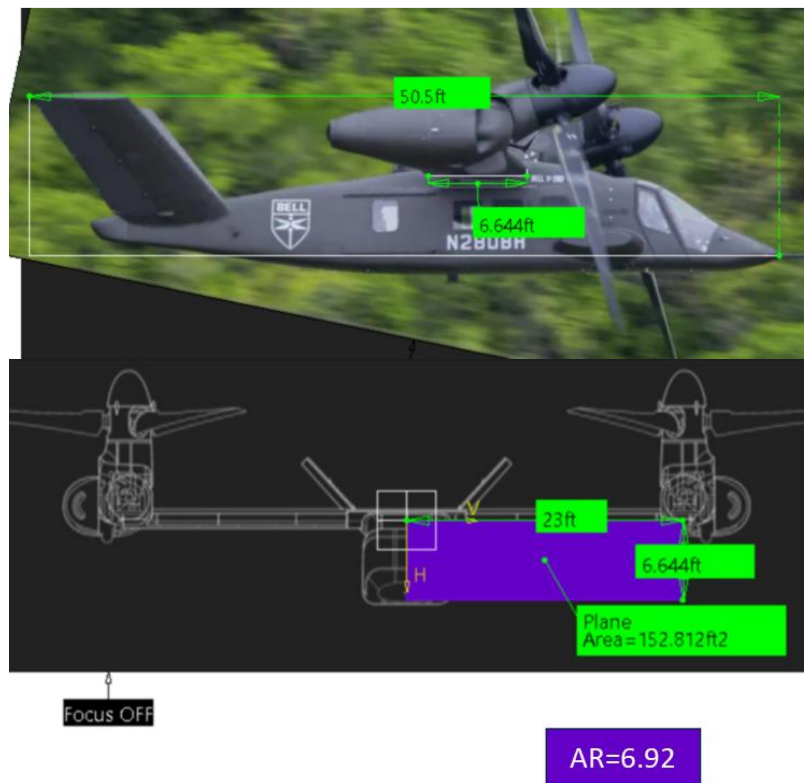


Figure A 9 V-280 aspect ratio (Drawing from [86] & [87]).

APPENDIX B – Data Used for Sizing

Table B 1 Parker™ Aircraft Engine-Driven Pumps data.

Model Number	Maximum Displacement [in³/rev]	Normal Operating Pressure [psi]	AS595 Maximum Recommended Speed [RPM]	Maximum Output Flow [GPM]	Approximate Dry Weight [lbs]	Power [hp]
AP05VC	0.09	3000	13060	4.8	2.4	10.08
AP05V	0.15	3000	11034	6.8	2.6	14.28
AP1V	0.31	3000	8684	11.1	7	23.31
AP2V	0.42	3000	7856	13.6	8	28.56
AP3V	0.52	3000	7321	15.7	9	32.97
AP4V	0.65	3000	6801	18.2	10.5	38.22
AP5V	0.82	3000	6299	21.2	11.5	44.52
AP6VSC	0.97	3000	5960	23.8	12	49.98
AP10VC	1.6	3000	5052	33.2	15.3	69.72
AP8V	1.35	3000	5344	29.7	16	62.37
AP12V	2.02	3000	4677	38.9	18.5	81.69
AP9VM	1.2	5000	5085	25.1	21.5	87.85
AP15V	2.4	3000	4420	43.6	25	91.56
AP19V	3	3000	4106	50.7	27.5	106.47
AP27V	4.3	3000	3646	64.5	29.8	135.45
AP20VM	3.05	5000	3737	46.9	41	164.15
AP36V	5.5	3000	3361	76	47	159.6

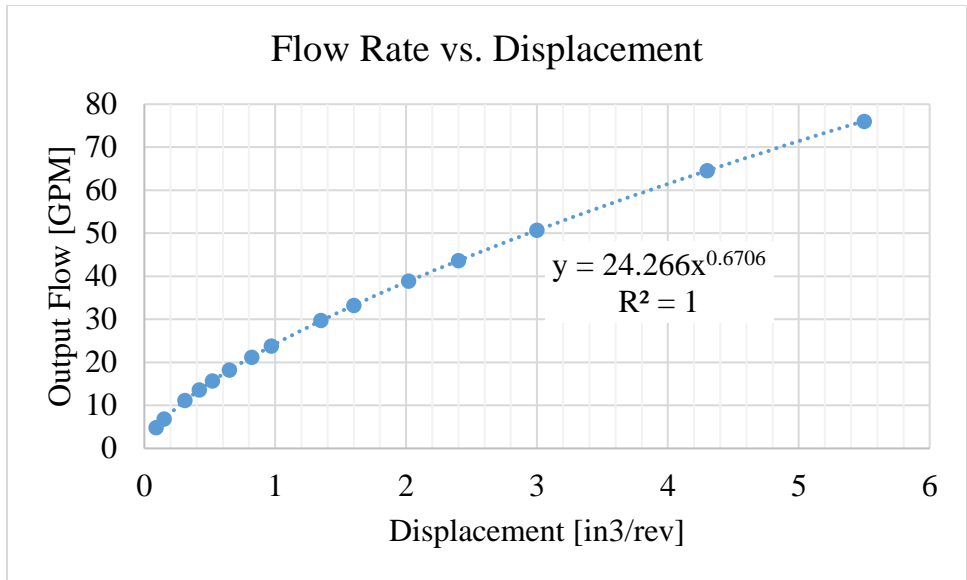


Figure B 1 Pump flow rate WRT displacement.

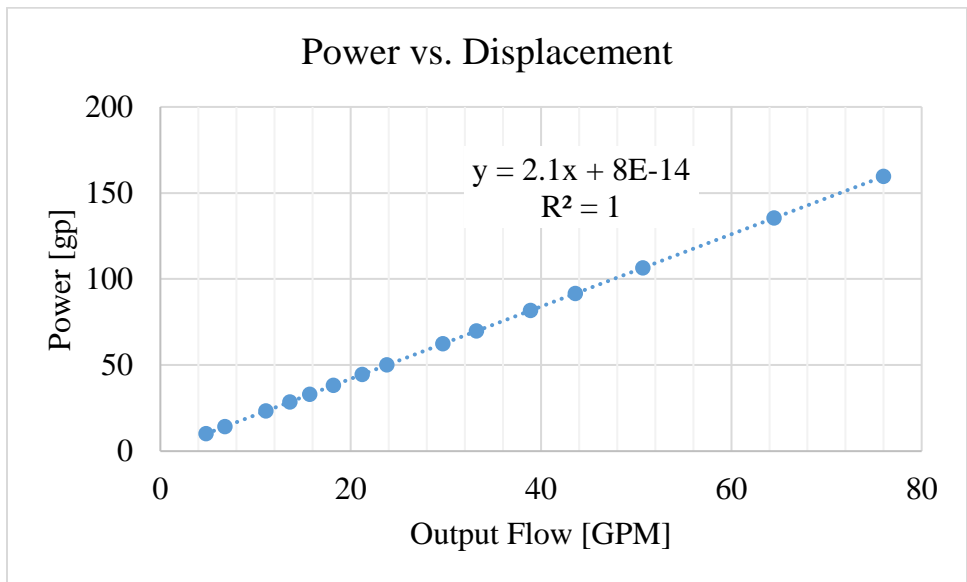


Figure B 2 Pump power to flow rate relation.

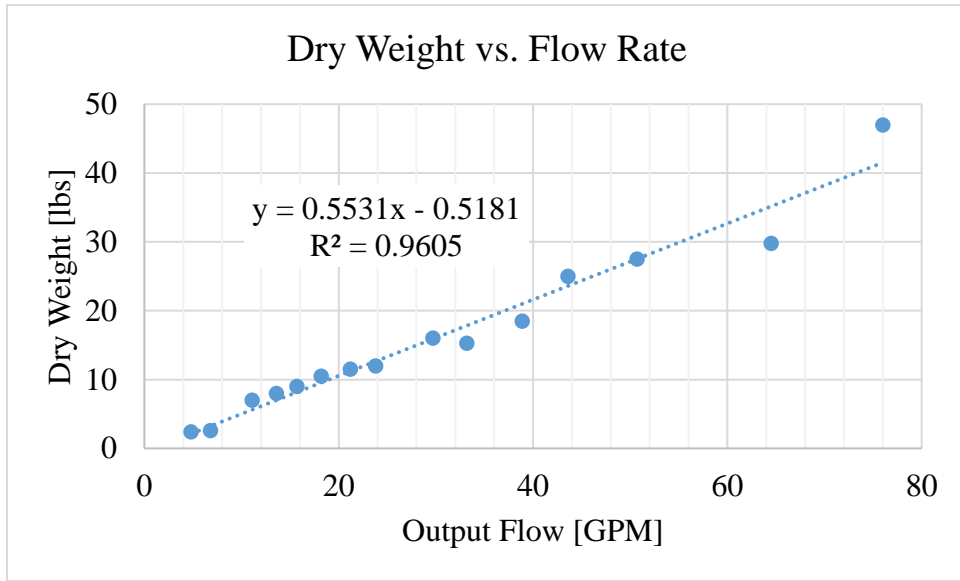


Figure B 3 Pump dry weight to flow rate relation.

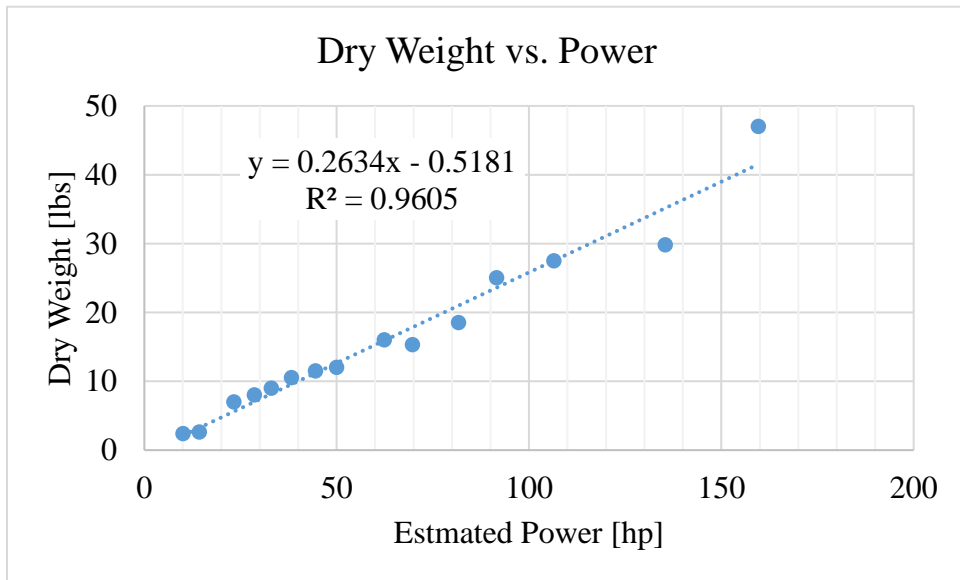


Figure B 4 Pump dry weight to power relation.

Table B 3 Bosch™ axial piston fixed/plug-in motor A10 series data.

Model Number	Displacement [in ³]	Normal Operating Pressure [psi]	Maximum Recommended Speed [RPM]	Inlet Flow [GPM]	Approximate Dry Weight [lbs]	Volume [gal]	Power [hp]	Torque [lb*ff]
10	0.65	4100	5000	14	11	0.03	33	34.6
11	0.7	4100	4200	12.7	14.3	0.04	30	37.5
14	0.86	4100	4200	15.6	14.3	0.04	37	46.5
16	0.98	4100	4200	17.9	14.3	0.04	42	53.1
18	1.1	4100	4200	20.1	14.3	0.04	47	59
23	1.43	4100	4900	30.4	26.5	0.16	71	77.4
28	1.73	4100	4700	35.4	26.5	0.16	83	93.7
37	2.24	4100	4200	40.7	37.5	0.18	95	120
45	2.71	4100	4000	47	37.5	0.18	111	146
58	3.53	4100	3600	55.2	48.5	0.21	130	190
63	3.84	4100	3400	56.8	48.5	0.21	133	207

Table B 2 Bosch™ axial piston fixed/plug-in motor A4 series data.

Model Number	Displacement [in ³]	Normal Operating Pressure [psi]	Maximum Recommended Speed [RPM]	Inlet Flow [GPM]	Approximate Dry Weight [lbs]	Volume [gal]	Power [hp]	Torque [lb*ff]
71	4.33	5076	3200	60.0	75.0	0.53	122	292
125	7.63	5076	2600	85.9	134.5	0.79	176	513
250	15.26	5076	2200	145.3	264.6	1.85	371	1027
500	30.51	5076	1800	237.8	485.1	2.91	704	2052
1000	61.02	5076	1600	422.7	1153.2	7.13	1251	4104

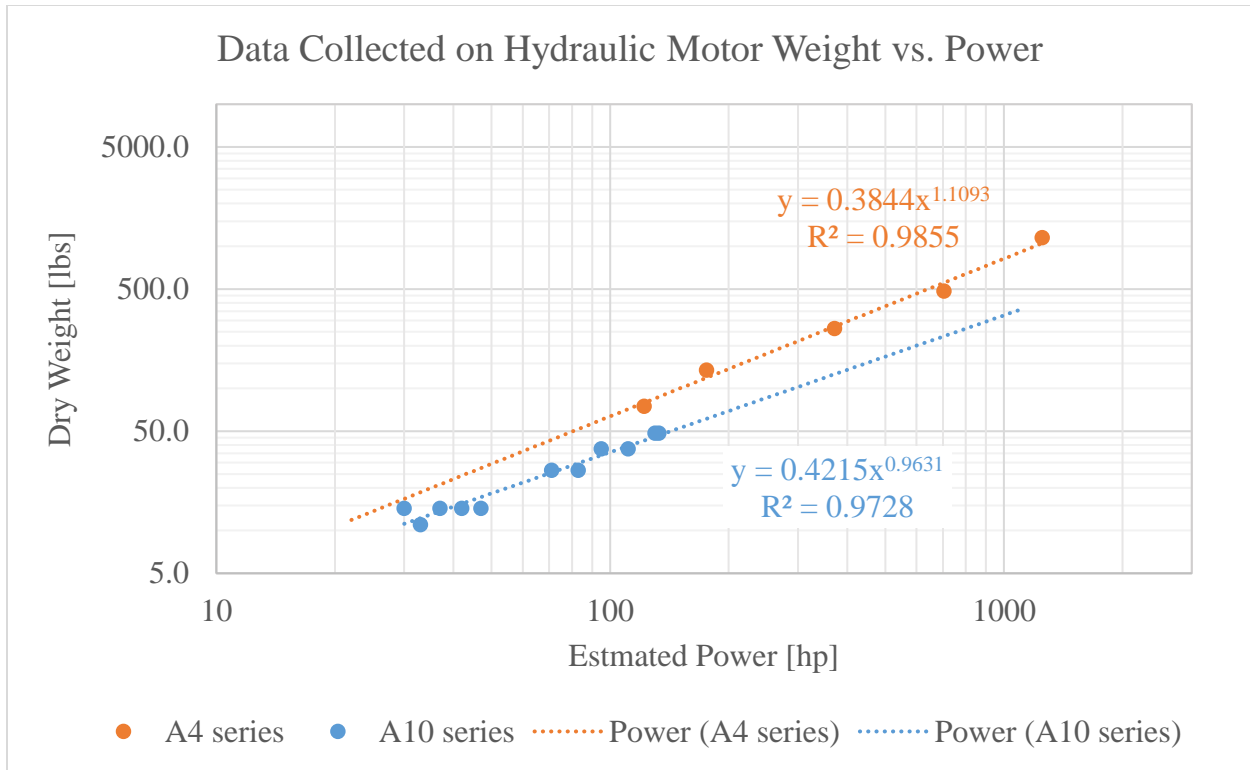


Figure B 5 Trend of the existing pump weight WRT rated power collected.

Table B 4 P35/P56 hose specific weight with various pressure and diameter in [lb/ft].

		Working Pressure [psi]					
		1000 [psi]	3000 [psi]	4000 [psi]	5000 [psi]	6000 [psi]	8000 [psi]
Part #	ID [in]						
4	0.25	0.10	0.16	0.20	0.21	0.21	0.36
6	0.375	0.10	0.23	0.28	0.28	0.31	0.50
8	0.5	0.29	0.29	0.35	0.45	0.45	0.63
10	0.625	0.33	0.33	0.44	0.54	0.54	0.68
12	0.75	0.42	0.58	0.58	0.75	0.78	0.84
16	1	0.61	0.79	1.34	1.17	1.17	1.22
20	1.25	1.24	1.74	1.74	1.95	1.95	2.27
24	1.5	1.32	2.01	2.07	2.66	2.66	3.32
32	2	1.75	2.75	4.35	4.37	4.37	5.03
40	2.25	2.04	3.12	4.25	4.52	4.52	5.96
48	3	2.77	4.32	5.93	6.29	6.28	8.34
Commercially Available				Extrapolated			

OTS Hose Weight Trend

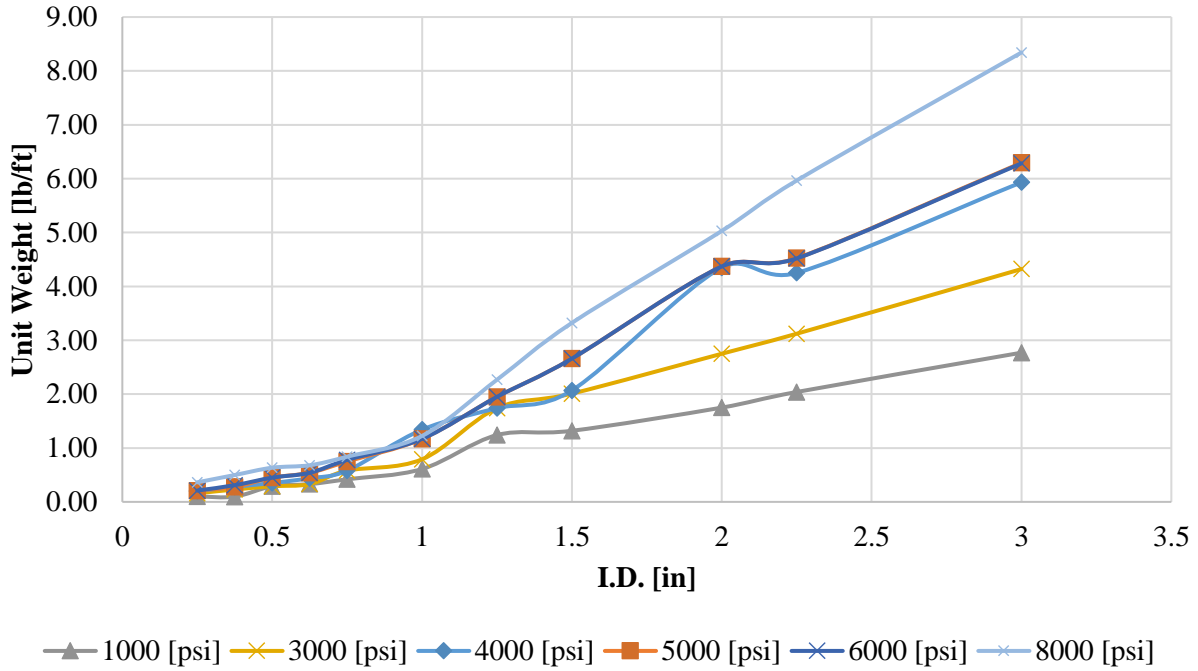


Figure B 6 Unit weight trend of Parker™ P35/P56 hydraulic hoses.

Table B 5 Minimum required thickness for given inner diameter and pressure.

ID [in]	AM 350 Steel (DA) Pipe Minimum Thickness [in]					
	1000 [psi]	3000 [psi]	4000 [psi]	5000 [psi]	6000 [psi]	8000 [psi]
0.25	1.97E-03	5.92E-03	7.89E-03	9.87E-03	1.30E-02	1.58E-02
0.375	2.96E-03	8.88E-03	1.18E-02	1.48E-02	1.95E-02	2.37E-02
0.5	3.95E-03	1.18E-02	1.58E-02	1.97E-02	2.61E-02	3.16E-02
0.625	4.93E-03	1.48E-02	1.97E-02	2.47E-02	3.26E-02	3.95E-02
0.75	5.92E-03	1.78E-02	2.37E-02	2.96E-02	3.91E-02	4.74E-02
1	7.89E-03	2.37E-02	3.16E-02	3.95E-02	5.21E-02	6.32E-02
1.25	9.87E-03	2.96E-02	3.95E-02	4.93E-02	6.51E-02	7.89E-02
1.5	1.18E-02	3.55E-02	4.74E-02	5.92E-02	7.82E-02	9.47E-02
2	1.58E-02	4.74E-02	6.32E-02	7.89E-02	1.04E-01	1.26E-01
2.25	1.78E-02	5.33E-02	7.11E-02	8.88E-02	1.17E-01	1.42E-01
3	2.37E-02	7.11E-02	9.47E-02	1.18E-01	1.56E-01	1.89E-01
3.75	2.96E-02	8.88E-02	1.18E-01	1.48E-01	1.95E-01	2.37E-01

Table B 6 Minimum weight for AM 350 (DA) piping.

ID [in]	Unit Weight [lb/ft]											
	100 [psi]	200 [psi]	220 [psi]	400 [psi]	600 [psi]	800 [psi]	1000 [psi]	3000 [psi]	4000 [psi]	5000 [psi]	6000 [psi]	8000 [psi]
0.25	-	-	-	-	-	-	0.01	0.02	0.02	0.03	0.04	0.04
0.375	-	-	-	-	0.01	0.01	0.01	0.04	0.05	0.06	0.08	0.10
0.5	-	-	-	0.01	0.01	0.02	0.02	0.06	0.09	0.11	0.14	0.18
0.625	-	0.01	0.01	0.01	0.02	0.03	0.03	0.10	0.13	0.17	0.22	0.27
0.75	-	0.01	0.01	0.02	0.03	0.04	0.05	0.14	0.19	0.24	0.32	0.39
1	0.01	0.02	0.02	0.03	0.05	0.07	0.08	0.25	0.34	0.43	0.57	0.70
1.25	0.01	0.03	0.03	0.05	0.08	0.10	0.13	0.40	0.53	0.67	0.89	1.10
1.5	0.02	0.04	0.04	0.07	0.11	0.15	0.19	0.57	0.77	0.96	1.29	1.58
2	0.03	0.07	0.07	0.13	0.20	0.27	0.33	1.01	1.36	1.71	2.29	2.80
2.25	0.04	0.08	0.09	0.17	0.25	0.34	0.42	1.28	1.72	2.17	2.90	3.55
3	0.07	0.15	0.16	0.30	0.45	0.60	0.75	2.28	3.06	3.86	5.15	6.31
3.75	0.12	0.23	0.26	0.47	0.70	0.93	1.17	3.56	4.78	6.03	8.05	9.86

Table B 7 Reference hydraulic component weight for 1,500 hp system [49].

TABLE III HYDRAULIC TRANSMISSION COMPONENTS AND TOTAL WEIGHT				
Component	Front Drive T-53		Rear Drive T-58	
	Dia. " x L. "	Total Weight	Dia. " x L. "	Total Weight
Pump	8.5 x 12	70.0	8.5 x 12	70.0
Motor	20 x 27	300.0	20 x 27	300.0
Mounting frame	17 x 2	60.0	17 x 2	60.0
Oil cooler	13.2 x 13.2 x 2.5	28.0	13.2 x 13.2 x 2.5	28.0
Piping	-	15.3	-	72.3
Oil	-	25.7	-	69.2
Accessory drive	22.4 x 1	27.1	22.4 x 1	27.1
Scavenge pump drive	-	0.4	-	0.4
Idler gear	-	0.4	-	0.4
Gen. drive	-	0.1	-	0.1
Tach. gen. drive	-	0.2	-	0.2
Valves	-	20.0	-	20.0
Scavenge pump	3 x 4	10.0	3 x 4	10.0
Tail rotor piping	-	30.8	-	24.4
Tail rotor fluid	-	12.4	-	10.0
Tail rotor motor	7.375 x 7.375	<u>75.0</u>	7.375 x 7.375	<u>75.0</u>

Table B 8 MOOG Model 810 Parameters [66].

Model 810 Parameters (See sheet 3 for dimensional details)				
Number of Passes	2		4	
Port Size	1/2 inch	3/4 inch	1/2 inch	3/4 inch
Estimated Weight (lb [kg])	35 [16]	50 [23]	50 [23]	75 [34]
Max. Estimated Torque @ 6000 psi (lb-ft [Nm])	120 [165]	175 [240]	235 [320]	340 [460]
Max. Estimated Torque @ 3000 psi (lb-ft [Nm])	65 [90]	90 [125]	120 [165]	175 [240]
DIM A, Housing and Shaft Flange Diameter	5.00 [127.0]	5.75 [146.1]	5.00 [127.0]	5.75 [146.1]
DIM B, Overall Length	7.88 [200.2]	8.53 [216.7]	11.14 [283.0]	12.39 [314.7]
DIM C, Clearance Between Shaft Flange and Housing Assembly	1.5 [38.1]	1.46 [37.1]	1.5 [38.1]	1.46 [37.1]
DIM D, Shaft Flange Mounting Face to First Housing Port	3.87 [98.3]	4.08 [103.6]	3.87 [98.3]	4.08 [103.6]
DIM E, Port to Port	1.63 [41.4]	1.93 [49.0]	1.63 [41.4]	1.93 [49.0]
DIM E, Shaft Port PCD	SAE	1.92 [48.8]	2.33 [59.2]	1.92 [48.8]
	NPT	1.92 [48.8]	2.25 [57.2]	1.92 [48.8]
	BSPP	1.92 [48.8]	2.33 [59.2]	1.92 [48.8]
	O-Ring	1.68 [42.7]	2.10 [53.3]	1.68 [42.7]
DIM G, Shaft Flange Clearance Hole PCD	4.5 [114.3]	5.00 [127.0]	4.5 [114.3]	5.00 [127.0]

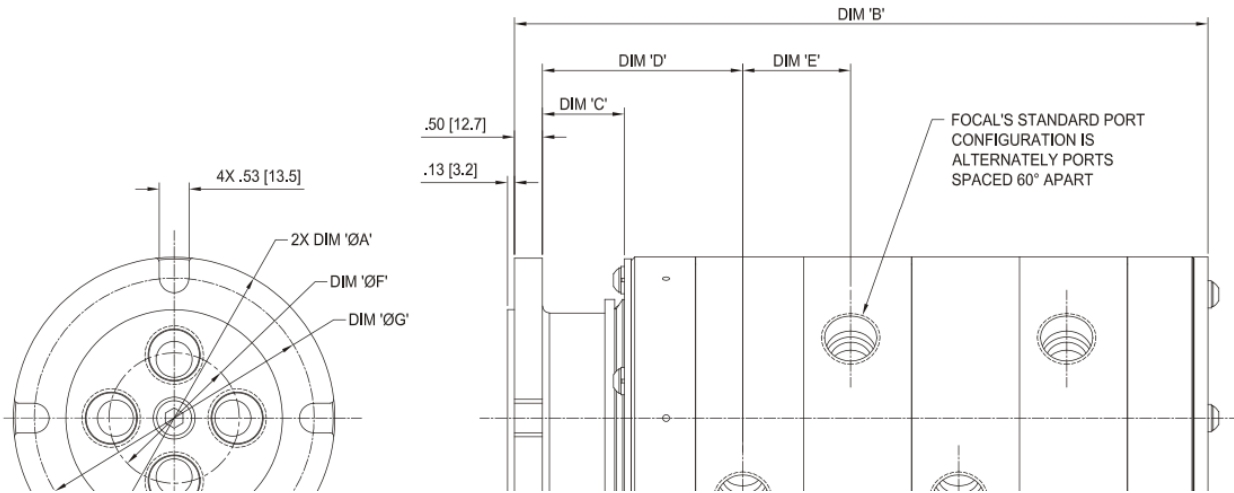


Figure B 7 Model 810 drawing with dimensions varying with variable dimensions.

Table B 9 Design assumption for Single-Aisle BLI electric weight estimates [53].

Component	Assumption	Efficiency	Size	Weight
Electric Motor	8 hp/lb	96.0%	3,500 hp	440 lb
Inverter	10 hp/lb	98.0%	3,500 hp	350 lb
Generator (2)	8 hp/lb	96.0%	2 @ 1,137 hp	480 lb
Cable (2×93')	3.85 kg/m	99.6%	1.44 MW	480 lb
	750V/1926 amps			
Circuit Protection	0.5*Cable Weight	-	-	240 lb
TMS	0.68 kW/kg	-	279 kW	910 lb
Total System	-	-	-	2,930 lb

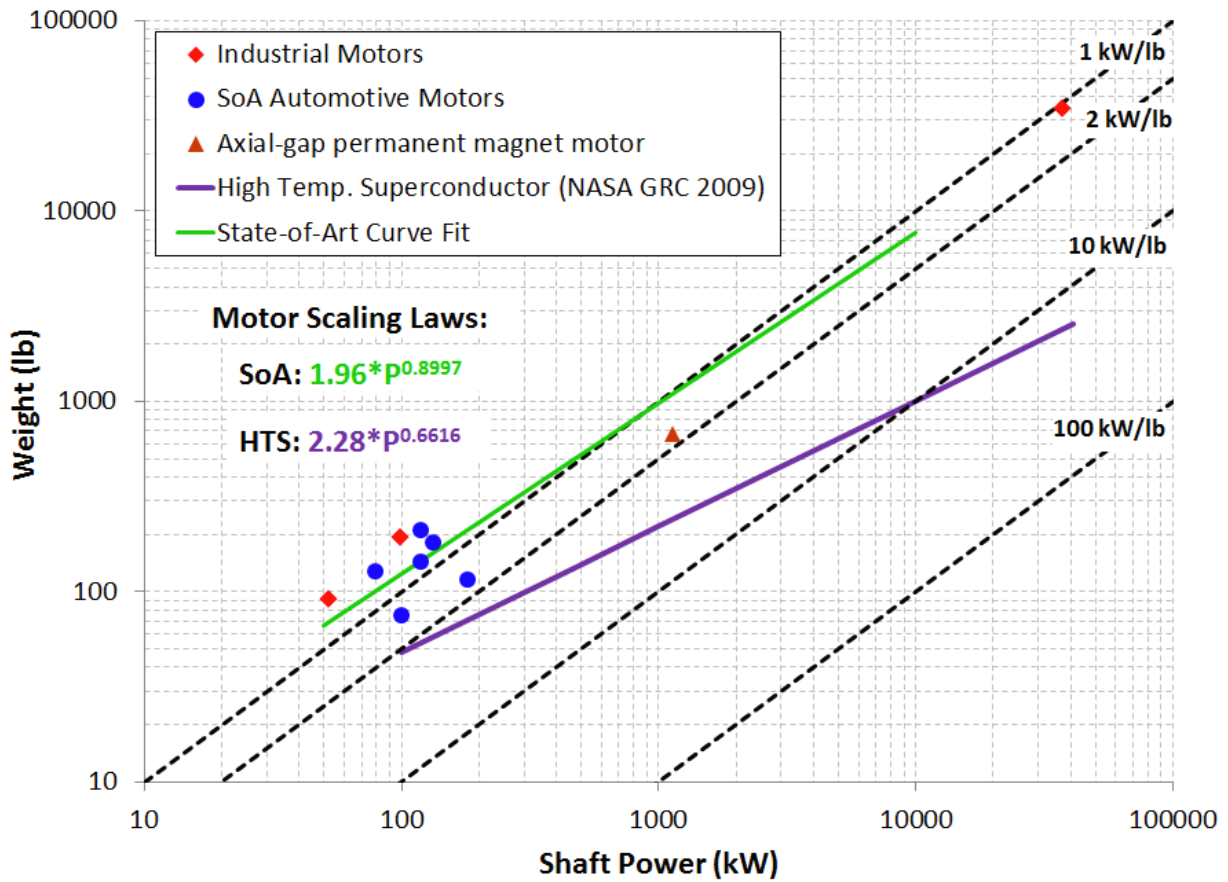


Figure B 8 Electrical motor scaling trends from [72] [81].

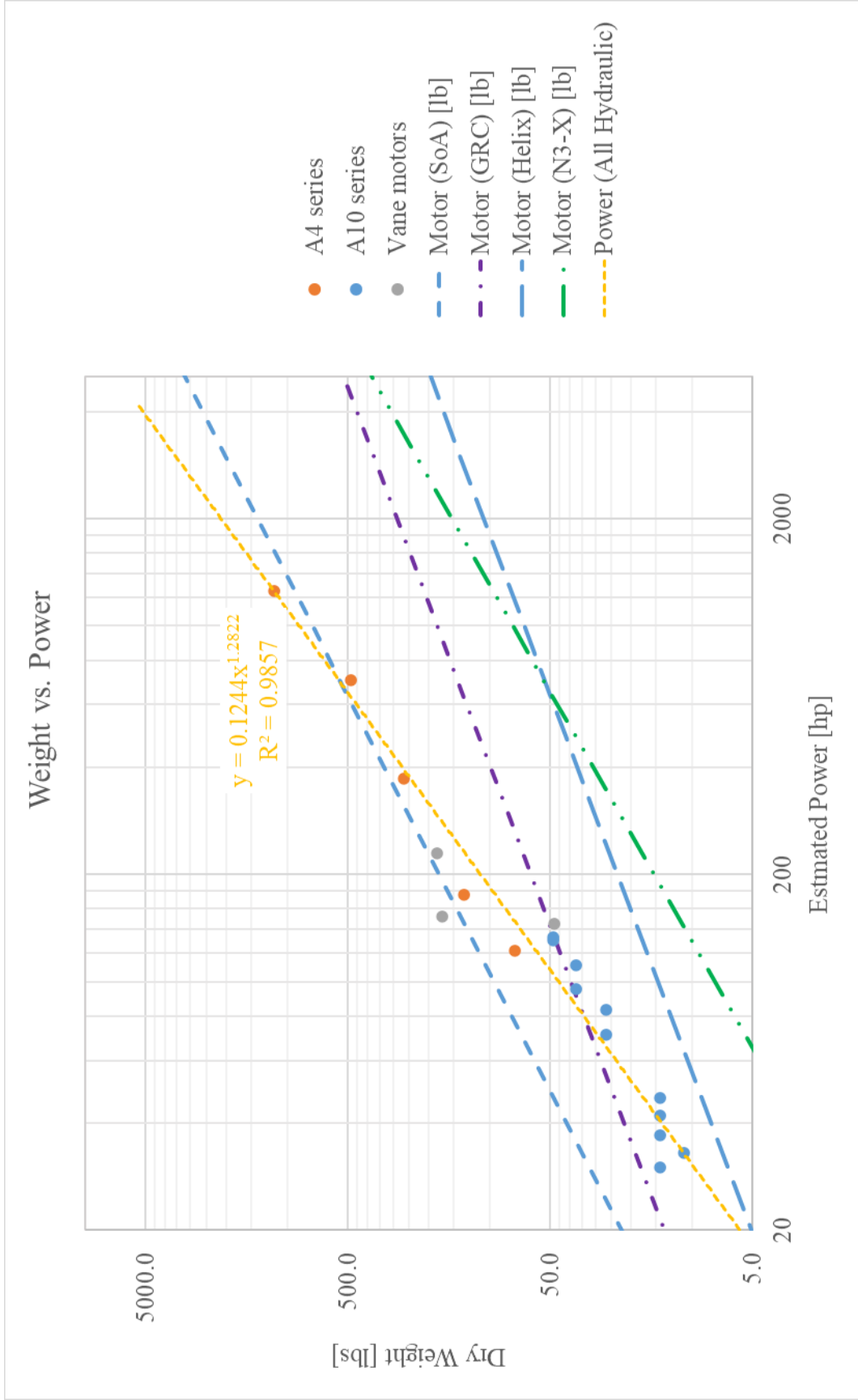


Figure B 9 Motor weight scaling trend for all motors considered.

Table B 10 Current carrying capacity and resistance of copper wire [76].

Size AWG	Nominal conductor area [circ.mils]	Nominal conductor area [mm ²]	Current Carrying Capacity (amps)			Max. resistance ohms/1000ft@20 °C tin plated conductor (See Note #2)
			105 °C	150 °C	200 °C	
24	475	0.2407	2.5	4	5	28.4
22	755	0.3826	3	5	6	16.2
20	1216	0.6162	4	7	9	9.88
18	1900	0.9627	6	9	12	6.23
16	2426	1.2293	7	11	14	4.81
14	3831	1.9412	10	14	18	3.06
12	5874	2.9764	13	19	25	2.02
10	9354	4.7397	17	26	32	1.26
8	16983	8.6054	38	57	71	0.7
6	26818	13.5889	50	76	97	0.44
4	42615	21.5933	68	103	133	0.28
2	66500	33.6960	95	141	179	0.18
1	81700	41.3980	113	166	210	0.15
1/0	104500	52.9509	128	192	243	0.12
2/0	133000	67.3921	147	222	285	0.09
3/0	166500	84.3668	172	262	335	0.07
4/0	210900	106.8646	204	310	395	0.06

Note #1: Rating is for 70°C ambient, 33 or more wires in the bundle for sizes 24 through 10, and 9 wires for size 8 and larger, with no more than 20 percent of harness current carrying capacity being used, at an operating altitude of 60,000 feet. For rating of wires under other conditions or configurations see paragraph 11-69.

Note #2: For resistance of silver or nickel-plated conductors see wire specifications.

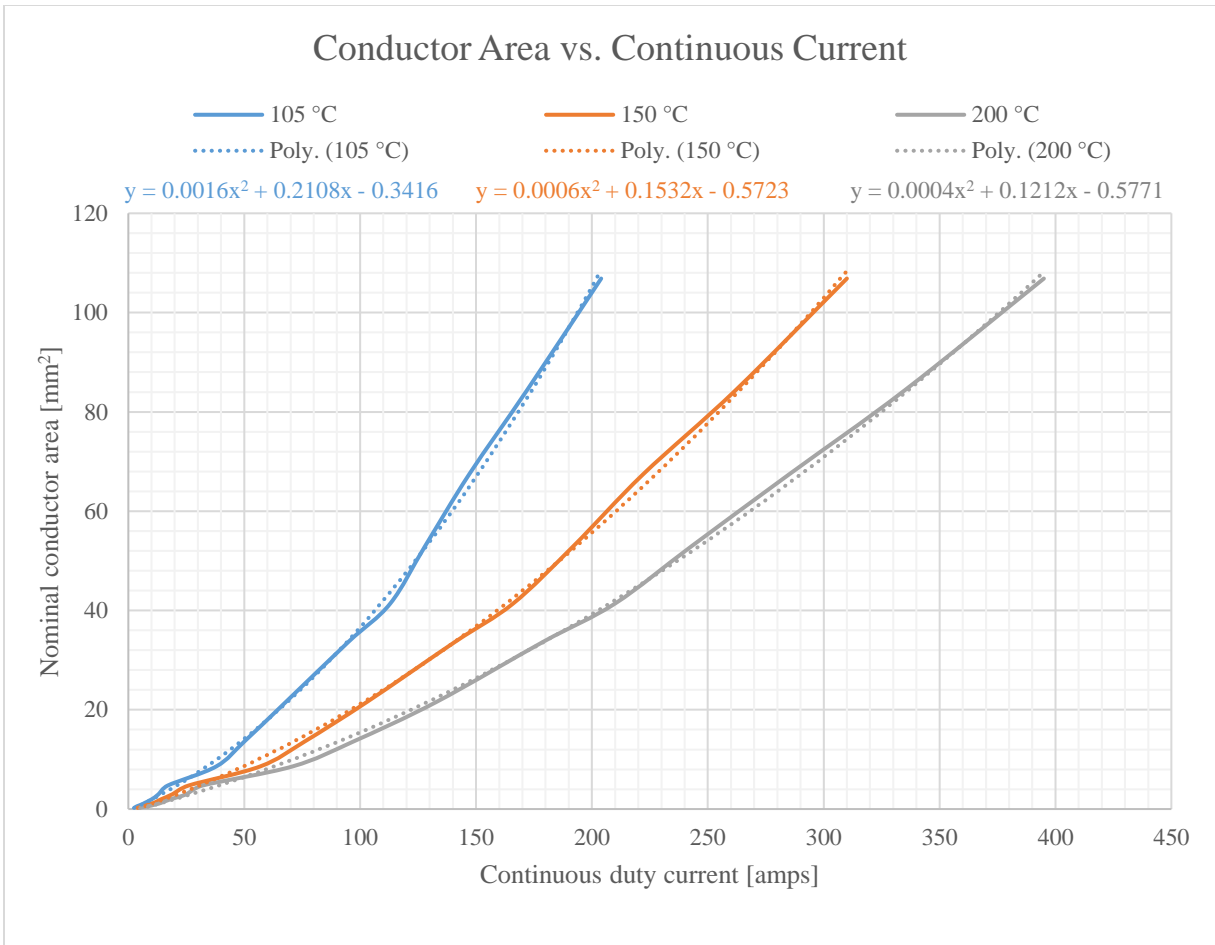


Figure B 10 Wire cross-sectional area WRT current comply with AC 43.13-1B.

Table B 11 HW263 cable data [77].

Size AWG/ kcmil	Nominal conductor area [mm ²]	Weight [lbs/ft]	Current Carrying Capacity (amps)		
			90 °C	100 °C	110 °C
18	1	0.016	20	16	17
16	1.3	0.018	23	23	25
14	2.1	0.025	32	37	40
12	3.3	0.032	38	45	48
10	5.2	0.051	51	58	62
8	7.6	0.071	68	72	77
6	12.5	0.108	91	96	103
4	21	0.173	121	128	137
2	34	0.242	162	169	181
1	43	0.335	187	194	208
1/0	54	0.42	217	227	243
2/0	70	0.494	250	262	281
3/0	86	0.627	289	300	321
4/0	109	0.82	335	351	376
262	132	0.945	382	407	436
313	159	1.113	427	455	487
373	189	1.419	476	516	553
444	227	1.578	531	588	630
535	273	1.976	597	630	709
646	326	2.348	671	731	783
777	394	2.795	753	822	881
1111	562	3.982	937	1025	1098

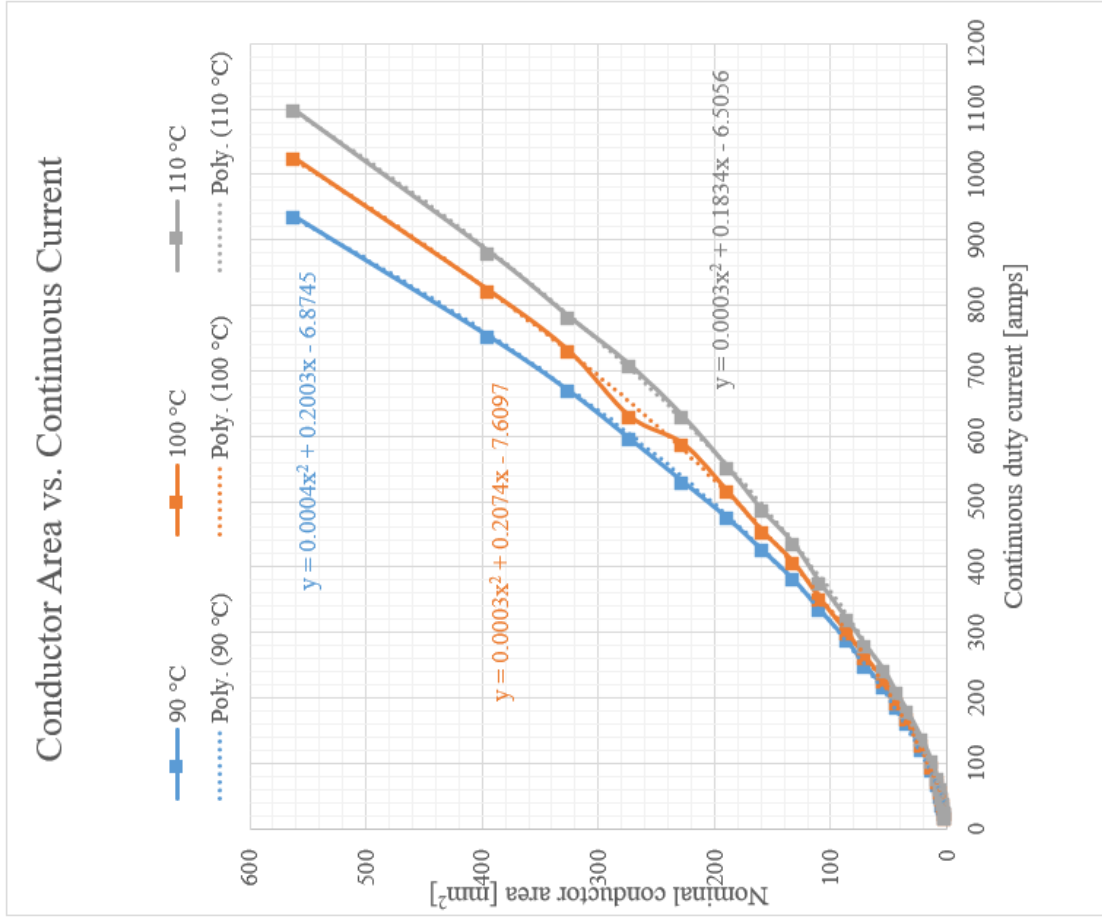


Figure B 11 HWC 263 cross-sectional area WRT current.

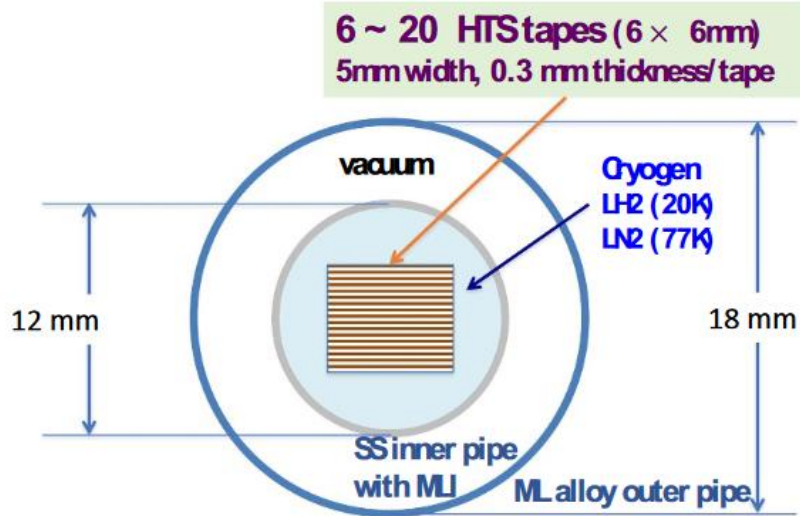


Figure B 12 Cross-section of the cryogenic pipe and conductor [78].

Table B 12 Weight per unit length of the cable system [78].

	Weight/length [kg/km]
Sum of the inner & outer cryogenic pipes	111.3
HTS tapes (6 layers)	134.4
Liquid nitrogen	56.1
Other parts	7.6
Sum	301.8

Table B 13 Rated current and weight-to-current per unit length [78].

Configuration	Temp. [K]	Rated current [kA]	Weight-to-current per length [kg/A/km]
6 tapes	77	0.6	0.503
	20	3.0	0.101
20 tapes	77	2.0	0.319
	20	10.0	0.064

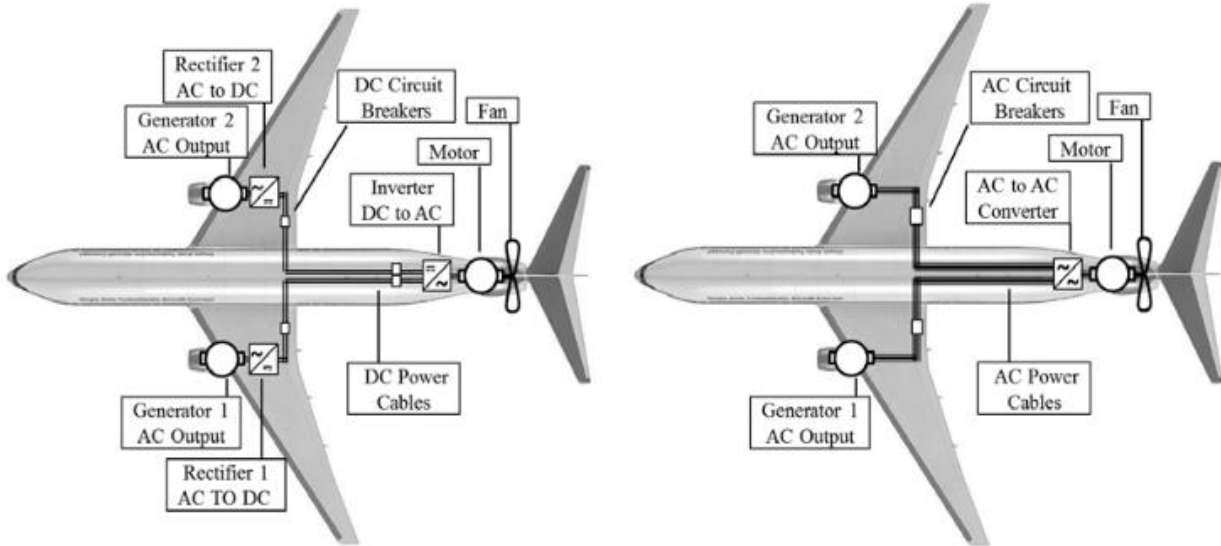


Figure B 13 STARC-ABL architecture: baseline (left) & advanced concepts (right) [79].

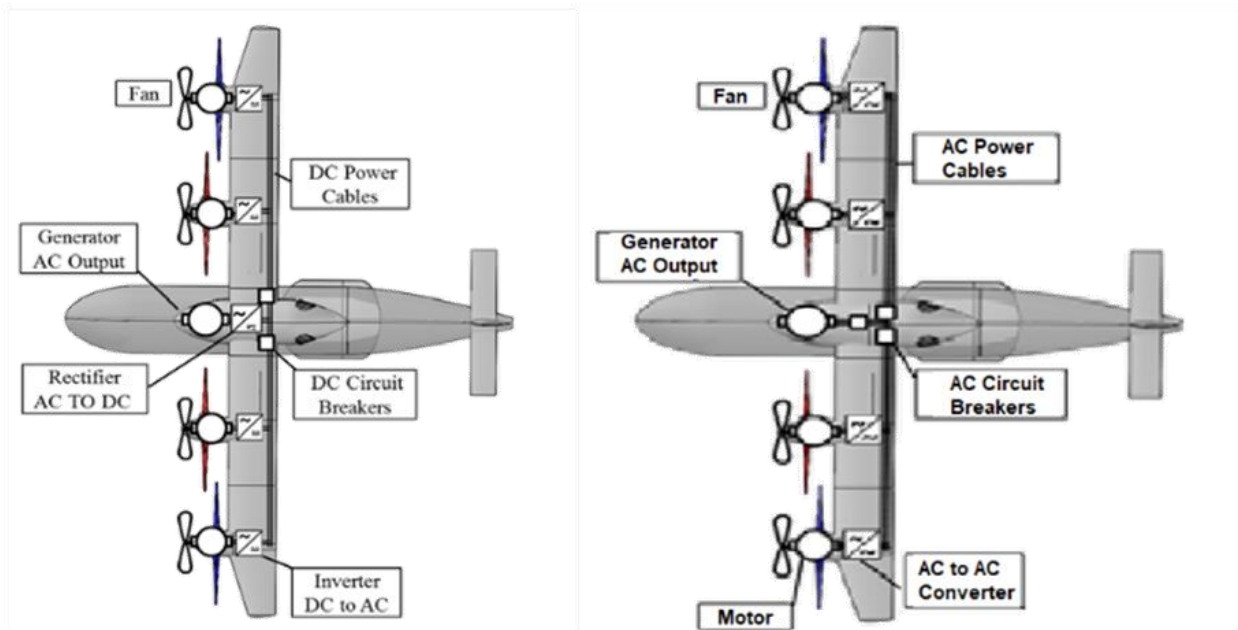


Figure B 14 RVL T EAP architecture: baseline (left) & advanced concepts (right) [79].

Table B 14 Electrified aircraft cooling loop comparison [79].

Loop Type	Platform	n	Technology	Rejected Power,kW	Coolant	Weight,kg	Required power, kW	Drag,lbf
engine + generator	STARC-ABL engine	2	baseline	175	engine oil	5.44E+01	4.00E-02	2.25E+00
	Tiltwing	1	baseline	173	engine oil	1.46E+01	2.84E+00	-1.11E+01
converter	STARC-ABL engine	2	baseline	29	PGW30	1.53E+01	3.00E-02	1.83E+00
	Tiltwing	1	baseline	48	PGW30	1.11E+01	2.26E+00	-8.55E+00
battery	PEGASUS battery	1	baseline	186	PGW30	1.00E+02	1.60E-01	1.06E+01
		1	advanced	178	PGW30	9.60E+01	1.50E-01	1.02E+00
	STARC-ABL BU	1	baseline	164	PGW30	5.86E+01	6.00E-02	6.53E+00
	PEGASUS inboard	2	baseline	66	PGW30	2.82E+01	1.70E-02	2.16E+00
converter + motor	PEGASUS tip	2	baseline	24	PGW30	1.20E+01	7.00E-03	8.33E+01
	PEGASUS BU	1	baseline	33	PGW30	1.50E+01	9.00E-03	8.00E-02
	Tiltwing	4	baseline	35	PGW30	7.11E+00	1.36E+00	-5.06E+00
	STARC-ABL engine	2	advanced	20	PSF-5	9.46E+00	5.00E-02	7.36E+01
motor (HEMM) *Engine coolant loop	Tiltwing	1	advanced	35	PSF-5	8.62E+00	1.41E+00	-5.14E+00
	STARC-ABL BU	1	advanced	66	PSF-5	3.19E+01	2.12E-01	3.05E+00
converter + motor (HEMM)	PEGASUS inboard	2	advanced	21	PSF-5	1.29E+01	5.00E-02	8.10E-01
	PEGASUS tip	2	advanced	6	PSF-5	4.78E+00	1.40E-02	2.25E-01
	PEGASUS BU	1	advanced	11	PSF-5	7.52E+00	2.50E-02	4.28E-01
	Tiltwing	4	advanced	14	PSF-5	4.58E+00	6.00E-01	-2.19E+00

Table B.15 Sizing relations for loops cooling converters in series with motors [79].

Vehicle Objective	Technology Level	Coolant	TMS Sizing Relations, weight(kg), power(kW), and drag (lbf)
STARC-ABL	Baseline	PGW30	$\text{weight} = 0.346 * \text{power}_{\text{rejected}} + 1.480$ $\text{power}_{\text{required}} = 3.65e - 4 * \text{power}_{\text{rejected}} - 1.19e - 4$ $\text{drag} = 4.06e - 2 * \text{power}_{\text{rejected}} + 4.41e - 5$
STARC-ABL	Advanced	PSF-5	$\text{weight} = 0.442 * \text{power}_{\text{rejected}} + 2.195$ $\text{power}_{\text{required}} = 3.13e - 3 * \text{power}_{\text{rejected}} + 4.01e - 3$ $\text{drag} = 4.55e - 2 * \text{power}_{\text{rejected}} - 1.05e - 2$
RVLT Tiltwing	Baseline	PGW30	$\text{weight} = 0.159 * \text{power}_{\text{rejected}} + 1.4824$ $\text{power}_{\text{required}} = 3.88e - 2 * \text{power}_{\text{rejected}} + 8e - 8$ $\text{drag} = -0.1446 * \text{power}_{\text{rejected}} + 0.0025$
RVLT Tiltwing	Advanced	PSF-5	$\text{weight} = 0.1902 * \text{power}_{\text{rejected}} + 1.8401$ $\text{power}_{\text{required}} = 4.36e - 2 * \text{power}_{\text{rejected}} + 9.2e - 3$ $\text{drag} = -0.1532 * \text{power}_{\text{rejected}} - 0.0228$
PEGASUS	Baseline	PGW30	$\text{weight} = 0.407 * \text{power}_{\text{rejected}} + 1.504$ $\text{power}_{\text{required}} = 2.65e - 4 * \text{power}_{\text{rejected}} + 1.33e - 4$ $\text{drag} = 3.30e - 2 * \text{power}_{\text{rejected}} + 5.87e - 3$
PEGASUS	Advanced	PSF-5	$\text{weight} = 0.5207 * \text{power}_{\text{rejected}} + 1.863$ $\text{power}_{\text{required}} = 2.25e - 3 * \text{power}_{\text{rejected}} + 1.15e - 3$ $\text{drag} = 3.80e - 2 * \text{power}_{\text{rejected}} + 1.11e - 2$

Table B 16 Tiltwing concept vehicle design [56].

	turboelectric	turboshaft	tailprop		turboelectric	turboshaft	tailprop
disk load (lb/ft ²)	30	30	30	DGW (lb)	14039	11856	14193
radius (ft)	6.10	5.61	6.14	WE (lb)	8918	6518	9068
solidity	0.3707	0.3707	0.3707	structure	3495	2973	3520
tail prop DL			20	wing group	822	686	831
radius (ft)			4.65	rotor group	503	431	502
solidity			0.2471	fuselage group	1129	1018	1137
wing load (lb/ft ²)	60	60	60	propulsion	3460	1810	3619
wing span (ft)	51.26	47.11	51.54	drive system	715	580	748
aspect ratio	11.23	11.23	11.23	systems	1338	1278	1294
power (hp)	4x731	4x862	4x731	flight controls	394	348	344
sfc MCP SLS		0.491		WO (lb)	8938	6538	9088
weight/power	0.198	0.230	0.198	V _{br} (knots)	200	184	192
turboshaft power	4730		4733	V _{be} (knots)	122	117	117
sfc MCP SLS	0.348		0.348	V _{max} (knots)	230	215	227
weight/power	0.132		0.132	payload (lb)	3000	3000	3000
generator power	3239		3242	range (nm)	400	400	400
weight/power	0.150		0.150	TO GW	13866	11654	14009
drag D/q (ft ²)	8.22	8.81	8.37	TO WO	8938	6538	9088
fuselage	2.58	2.58	2.58	TO fuel Wt (lb)	1928	2116	1921
rotor	2.18	3.39	2.29	fuel burn (lb)	1753	1923	1747
wing	2.22	1.88	2.25	cruise speed (knots)	200	183	192
D/q / (W/1000) ^{2/3}	1.43	1.68	1.44	aircraft L/D _e = WV/P	7.22	7.28	7.70
battery cap (MJ)	288		288	aircraft FM	0.67	0.76	0.68
tank cap (lb)	2101	2318	2105	V/V _{tip}	1.23	1.12	1.18
battery wt (lb)	441		441	C _T /s	0.138	0.137	0.137
fuel tank wt (lb)	248	267	249	total hover FM	0.79	0.79	1.05
				total propulsive eff	0.82	0.85	0.82
				W _{battery} /GW	0.032	0.000	0.032
				WO/GW (wo battery)	0.613	0.561	0.617
				WO/GW	0.645	0.561	0.649
				W _{fuel} /GW	0.139	0.182	0.137
				W _{payload} /GW	0.216	0.257	0.214

APPENDIX C– Additional Information

Table C 1 The hydraulic component weight, of various takeoff weight.

Hydrostatic (Tilt motor)									
MTOW	5000	10000	20000	30000	40000	50000	60000	70000	80000
Centerbox	33	67	134	201	268	335	402	469	536
Hydrostatic Pump	84	168	335	503	671	839	1,006	1,174	1,342
Rotor Motor	176	342	667	986	1,300	1,612	1,922	2,229	2,535
Hose (wet)	37	93	231	395	578	776	988	1,211	1,445
Support	64	127	255	382	510	637	765	892	1,020
Rotary union	57	102	162	206	242	273	300	325	347
Total	450	899	1,785	2,673	3,569	4,472	5,382	6,300	7,225
Weight Fraction	0.09	0.09	0.09	0.09	0.09	0.09	0.09	0.09	0.09

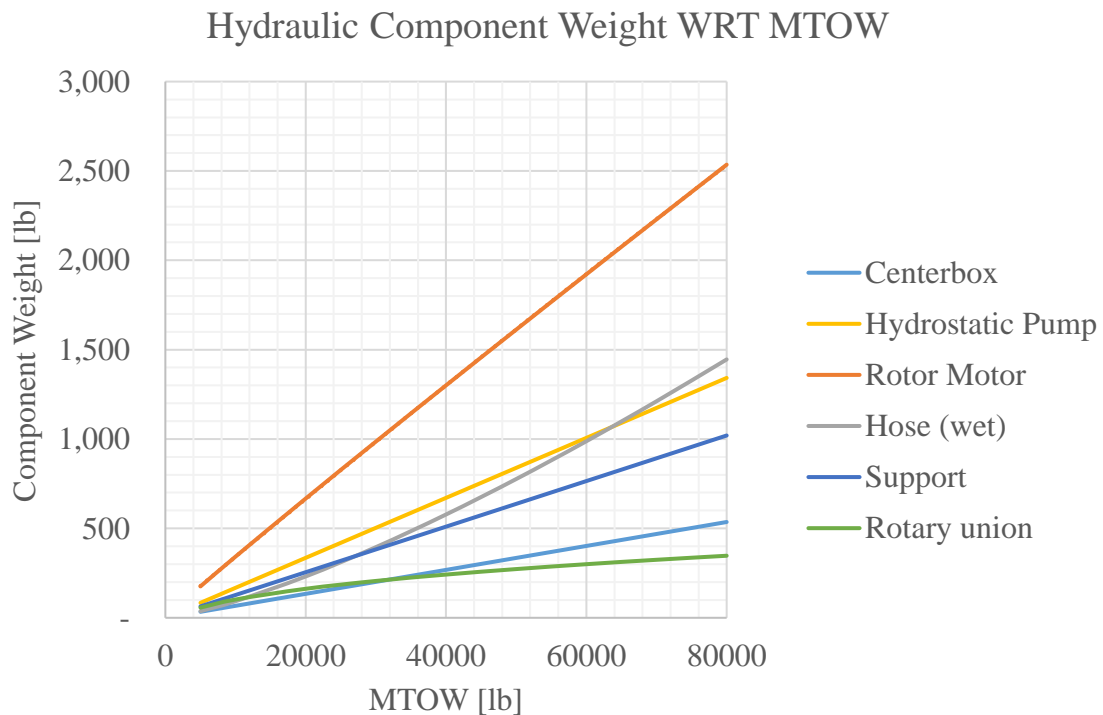


Figure C 1 The hydraulic component weight trend over takeoff weight.

Table C 2 The electric transmission component weight with GRC components.

Electric (HTS GRC)									
MTOW	5000	10000	20000	30000	40000	50000	60000	70000	80000
Centerbox	33	67	134	201	268	335	402	469	536
Motor Generator	161	255	403	527	638	740	834	924	1009
Inverter	118	236	473	709	945	1181	1418	1654	1890
Rotor Motor	204	322	510	667	807	935	1055	1168	1276
Battery	31	61	123	184	246	307	369	430	491
Wire	2	9	35	81	150	246	371	526	715
Support	263	529	1067	1614	2174	2746	3333	3936	4555
Rotary union	0.2	1	4	12	24	42	68	103	148
Total	813	1481	2748	3995	5252	6533	7850	9210	10621
Weight Fraction	0.16	0.15	0.14	0.13	0.13	0.13	0.13	0.13	0.13

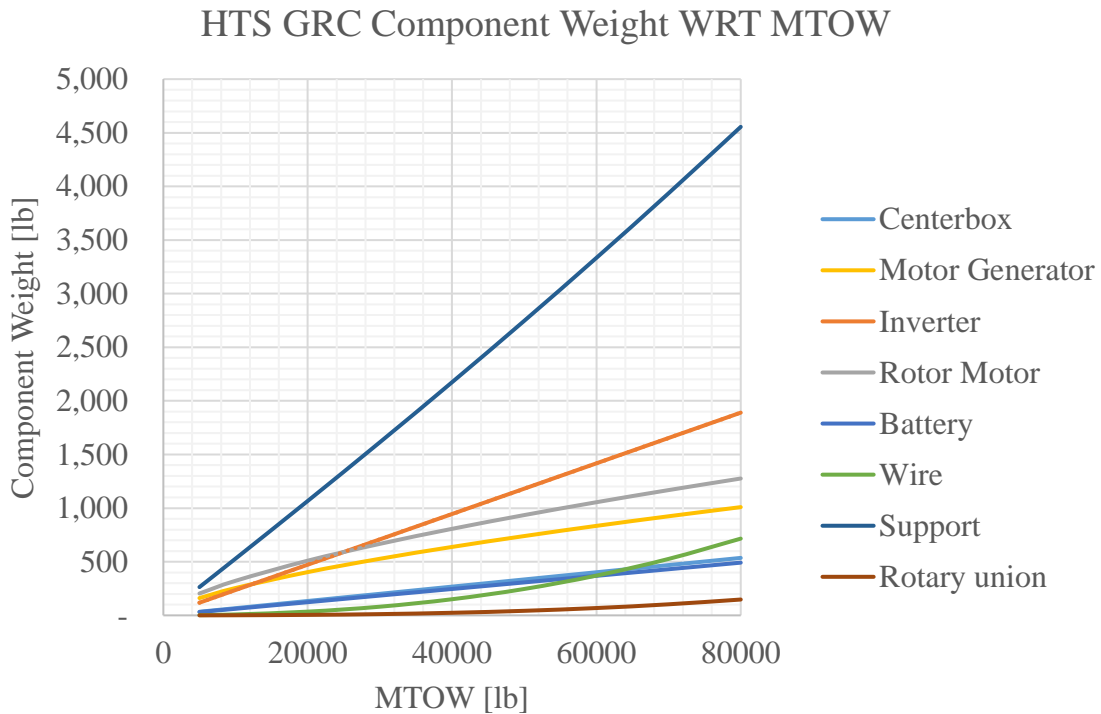


Figure C 2 GRC components weight trend over takeoff weight.

Table C 3 The electric transmission component weight with N3-X assumption.

Electric (Cryo. N3-X)									
MTOW	5000	10000	20000	30000	40000	50000	60000	70000	80000
Centerbox	33	67	134	201	268	335	402	469	536
Motor Generator	28	56	112	167	223	279	335	391	446
Inverter	118	236	473	709	945	1181	1418	1654	1890
Rotor Motor	64	129	258	386	515	644	773	902	1030
Battery	31	61	123	184	246	307	369	430	491
Wire	2	5	14	25	38	54	71	89	109
Support	175	352	705	1060	1416	1773	2131	2489	2848
Rotary union	0.2	1	4	12	24	42	68	103	148
Total	452	907	1822	2745	3676	4615	5565	6526	7499
Weight Fraction	0.09	0.09	0.09	0.09	0.09	0.09	0.09	0.09	0.09

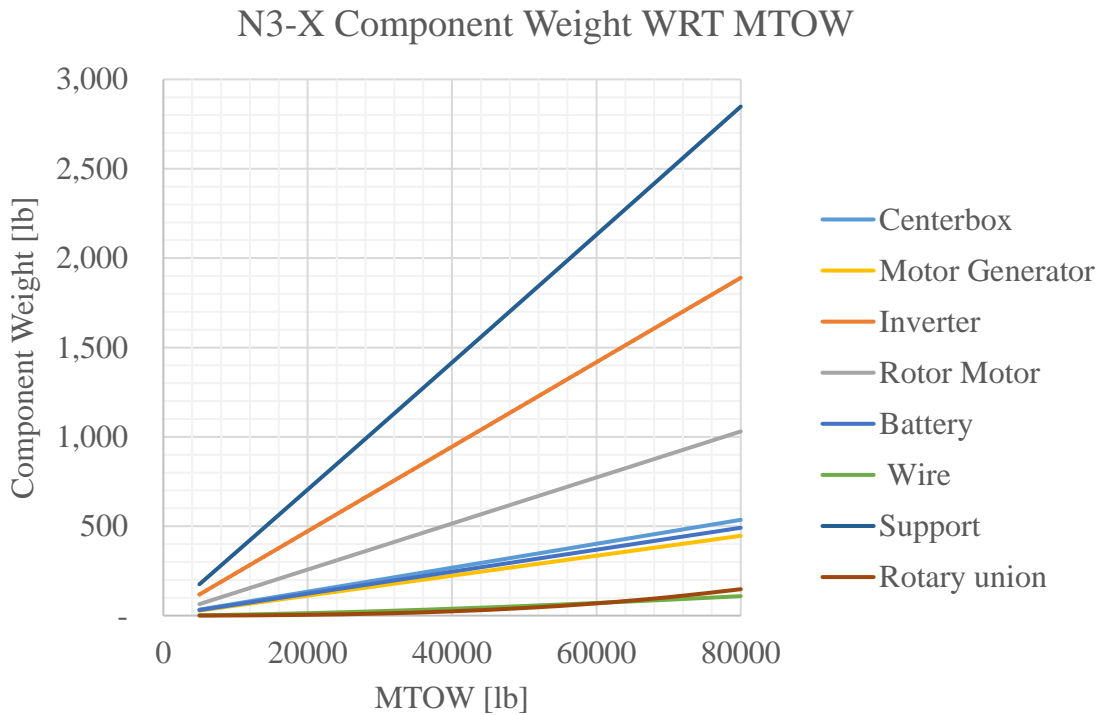


Figure C 3 N3-X assumption components weight trend over takeoff weight.

Table C 4 The electric transmission component weight using Helix motor.

Electric (Helix)									
MTOW	5000	10000	20000	30000	40000	50000	60000	70000	80000
Centerbox	33	67	134	201	268	335	402	469	536
Motor Generator	120	190	301	393	476	551	622	689	753
Inverter	55	110	220	330	440	551	661	771	881
Rotor Motor	120	190	301	393	476	551	622	689	753
Battery	40	80	160	240	319	399	479	559	639
Wire	9	35	138	321	597	977	1472	2090	2841
Support	25	57	149	281	459	689	976	1325	1741
Rotary union	0.2	1	4	12	24	42	68	103	148
Total	403	730	1406	2171	3059	4096	5302	6695	8290
Weight Fraction	0.08	0.07	0.07	0.07	0.08	0.08	0.09	0.10	0.10

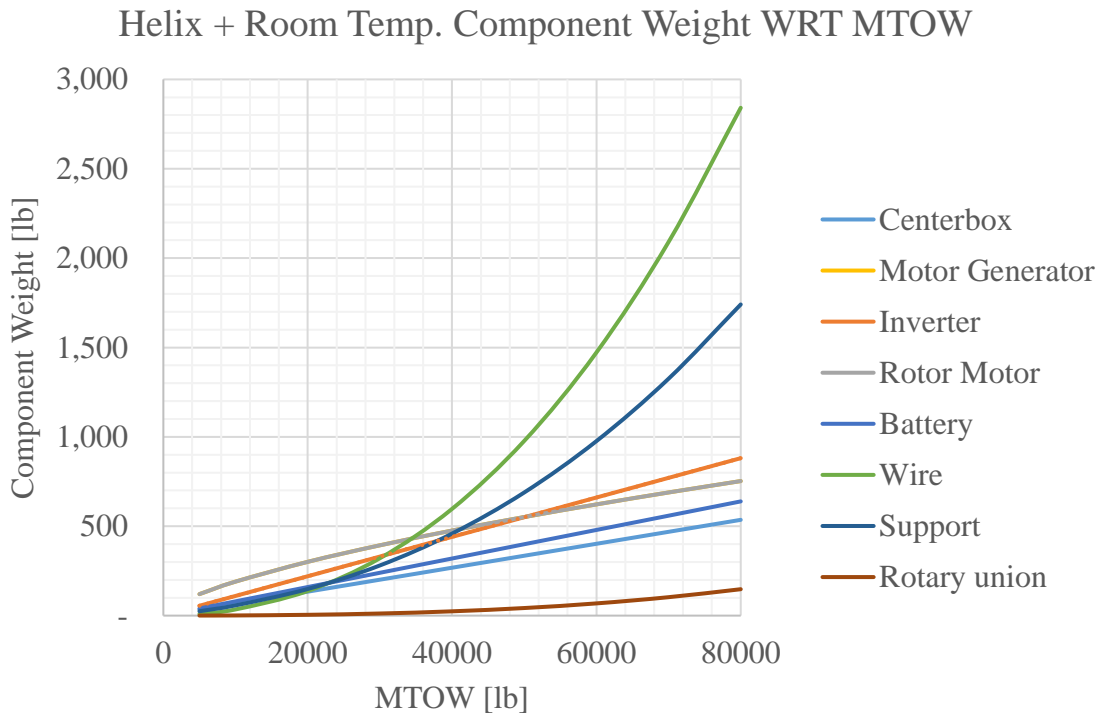


Figure C 4 Helix motor transmission weight over takeoff weight.

Table C 5 Electric transmission component weight using Helix motor + HTS cable.

Electric (Helix+HTS)									
MTOW	5000	10000	20000	30000	40000	50000	60000	70000	80000
Centerbox	33	67	134	201	268	335	402	469	536
Motor Generator	120	190	301	393	476	551	622	689	753
Inverter	55	110	220	330	440	551	661	771	881
Rotor Motor	120	190	301	393	476	551	622	689	753
Battery	40	80	160	240	319	399	479	559	639
Wire	2	5	14	25	38	54	71	89	109
Support	26	54	109	166	224	283	343	403	465
Rotary union	0.2	1	4	12	24	42	68	103	148
Total	397	697	1243	1760	2266	2767	3268	3772	4282
Weight Fraction	0.08	0.07	0.06	0.06	0.06	0.06	0.05	0.05	0.05

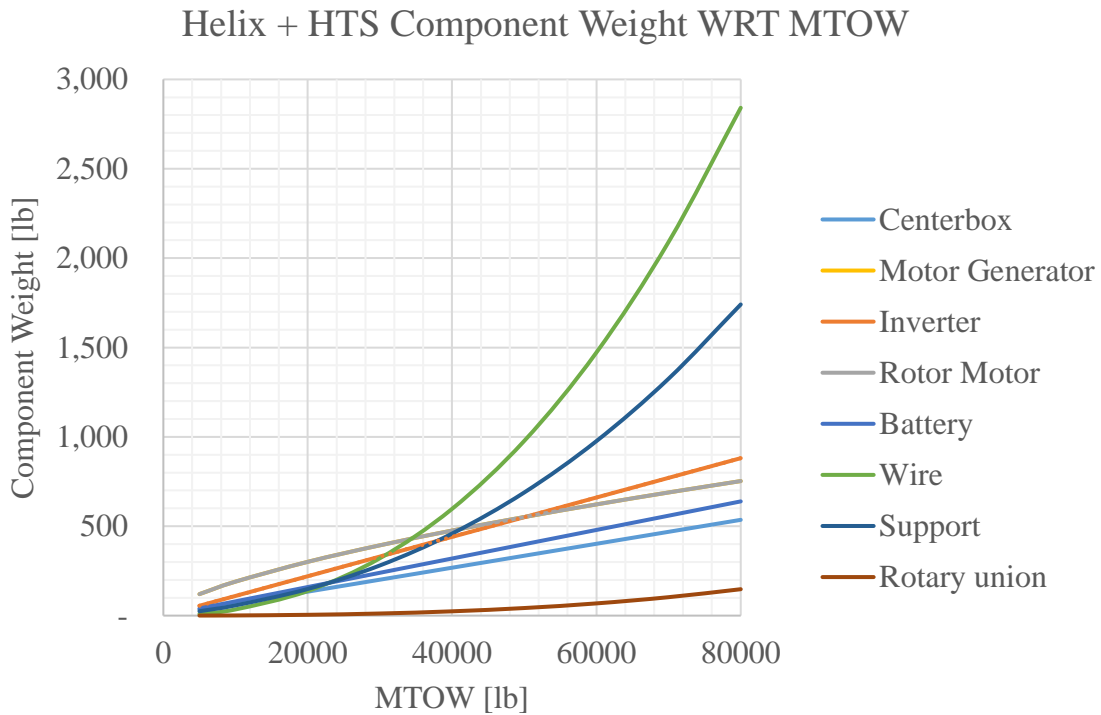


Figure C 5 Helix motor and HTS cable transmission weight over takeoff weight.

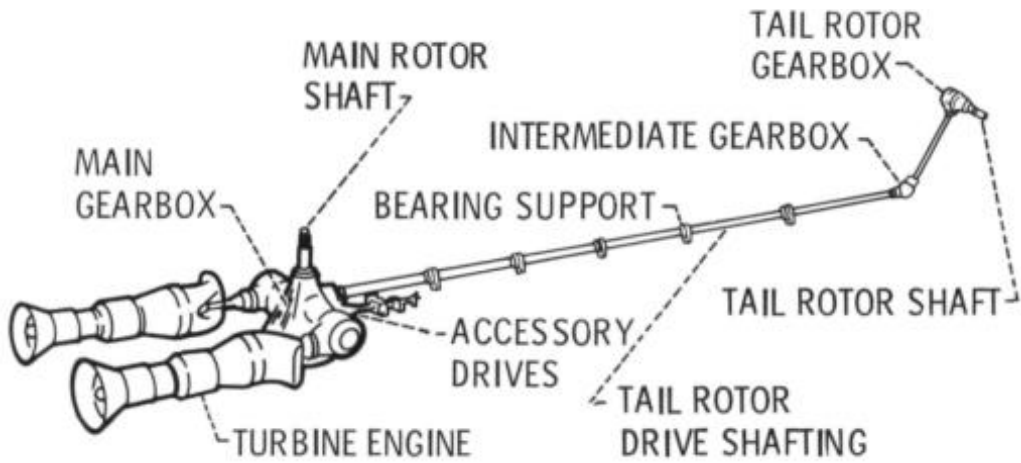


Figure C 6 Typical transmission system in single-rotor helicopter from [82].

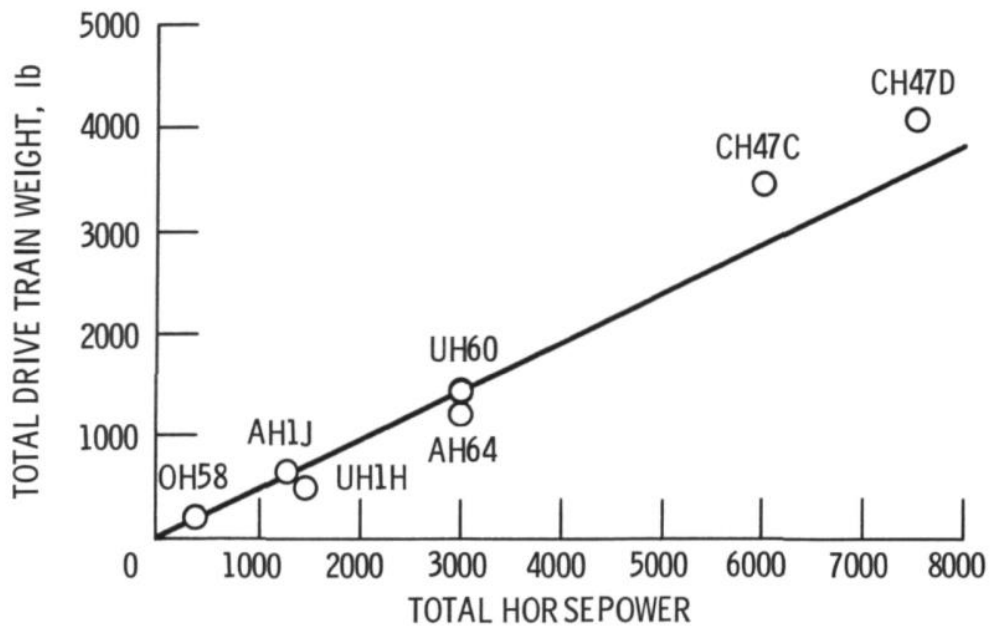


Figure C 7 Weight trends for current helicopter drive trains from [82].